

University of Louisville

## ThinkIR: The University of Louisville's Institutional Repository

---

Electronic Theses and Dissertations

---

12-2022

### The impact of PEGylation on cellular uptake and in vivo biodistribution of gold nanoparticle MRI contrast agents.

Nagwa El-Baz  
*University of Louisville*

Follow this and additional works at: <https://ir.library.louisville.edu/etd>



Part of the [Nanomedicine Commons](#)

---

#### Recommended Citation

El-Baz, Nagwa, "The impact of PEGylation on cellular uptake and in vivo biodistribution of gold nanoparticle MRI contrast agents." (2022). *Electronic Theses and Dissertations*. Paper 4008.  
<https://doi.org/10.18297/etd/4008>

This Doctoral Dissertation is brought to you for free and open access by ThinkIR: The University of Louisville's Institutional Repository. It has been accepted for inclusion in Electronic Theses and Dissertations by an authorized administrator of ThinkIR: The University of Louisville's Institutional Repository. This title appears here courtesy of the author, who has retained all other copyrights. For more information, please contact [thinkir@louisville.edu](mailto:thinkir@louisville.edu).

THE IMPACT OF PEGYLATION ON CELLULAR UPTAKE AND IN VIVO  
BIODISTRIBUTION OF GOLD NANOPARTICLE MRI CONTRAST AGENTS

By

Nagwa El-Baz

B.S., Pharmacy School, Mansoura University, 2001

M.S., University of Louisville, 2018

A Dissertation

Submitted to the Faculty of the

School of Medicine of the University of Louisville

In Partial Fulfilment of the Requirement

for the Degree of

Doctor of Philosophy in Pharmacology and Toxicology

Department of Pharmacology and Toxicology

University of Louisville

Louisville, Kentucky

December 2022

Copyright 2022 by Nagwa El-Baz

All rights reserved



THE IMPACT OF PEGYLATION ON CELLULAR UPTAKE AND IN VIVO  
BIODISTRIBUTION OF GOLD NANOPARTICLE MRI CONTRAST AGENTS

By

Nagwa El-Baz

B.S., Pharmacy School, Mansoura University, 2001

M.S., University of Louisville, 2018

A Dissertation Approved on

November 17<sup>th</sup>, 2022

by the following Dissertation Committee:

---

Martin O'Toole, Ph.D.

---

Paula Bates, Ph.D.

---

Geoffrey Clark, Ph.D.

---

Hermann Frieboes, Ph.D.

---

Jill Steinbach-Rankins, Ph.D.

## DEDICATION

This dissertation is lovingly dedicated to

My father

Abd El-Fattah, who will be on my heart forever

My mother

Hend, who always gives me too much

For my husband

Ayman, for his constant support and love

My sister and brothers

Mona, Sherif, and Ahmed

And my very lovely kids

Maryam & Ahmed

## ACKNOWLEDGEMENT

First, I would like to express my appreciation and gratitude to my mentor Dr. Martin O'Toole for his spectacular support, guidance, and patience over the past 7 years. I really appreciate the opportunity I had to pursue my master and PhD degrees under his supervision and to learn about the state-of-the-art in gold nanoparticle synthesis and applications.

I would like to thank my doctoral committee: Dr. Paula Bates, Dr. Geoffrey Clark, Dr. Hermann Frieboes, and Dr. Jill Steinbach-Rankins for their valuable suggestions, comments, and guidance throughout the past years.

In addition, I would like to thank Dr. Jason Xu for running the ICP-MS samples and for his help in answering any question.

I also want to thank all the current and former lab members: Kurtis James and Dr. Rajat Chauhan who taught me gold nanoparticle synthesis. Betty Nunn for her great help in animal studies and for always being willing to help out. Nicholas Allen and Md Emtias Chowdhury for helping and support.

Thank you to the Department of Pharmacology and Toxicology for providing me the opportunity to pursue my graduate degree, I would like to thank Dr. David Hein, Dr. Christopher States, Dr. Leah Siskind, and Dr. Sandra Wise. Thanks for the Integrated Program in Biomedical Science (IPBS) for providing support for two years.

I also want to thank the Graduate Student Council for supporting part of my research. Finally, I must thank all my family for their great help.



## ABSTRACT

### THE IMPACT OF PEGYLATION ON CELLULAR UPTAKE AND *IN VIVO* BIODISTRIBUTION OF GOLD NANOPARTICLE MRI CONTRAST AGENTS

Nagwa El-Baz

November 17<sup>th</sup>, 2022

Gold nanoparticles (GNPs) have become a pivotal platform for the delivery of pharmaceutical and diagnostic agents as well as for general therapeutic purposes. Despite their potential for use in biomedicine, their interaction with serum proteins is crucial as it could change their biological profile due to the formation of a protein corona, which can affect their delivery to target tissues in the body. Grafting the GNPs with polyethylene glycol (PEG) is widely used in research to decrease opsonization of the particles by serum proteins and decrease the uptake by the reticuloendothelial system.

Here in this dissertation, we have developed a library of 4 and 10 nm GNPs conjugated with a gadolinium chelate as MRI contrast agent, cancer-targeting aptamer AS1411 (CRO aptamer was used as control), and with or without polyethylene glycol (PEG) of different molecular weights (Mw: 1, 2, and 5 kDa).

We have quantified the amount of proteins that adsorbed on the surface of PEGylated and non-PEGylated GNPs after incubation in human serum proteins. Additionally, we have quantified the uptake of nanoparticles with and without protein corona by the human breast cancer cell line MDA-MB-231 and the murine monocyte/macrophage cell line RAW 264.7.

Furthermore, we have investigated the *in vivo* biodistribution of GNPs using the murine

model of 4T1 mammary carcinoma in BALB/c female mice.

The *in vitro* results showed that PEG failed to decrease protein adsorption and the cellular uptake by macrophage cells was contingent on the different configurations of the aptamers and the length of PEG chain. While *in vivo* biodistribution showed that PEG increased the uptake by tumor cells for some GNPs, it did not decrease the uptake of GNPs by macrophage-rich organs.

## TABLE OF CONTENTS

Content:	PAGE
DEDICATION	iii
ACKNOWLEDGMENTS	iv
ABSTRACT	vi
LIST OF TABLES	xii
LIST OF FIGURES	xiii
CHAPTER 1: INTRODUCTION	1
Part 1. Gold Nanoparticles: History, Synthesis, Properties, Applications, and Challenges	1
1.1. Colloidal Gold History	2
1.2. Synthesis of Gold Nanoparticles (GNPs)	3
1.3. Properties of GNPs	5
1.4. Formation of GNP Bioconjugates	6
1.5. Application of GNPs	7
Diagnostic Applications	8
Therapeutic Applications	11

1.6. Challenges Facing GNPs in Biomedicine	17
1.7. Strategies to Increase Blood Circulation Half-Life and the Selective Delivery of GNPs	21
Part 2. Focus of This Dissertation	23
Specific Aims	24
CHAPTER 2: MATERIALS AND METHODS	27
2.1. Materials	27
2.2. GNPs Synthesis	29
2.3. Chemical Synthesis of Gadolinium (III) DO3A-SH (Gd)	30
2.4. Annealing and Preparing of AS1411 and CRO for Conjugation to GNPs	30
2.5. Preparation of PEG Solutions	31
2.6. Conjugation of Gd(III)-DO3A-SH (Gd), AS1411/ and or CRO, and mPEG to GNP	31
2.7. Quantification of AS1411 and CRO per Nanoparticle	32
2.8. Quantification of Gadolinium	32
2.9. Protein Quantification by Bicinchoninic Acid (BCA) Assay	33
2.10. Gel Electrophoresis	33
2.11. MDA-MB-231 and RAW 264.7 Cells Culture	33

2.12. Cellular Uptake Studies	34
2.13. In vivo Biodistribution Study	34
2.14. Statistical Analysis	35
CHAPTER 3: RESULTS OF GNPs CHARACTERIZATION AND PROTEIN ADSORPTION STUDIES	36
3.1. Development and Characterization of 4 & 10 nm GNPs Conjugates with AS1411/CRO, Gd (III)-DO3A, and PEGs (1, 2, and 5 kDa)	36
3.2. Determination of the Adsorption of Serum Proteins on the GNP Surfaces	44
3.2.1. Quantification of the Amount of Bound Proteins on the Surface of GNPs by Bicinchoninic Acid Assay (BCA).	44
3.2.2. Quantification of the Amount of Bound proteins on the Surface of GNPs by NuPAGE Bis-Tris gel Electrophoresis	49
CHAPTER 4: RESULTS OF <i>IN VITRO</i> AND <i>IN VIVO</i> STUDIES	53
4.1. Determination of the Uptake of the Incubated Particles with and without Serum Proteins by Macrophage and Cancer Cells.	53
4.1.1. Uptake by Macrophage Cells	53
4.1.2. Uptake by cancer cells	61
4.2. Determination of the uptake of the particles by tumor cells	66

through *in vivo* biodistribution study.

4.3. Magnetic resonance imaging (MRI) data analysis	77
CHAPTER 5: DISCUSSION and CONCLUSION	82
REFERENCES	89
LIST of ABBREVIATIONS	105
CURRICULUM VITAE	109

## LIST OF TABLES

TABLE	PAGE
2.1. Demonstration of the amount of functionalizing agents	31
3.1. Quantification of the amount of oligonucleotides	41
3.2. Quantification of gadolinium	42
4.1. Relaxivity enhancement % by different concentrations of 4 nm GNP-Gd-AS1411	78
4.2. Relaxivity enhancement % of each MRI contrast agents at 24 h post-injection.	79
4.3. Relaxivity enhancement % of each MRI contrast agents at 72 h post-injection.	79

## LIST OF FIGURES

FIGURE	PAGE
1.1. Schematic illustration of GNPs applications in biomedicine	7
1.2. Demonstration of the challenges that face GNPs in biomedicine.	18
1.3. Schematic illustration the formation of protein corona on gold nanoparticle surface	19
1.4: Schematic illustration of the construction of the proposed MRI contrast agents	24
1.5. Demonstration of the <i>in vitro</i> and the <i>in vivo</i> study	26
3.1. UV-vis spectra of citrate capped and conjugated GNPs.	39
3.2. Characterization of GNPs: the average hydrodynamic diameter	40
3.3. Characterization of GNPs: Zeta ( $\zeta$ ) potential of citrate capped and conjugated	41
3.4. Quantification of the amount of adsorbed proteins after incubation of 4 and 10 nm GNP-AS1411 with 10% human serum.	46
3.5. Quantification of the amount of adsorbed proteins after incubation of 4 and 10 nm GNP-CRO with 10% human serum.	47



3.6. Comparison between 4 and 10 nm GNPs indicates that the amount of adsorbed proteins on 10 nm GNPs is almost 2-fold the amount found on 4 nm GNPs.	48
3.7. Activation of the complement system by GNPs.	49
3.8. Bis Tris gel electrophoresis of isolated protein from 4 nm GNP/AS1411 and GNP/CRO.	51
3.9. Bis-Tris gel electrophoresis of isolated proteins from 10 nm GNP/AS1411 and GNP/CRO.	52
4.1. Effect of 4 and 10 nm GNP-AS1411 human serum proteins corona on the uptake by macrophage RAW 264.7 cells.	55
4.2. Effect of 4 and 10 nm GNP-CRO human serum proteins corona on the uptake by macrophage RAW 264.7 cells.	57
4.3. Quantification of the amount of gadolinium in macrophage cells RAW 267.7 at 90 minutes and 4 h. after treatment with GNP-AS1411	59
4.4. Quantification of the amount of gadolinium in macrophage RAW 264.7 cells at 90 minutes and 4 h. after treatment with GNP-CRO	60
4.5. Effect of 4 and 10 nm GNP-AS1411 human serum protein corona on the uptake by cancer MDA-MB231 cells.	62
4.6. Effect of 4 and 10 nm GNP-CRO human serum protein corona on the uptake by cancer MDA-MB231 cells.	63
4.7. Quantification of the amount of gadolinium in cancer cells MDA-MB-231 at 90 minutes and 4 h. after treatment with GNP-AS1411.	64

4.8. Quantification of the amount of gadolinium in cancer cells MDA-MB-231 at 90 minutes and 4 h. after treatment with GNP-CRO.	65
4.9. Figure 4.9: Quantification of 4 nm GNPs accumulation in the tumor, liver, and spleen of mice that injected with non-PEGylated and PEGylated (PEG Mw: 1kDa) 24 and 72 h post injection.	68
4.10. Quantification of 10 nm GNPs accumulation in the tumor, liver, and spleen of mice that injected with non-PEGylated and PEGylated (PEG Mw: 1kDa) 24 and 72 h post injection.	69
4.11. Quantification of the uptake of 4 nm GNPs by tumor cells, the graph shows the percentage of the injected dose.	70
4.12. Quantification of the uptake of 10 nm GNPs by tumor cells, the graph shows the percentage of the injected dose.	71
4.13. Quantification of the uptake of GNPs by liver cells.	72
4.14. Quantification of the uptake of GNPs by spleen cells.	73
4.15. Quantification of the amount of gadolinium in tumor tissues in g of Gd/g tissue at 24 post injection.	74
4.16. Quantification of the amount of gadolinium in liver tissues in g of Gd/g tissue at 24 post injection.	75
4.17. Quantification of the amount of gadolinium in spleen tissues in g of Gd/g tissue at 24 post injection	76
4.18. Relaxivity enhancement % of each MRI contrast agents at 24 h post-injection	80

## CHAPTER 1

### INTRODUCTION

#### **Part 1. Gold nanoparticles: history, synthesis, properties, applications, and challenges**

Recently, gold nanoparticles (GNPs) have become a fundamental part of clinical medicine and research. Their ease of synthesis and ability to be conjugated with various numbers of specific biomolecules such as proteins, carbohydrates, antibodies, DNA, RNA, and imaging moieties [1], make them promising agents for delivery of pharmaceutical and diagnostic agents as well as therapeutics. Furthermore, their nano-size facilitates their uptake by body cells via endocytosis [2], and accumulation in tumors by the enhanced permeability and retention effect (EPR), as nano-sized molecules leak preferentially into cancerous tissue via permeable vessels and accumulate in tumor cells. Moreover, conjugation of drugs and biomolecules with GNPs amplifies their efficacy, which leads to a decrease in the dose that is needed to achieve a desired outcome [1].

## **1.1 Colloidal gold history:**

Colloidal gold history can be traced back to the fourth century B.C. as it was found in Chinese, Arabic, and Indian scientists' literature [3]. In the Middle Ages in Europe, Paracelsus prepared a gold colloid solution by reducing auric chloride with alcohol or oil plant extract. He used the gold colloid for treating mental disorders and syphilis [3]. In 1618, Francisco Antonii published the first book on colloidal gold that contains information on its preparations and medical applications. After that, gold colloid was used for treating ulcers, epilepsy, diarrhea, and alcoholism [4], easing the suffering of cancer patients [5], alleviating rheumatoid arthritis, and as a means of life prolongation (elixir of longevity) [3].

Despite the long history of gold colloid, it didn't attract the attention of modern scientists until Michael Faraday's research in 1857. He was the first to report that colloidal gold has different properties than bulk gold [1]. Later a revolution in immunochemistry came in 1971 when British scientists W. P. Faulk and G. M. Taylor reported the use of gold colloid with conjugated antibodies for direct electron microscopic visualization of Salmonella antigens, representing the first time of using gold colloid conjugated as an immunochemical marker [6]. From this time on gold colloid biomolecule conjugates became widely investigated in biomedical and chemical laboratories.

## **1.2 Synthesis of gold nanoparticles (GNPs):**

There are different ways of synthesizing GNPs with major approaches categorized as either top-down or bottom-up [7]. Top-down protocols are usually chemical and physical processes used to break up a bulk element into smaller pieces. Bottom-up protocols are used to synthesize GNPs using smaller precursors, such as metallic salt or molecular seeds that nucleate into a nanometric scale. Synthesis can be also categorized into chemical, physical, and biological methods.

### ***1.2.1. Physical methods:***

This method depends on energy transfer in the material that is irradiated by ionizing and non-ionizing radiation, which initiate reduction reactions that form nucleation of nanoparticles.  $\alpha$ (UV), and  $\gamma$  radiation as examples [7]. The principle of radiation science divides the radiation effects into direct and indirect effects. The direct effect attributes to the energy transfer while the indirect one attributes to forming the reactive species over the solvent as a result of the direct effect [8]. Water is the most common solvent in gold nanoparticles synthesis when water gets exposed to radiation (water radiolysis), it generates  $\text{OH}\bullet$  (hydroxyl radicals),  $\text{H}\bullet$  (hydrogen radicals),  $e_{\text{aq}}^-$  (solvated electrons),  $\text{H}_2\text{O}_2$  (peroxide), and  $\text{O}_2^-$  (superoxide) along with the following species  $\text{H}_2$ ,  $\text{H}^+$ ,  $\text{O}$ , and  $\text{H}_2\text{O}_2$  [8, 9].  $\text{OH}\bullet$  and  $e_{\text{aq}}^-$  play a major role in GNPs synthesis, they are responsible for the nucleation process by reduction of  $\text{Au}^{+3}$  into Au [9].

### **1.2.2. Biological methods:**

Biological methods are known as favorable to the environment or green methods because of the biocompatibility of the precursors and reduction of the use of toxic chemicals [10]. The use of microorganisms, fungi, algae, and plants in the synthesis of GNPs is a relatively new addition and it seems promising for large-scale synthesis. Plants contain proteins and secondary metabolites that have a high reducing capacity, which reduces the gold ions into metallic gold [11,12]. There are many examples of plant extracts used in GNP synthesis such as phenolic acids, proteins, alkaloids, sugars, and terpenoids [13, 14, 15, 16]. Using plants for GNPs synthesis is favored not only its efficiency but also because of its stabilizing properties [13, 14, 15, 16]. Microorganisms secrete a large number of enzymes that mediate GNPs synthesis. There are many bacterial, fungal, and actinomycete species, such as *Fusarium oxysporum*, *Verticillium* sp., *Thermomonospora* sp., *Rhodococcus* sp. that have been used for GNPs synthesis intracellularly or extracellularly [17, 18].

### **1.2.3. Chemical methods:**

These are the most common methods in laboratories for GNP production due to the relative ease of synthesis. Many protocols have been reported for GNPs synthesis, but the most common one is the reduction of tetrachloroauric acid ( $\text{HAuCl}_4$ ) by using different reducing agents such as sodium/potassium borohydride [19, 20], sodium citrate [21], hydrazine [22], and dimethyl formamide [23]. Despite Hauser E.A. and Lynn J.E. being the first scientists to report the synthesis of GNPs using  $\text{HAuCl}_4$  and trisodium citrate ( $\text{Na}_3\text{C}_6\text{H}_5\text{O}_7$ ) in 1940 [24], Turkevitch and co-workers refined the citrate reduction

method, and their work (in 1951) became a milestone of GNPs synthesis [24]. They reported GNPs with 10-20 nm diameters. In 1973, their method was further refined and improved by Frens, and it was possible to obtain a precise size of GNPs [25, 26]. Later in 1994, Brust and Schiffrin reported their two-phase method, and it was the first method that allowed the ease of production of thermally stable and air-stable GNPs. Their research had a large impact on the whole field of GNP synthesis and inspired many other researchers [27].

### **1.3. Properties of GNPs**

GNPs have a huge surface area in comparison with the same mass of bulk material, which allows conjugation of a tremendous number of specific biomolecules. GNPs possess many attributes such as shape and size-related optoelectronic properties (e.g. a slight deviation in GNPs size can give completely different properties), intrinsic ability to absorb light, ease of synthesis, good biocompatibility, and low toxicity [28]. Spherical GNPs exhibit a wide range of colors (orange, red, and purple), depending on the core size (1 to 100 nm) of the nanoparticle [29, 30]. The absorption peak, called the surface plasmon resonance (SPR), results from resonance between incident electromagnetic radiation and surface conduction electrons in the gold. This absorption band can be tuned from the visible to near-infrared (NIR) region by changing the nanoparticle size or shape, or varying environmental factors such as solvent, surface ligands, and temperature [31, 32]. Aggregation of GNPs results in red-shifting of the SPR and changes the color of the solution from red to blue due to the interparticle plasmon coupling [33].

#### **1.4. Formation of GNP bioconjugates:**

Specific biomolecules can be conjugated to the surface of GNPs by either covalent or non-covalent conjugation [1].

**Non-covalent conjugation:** This attachment may be achieved in either of two ways, electrostatic adsorption or specific affinity. Electrostatic adsorption is the simplest way, and there is no chemical reaction needed [1]. GNPs and biomolecules should have opposite charges to achieve attraction, and it depends on the pH and ionic strength of the medium. This approach is completely random in that GNPs and the bioconjugates can be attached in any direction and arrangement.

The specific affinity conjugation can be achieved by either biological interrelated molecules such as biotin-streptavidin or chemically synthetic molecules such as nickel-mediated interaction with His-tagged proteins [1]. This approach is highly selective and strong enough to maintain the conjugation under mild conditions. The most important advantage of non-covalent conjugation is the reversibility of the conjugation, which makes it very suitable for some applications such as drug delivery and sensing.

**Covalent conjugation:** can be achieved by direct attachment to GNPs or through linkers (surface ligand), and both ways depend on Au-thiol chemistry. Molecules containing thiol groups, such as proteins that contain surface cysteine residues can attach directly to GNPs through a gold thiol bond that is near covalent bond strength. This is considered a convenient method to attach proteins to GNPs. In-direct attachment of other molecules to GNPs can occur through linkers that have a thiol group at one end to attach to gold and chemically active functional groups at the other for forming molecular



attachments. The gold-thiol interaction forms coordinate-covalent bonds that provide stable conjugations, with its near irreversibility being suitable for some applications in complicated biological environments (pH and biological fluids)[1].

### **1.5 Application of GNPs:**

Gold nanoparticles have been used in a wide variety of applications in biomedicine due to their unique properties, we classified their applications into two main categories, diagnostic and therapeutic.

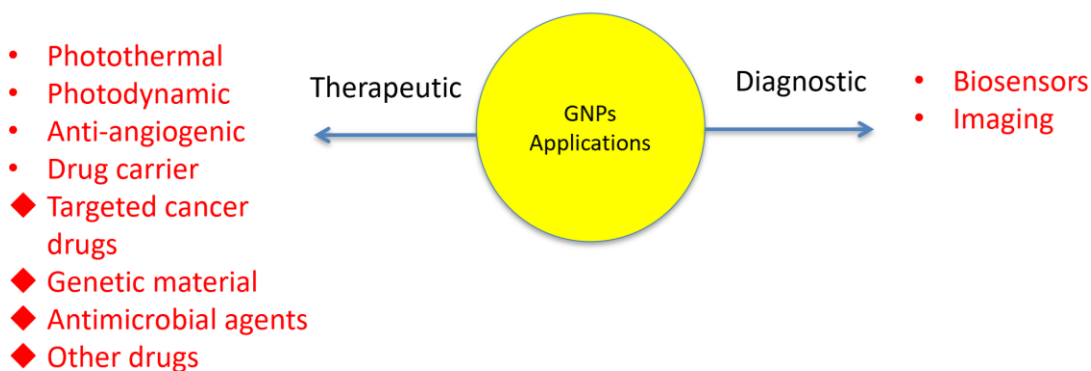


**Figure 1.1: Schematic illustration of GNPs applications in biomedicine**

## **Diagnostic applications:**

### ***Biosensors:***

Gold nanoparticles are used as very sensitive biosensor agents for detecting biomolecules such as carbohydrates, proteins, nucleotides, and toxins [34]. The sensing strategy can be colorimetric, electrical and electrochemical, fluorescence-based, or capitalize on the presence of the GNP surface plasmon resonance. Colorimetric detection depends on the change of GNPs color due to aggregation. Electrical and electrochemical detection schemes depend on the GNPs conductivity and the high surface area of gold. Fluorescence-based biosensors rely on fluorescence quenching properties of GNPs, and surface plasmon resonance-based biosensors use optical detection of the intrinsic optical properties (SPR) of gold nanoparticles [35]. GNPs play an important role in the bio-barcode assay, which is an extraordinarily sensitive assay for proteins and nucleic acids detection. The operating principle of the bio-barcode assay utilizes two types of particles: (a) a magnetic microparticle (MMP) with recognition elements (such as antibodies) for the target of interest and (b) GNPs conjugated with a second recognition moiety and hundreds of thiolated single-strand oligonucleotide barcodes. Upon detection of the target molecule, the two different particles form a sandwich around it, and a magnetic field is applied to collect the sandwich structures. The oligonucleotide barcodes are subsequently released which allows identification and quantification of the target [28, 36, 37].

### ***Imaging:***

Recently, GNPs-based imaging agents became a hot topic in the field of imaging. In particular, they are extensively investigated as cancer-specific imaging probes, based upon their conjugation with cancer-targeted molecules (aptamers and antibodies), which leads to selective accumulation in cancerous cells. The SPR and the intrinsic light scattering properties make GNPs

good agents for imaging applications such as computed tomography (CT), photoacoustic tomography (PAT) [1], dark-field microscopy [38], photothermal heterodyne imaging techniques [39], coherence tomography (OCT) [40, 41], and Raman spectroscopy [42].

GNPs serve as a good platform for CT contrast agents due to the higher atomic number and electron density of gold (79 and 19.32 g/cm<sup>3</sup>, respectively) in comparison with iodine which is the currently used CT contrast agent (53 and 4.9 g/cm<sup>3</sup>) [37]. Moreover, the higher molecular weight of gold exhibits an enhanced absorption coefficient (5.16 cm<sup>2</sup>g<sup>-1</sup>) as compared with the iodine absorption coefficient (1.94 cm<sup>2</sup>g<sup>-1</sup>) [43, 44]. GNPs have been used as CT cancer-targeted contrast agents. Meir et al. reported the use of GNP-labeled melanoma T cells for tumor targeting in mice bearing human melanoma xenografts. The result showed a maximum CT signal intensity at the tumor site after 48 h of injection whereas there was no signal detected at the tumor site before injection [45]. Cao et al. also used GNPs with lactobionic acid (LA)-modified dendrimers (LA-Au DENPs) for targeting hepatocellular carcinoma (HCC) in xenograft mice. LA-Au DENPs showed high CT signal intensity in comparison with Omnipaque (commercial iodine CT contrast agents [46].

In addition to CT imaging, tethering gadolinium with gold nanoparticles introduced a high performance magnetic resonance imaging (MRI) contrast agent. The enhancement in contrast that produced by MRI gadolinium-based contrast agent is measured in terms of relaxivity, and it can achieve by two ways: by boosting the relaxivity of the contrast agent or by increasing the gadolinium concentration. Conjugation of gadolinium chelate to GNPs avails these two factors, as GNPs slows the rotational motion of gadolinium and thus boosts the relaxivity [47-49].

Darkfield microscopy (DFM) is widely used for scanning live cells. Its principle is based on blocking off the light source by the specimen, causing the scattering of light and only the scattered beams are captured by the monochromator. The limitation of this method is the low intensity of light of the final image [50,51]. GNPs were introduced to DFM and have been used

successfully for reducing fluctuations in scattered light, which leads to improving the light intensity of the final image. The intensity of scattered light is determined by the shape and size of GNPs. Patskovsky et al. used GNPs conjugated with PEG and CD44<sup>+</sup> antibodies for DFM of human breast cancer cells (MDA-MB-231) that over-express CD44<sup>+</sup>. The cells showed bright light illumination due to the attachment of GNPs-conjugate with CD44<sup>+</sup> in comparison to CD44<sup>-</sup> BT-474 cells that showed no light emitted [52]. Qian et al. reported the use of GNPs as a contrast agent in DFM to monitor the living stages of cancer cells [53]. GNPs-peptide conjugates were delivered to cancer cells in nuclear and cytoplasmic regions to monitor chromosomal dynamics during mitosis and to study the different phases of cells from birth to division. These results introduce GNPs as promising nanoprobe in DFM for studying cellular mechanisms.

In addition, GNPs play an important role in live cell Raman imaging, due to their surface-enhanced Raman scattering (SERS) effect [54,55]. Kang et al. reported the use of GNPs for monitoring the changes in cell morphology during death induced by highly toxic KCN. Different organelles were targeted with GNP-conjugates to obtain a high-resolution Raman image [56]. Moreover, different shapes of GNPs (shells, rods, stars, and spheres) have become one of the most widely used contrast agents in photoacoustic imaging (PAI) based on their optical properties and SPR [57]. Song et al. used 10 nm GNPs conjugated with hydrolysis-susceptible citraconic amide moieties as a cancer-targeted contrast agent for PAI. GNPs accumulated in cancer cells due to the electrostatic attraction induced by the acidic pH of the cancer cells. The PA signals of the contrast agents at pH 5.5 in xenograft mice were two fold higher in comparison with the PA signals of healthy animals and the PA signals of others animals injected with non-susceptible SANs. [58].

## **Therapeutic applications:**

### ***Photothermal therapy (PTT):***

Photothermal therapy has been used for cancer treatment since the eighteenth century by applying local heating using microwave, radio, and ultrasonic radiation or general heating to 41-47 °C for 1 h [59]. This method has limitations because healthy tissues get affected by the heat too. The development of laser radiation made a revolution in photothermal therapy, which limited heat exposure to only cancer cells [60].

Photothermal damage of cancer cells using GNPs is extensively addressed as a promising platform in the treatment of cancer and infectious diseases. The principle of this method is based on the high ability of GNPs to absorb light in the visible and near-IR region. When particles get irradiated with a corresponding light beam, they become very hot and induce disruption of cell membrane permeability and protein denaturation, which leads to irreversible damage to cancerous cells [61].

Pitsillides et al. pioneered the PTT using a novel selective cell targeting technique. They used a short laser pulse (532 nm) focused on monoclonal antibodies conjugated with GNPs (20 and 30 nm) [62]. The acceptance of new techniques of PTT in the medical field relies on future advancements in several factors, including: (i) the prevalence of GNPs with optimal optical properties, (ii) the development of efficient techniques to deliver the particles to the cancerous or diseased tissues, and (iii) delivering the optical radiation to the targeted sites.

***Photodynamic therapy (PDT):***

Photodynamic therapy is used for treating cancer and skin disease [63], this method can be achieved by using a photosensitizer agent and visible light at a certain wavelength corresponding to the peak of dye absorption [64]. The photosensitizer can be applied intravenously, orally, or directly on the skin. When the photosensitizer agent gets irradiated with the light beam, it generates singlet oxygen and free radicals along with the heating effect, which mediates necrosis and apoptosis of diseased tissues [65]. PDT is limited by the low effectiveness of molecular dyes for heating tissues due to small absorption cross-section and also the longevity of the dye in the body that results in patient sunlight sensitivity [3].

Introducing GNPs to PDT improves the efficiency of this method, as GNPs increase the fluorescence intensity of the photosensitizers if they are placed at an optimum distance from the dyes [66, 67]. Moreover, GNPs have a high surface area, which allows maximum absorption of light and loading with a high number of photosensitizer molecules.

Jing Lin et al. reported a multifunctional theranostic platform consisting of GNPs conjugated with chlorin e6 (Ce6), and polyethylene glycol (PEG). GNPs absorb light near the IR region (650-800 nm), and when irradiated by 671 nm laser irradiation they produce enough heat to excite Ce6 to produce singlet oxygen and other free radicals. Moreover, the efficient loading of Ce6 onto GNPs increases the accumulation of Ce6 inside cancer cells, which leads to visualization by fluorescence [68].

### ***GNPs as drug carriers:***

GNPs have shown a unique role as non-toxic drug carriers. Owing to their extensive surface-to-volume ratio, they can be loaded with high numbers of different biomolecules [69, 70] such as: antibodies, vaccines, recombinant proteins, and nucleotides. GNPs also can be used to deliver drugs with low solubility and poor pharmacokinetics [71, 72], or to deliver drugs that have susceptibility to enzymatic degradation and poor cellular penetration (e.g., siRNA) [73, 74].

### **GNPs in targeted cancer drug delivery:**

Circulating GNPs have a preference to accumulate in tumor and inflammatory sites due to the defective architecture of the blood vessels that supply these sites [75, 76]. Once the particles get in the vessels, they stay lodged due to the characteristically reduced lymphatic drainage and their low diffusivity. This phenomenon is widely known as the enhanced permeability and retention (EPR) effect [77, 78]. El-Sayed and co-workers reported the use of GNPs conjugated to thiol-PEGylated tamoxifen derivatives to use EPR-based GNP accumulation in breast cancer cells [79]. The large surface area to volume ratio of GNPs provides high drug loading and lowers the minimum effective dosage relative to free drug molecules.

Dhar *et al.* reported the conjugation of GNPs with doxorubicin hydrochloride (DOX), which increased DOX toxicity to cancer cells compared with the free drug due to the efficient uptake of GNPs-DOX complex by endocytosis and retention in the cells, while free DOX diffuses passively across the membrane. This research demonstrates that

GNPs can help reduce the effective dosage of DOX (reduce its side effects), and aid in the transport of DOX across the blood-brain barrier [80].

Brown *et al.* showed the increased potency of oxaliplatin, a non-selective cytotoxic analog of cisplatin used in treating colorectal cancer, conjugated with GNPs through thiolated PEG linkers [81]. They reported a fivefold increase of cytotoxicity in comparison with free oxaliplatin, which was attributed to uptake through endocytosis into cancer cells.

It was also reported that GNPs were conjugated to many antitumor drugs, e.g., paclitaxel [82], methotrexate [83], daunorubicin [84], gemcitabine [85], 6-mercaptopurine [86], 5-fluorouracil [87], cisplatin [88], Herceptin [89], and  $\beta$ -lapachon [90]. The tremendous amount of studies dedicated to GNPs and cancer therapy has proved very promising and could be a turning point in the field of targeted drug-delivery.

### **GNPs in gene therapy:**

Recently, it has been demonstrated that GNPs can be successfully conjugated with nucleic acids such as antisense oligonucleotides and small interfering RNA (siRNA) and delivered to cells for gene regulation [91, 92]. GNPs have been found to protect nucleic acids from degradation by nucleases and provide efficient cell transfection.

Patel *et al.* reported heterofunctionalized nanoparticles conjugates consisting of GNPs loaded with antisense oligonucleotide and synthetic peptides. The synthetic peptides are used to target specific subcellular components for delivery of the antisense oligonucleotides for gene knockdown [93].



Liangliang Hao *et al.* conjugated GNPs with synthetic miRNA-205 to suppress tumor growth through down-regulation of protein kinase C epsilon (PRKCE). Researchers demonstrated that the conjugation of miRNA to GNPs significantly reduces PC-3 cell viability compared to using miRNA alone. Also, GNPs-miRNA conjugates enter the cells without the use of transfection agents [94].

### **GNPs deliver antimicrobial agents:**

While GNPs themselves do not display antimicrobial activity, their conjugation with antibiotics decreases the survival of bacteria [95]. Akhilesh Rai *et al.* reported the conjugation of cefaclor (a second generation antibiotic) with 22-52 nm GNPs. The results showed that the cefaclor-GNPs complex has potent antimicrobial activity against Gram-positive and Gram-negative bacteria in comparison to using cefaclor or GNPs alone [96].

Selvaraj *et al.* reported the conjugation of GNPs with 5-fluorouracil (5FU) has antibacterial and antifungal effects against *Staphylococcus aureus*, and *Micrococcus luteus*, *Escherichia coli*, *Aspergillus fumigatus*, and *Aspergillus niger* [97].

Also, it was demonstrated that GNPs overcome some antibiotic resistance mechanisms by delivering a dense mass of the antimicrobial, where each GNP is loaded with a number of antibiotic moieties that act as a single group against the bacteria leading to disruption of the cell wall before the antibiotics can be recognized by the bacterial cell defensive enzymes.

In contrast, Saha *et al.* [98] and Grace and Pandian [99] reported that they could not generate stable conjugation of GNPs and antibiotics (ampicillin, streptomycin,

kanamycin, aminoglycosides, and quinolone antibiotics). Although these researchers demonstrated that the increase in the antimicrobial activity using GNPs could range from 12 to 40%, and the activity depends on the complex antibiotic GNPs interactions with their environments and with the bacterial cells.

### **GNP delivery of other drugs:**

There are other drugs that have been reported in the literature in conjugation with GNPs. Bowman *et al.* designed GNP (2 nm)-SDC-1721 complexes, where SDC-1721 is a fragment of the potent HIV inhibitor TAK-779. The conjugation of GNPs with SDC-1721 resulted in inhibitory activity comparable to TAK-779, whereas SDC-1721 alone didn't show any inhibitory effect. This study showed the conversion of inactive drugs to an active form with conjugation with GNPs [100].

Joshi *et al.* reported the conjugation of bare GNPs and aspartate-coated GNPs with insulin hormone. The complex was delivered to diabetic Wistar rats by oral and intranasal routes. The results showed that the intranasal administration resulted in a significant reduction in blood glucose levels. These results also were comparable to that achieved by another drug that relieves type 1 diabetes mellitus [101].

Nie *et al.* developed a new synthetic antioxidant using GNPs loaded with Trolox (vitamin E analog) with better activity than Trolox alone. The results of the DPPH\* (2,2-diphenyl-1-picrylhydrazyl) assay showed that the rate constant for the reaction of GNPs-Trolox complex with DPPH\* radical was eight times greater than that for Trolox [102].

### ***GNPs have anti-angiogenic effects:***

It has been reported that naked GNPs exhibit an anti-angiogenic effect through reducing the viability, tube formation, and migration of human umbilical vein endothelial cells [103, 104]. It

also has been reported by other researchers that GNPs inhibited vascular endothelial growth factor-A (VEGF-A), which induced migration of human retinal microvascular endothelial cells [105]. GNPs were also shown to reduce the permeability and density of vessels in many cancer models [106]. Many molecular mechanisms have been shown to contribute to the anti-angiogenic effect of GNPs. They suppressed the activity of the VEGF-A/VEGR2 axis and its downstream signaling in different endothelial cells [107, 108]. Moreover, GNPs were shown to inhibit intracellular calcium release and reduce Ras homolog family member A (RhoA) activity mediated by VEGF-165 [109]. Furthermore, GNPs downregulated the levels of pro-angiogenic factors Ang-1 and Ang-2 in cancerous tissues [109].

### **1.6 Challenges facing GNPs in biomedicine:**

Despite the numerous applications of GNPs in biomedicine, there are some challenges and obstacles that face them and need to be investigated.

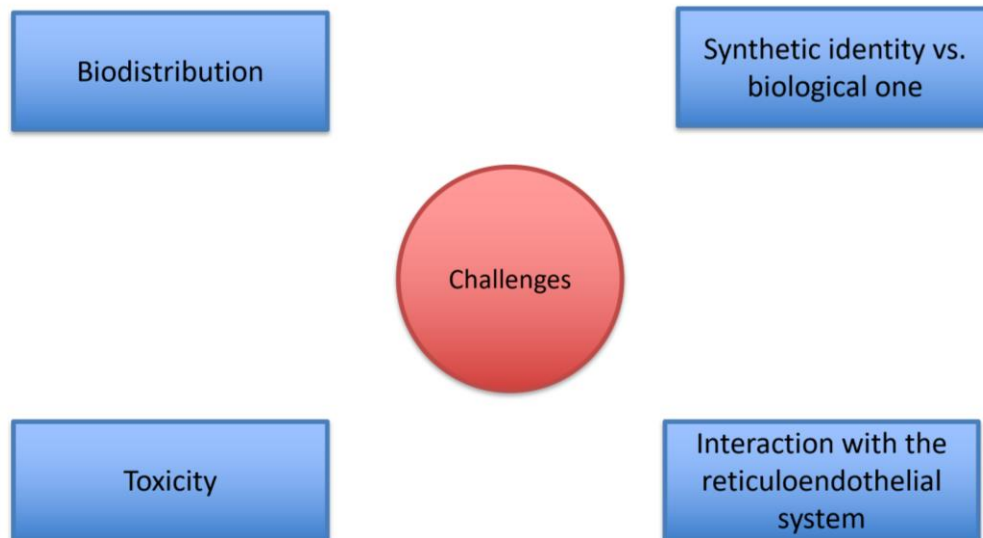


**Figure 1.2: Demonstration of the challenges that face GNPs in biomedicine**

### ***1.6.1. Biodistribution:***

The biodistribution of GNPs affects their therapeutic value. Biodistribution is highly regulated by the surface chemistry, surface charge, the diameter of the particles, and the route of administration [110-113]. Sonavane et al. reported that particle size is an important factor of drug permeation. Using citrate capped GNPs of different sizes (15, 100, and 200 nm), Particles were applied to excised rat skin using Franz diffusion cells, the smallest size (15 nm) showed the highest permeation coefficient in comparison to the largest ones, also the 15 nm GNPs penetrated into the deep region of the skin while the 100 and 200 nm GNPs stayed on the surface [114]. In another study done by the same group, mice were injected intravenously with 15, 50, 100, and 200 nm GNPs, the amounts of gold were evaluated in blood, liver, spleen, lung, stomach, brain, and heart. The highest amounts of gold were detected in the liver, spleen, and lung regardless of size. The smallest size (15 nm) showed the highest accumulation in blood and all organs and only 15 and 50 nm crossed the blood-brain barrier. The largest size GNPs (200 nm) showed the lowest accumulation in blood and all organs except the liver, spleen, and lung [115]. Other studies have reported that smaller particles size are accumulated in all body organs while larger ones are accumulated mostly in the liver and spleen [112, 116]. Khan and co-workers have used different types of dendrimer encapsulated gold nanoparticles with different sizes and different surface charges. B16 mouse melanoma tumor models were injected by the particles and biodistribution was evaluated by ICP-MS analysis. Results showed that surface charge and particle size achieved a selective targeting of certain organs without loading the particles with any specific targeting agents [117].

### 1.6.2. *Synthetic identity vs. biological identity:*

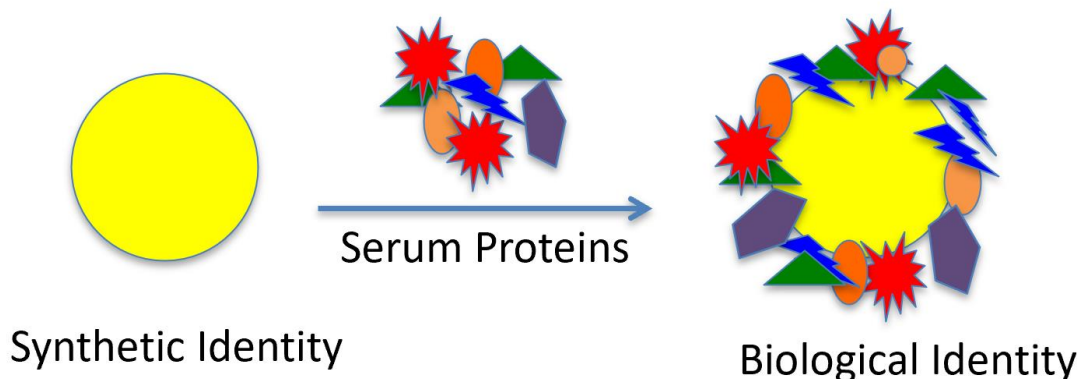


**Figure 1.3: Schematic illustration of formation of protein corona on gold nanoparticle surface**

Once GNPs get in the blood circulation, they interact with abundant proteins in the blood. Some of these proteins interact with the particles and get adsorbed on their surface leading to the formation of the protein corona, which affects the physical and the chemical properties of the GNPs and changes their synthetic identity, thereby forming a new biological identity that is completely different in size, shape and surface chemistry. Furthermore, the protein corona can lead to particle aggregation. The biological identity of GNPs determines their pharmacokinetic and pharmacodynamic properties and affects their biological fate [118, 119]. The thickness and identity of protein corona are dictated by the surface chemistry, charge, particle size, duration of exposure, and the nature of the biological environment (blood or interstitial fluid).

### 1.6.3. *Interaction with the reticuloendothelial system (RES):*

Controlling the interaction of GNPs with the RES is a fundamental challenge to the successful use of GNPs in a therapeutic context. GNPs can interact with cells and molecular

components of the immune system (monocytes, macrophages, and proteins) leading to the release of pro-inflammatory cytokines that activate or suppress the immune response [120]. On the other hand, interaction with the RES impacts the efficiency of the particles themselves, as their uptake by the RES can shorten their blood residence time and impact their biological fate. Once GNPs get in blood circulation, they activate the cleavage of C3 protein into two small units, C3a and C3b. C3b (opsonin protein) binds to GNPs in a process called opsonization and initiates a cascade of complement reactions which flags the nanoparticles for phagocytosis by scavenger cells [121-126]. The physicochemical properties of GNPs (e.g. shape, diameter, surface charge, surface loading, and hydrophobicity) dictate their interaction with the immune system [127-130]. Furthermore, the different routes of GNP administration (e.g., intravenous, intradermal, nasal, intramuscular, subcutaneous, and inhalation) can evoke different immune responses [131, 132]

There are four endocytic mechanisms for nanoparticle uptake by the immune system: macropinocytosis, pinocytosis, phagocytosis, and clathrin/caveolar mediated endocytosis. Usually, the uptake of nanoparticles takes place with more than one endocytic mechanism [133, 120].

Attributable to the immunological properties of GNPs, they can be used as agents for manipulating the innate immune system (stimulation or suppression). Vaccines and cancer immunotherapy are applications of these properties [134, 135]. The main principle is to stimulate the immune system to generate the pro-inflammatory signal in response to the antigens of foreign objects and tumors. In addition to stimulation of the immune system, GNPs also can elicit a suppression effect, which is used for the treatment of autoimmune diseases, atopic disorders, allergies, and organ transplantation [136].

#### **1.6.4 Toxicity:**

The toxicological properties of GNPs in literature are controversial. Some studies have shown that GNPs are toxic, while others have reported the opposite [137]. The variance in

toxicity of GNPs can be attributed to their sizes, shapes, surface loadings and charge, surface volume ratio, and their modification in the biological environment [138-141]. A group of researchers has reported that 13 nm PEGylated GNPs induced inflammation in the liver over two phases. The first phase occurred immediately after injection and the second one occurred after 7 days, they also found that the number of cells that underwent apoptosis over the two phases increased [142]

As observed before, the liver and spleen are the major organs that have the highest accumulation of GNPs, which may lead to their toxicity [143]. Furthermore, the interaction of GNPs with the different components of the immune system can cause immunotoxicity, due to the formation of reactive oxygen species (ROS) in cells which can lead to indiscriminate protein and membrane damage. Moreover, repetitive stimulation of the immune system can lead to autoimmune diseases and allergic reactions, while suppression can cause cancer and infectious diseases [120, 144].

### **1.7 Strategies to increase blood circulation half-life and the selective delivery of GNPs:**

Different strategies have been reported in the literature to attain longer blood circulation half-lives of GNPs by modifying the nanoparticles with biocompatible agents. Examples of these agents are:

***Serum albumin protein:*** the most abundant protein in the blood, it contains many carboxyl and sulfhydryl groups, which allow it to bind to GNP surfaces. Conjugation of GNPs with serum albumin increases their stability, bioavailability, and blood circulation time by decreasing binding to blood proteins, and provides selective targeting of tumor cells [145- 147].

***Red blood cell (RBCs, erythrocytes) membranes:*** first introduced as a drug carrier in 1953 when Gardos loaded erythrocyte ghosts with ATP. Using erythrocytes as a carrier of nanoparticles provides numerous benefits such as prolonging the lifespan up to 120 days, improving the nanoparticles' stability, decreasing the uptake by the immune system, and increasing the biocompatibility of the drug [148-151].

***Hyaluronic acid:*** It has shown that conjugation of GNPs with hyaluronic acid (a linear polysaccharide) increases their biocompatibility, increases the cellular uptake of large-sized nanoparticles, and decreases the adsorption of blood proteins on GNPs surfaces. In addition, it has been reported that hyaluronic acid acts as a ligand for many cell receptors (e.g. cluster of differentiation 44 receptor or CD44) [151-156]

***Polyethylene glycol (PEG):*** a condensation polymer of ethylene oxide and water. Grafting GNPs with PEG (the process known as PEGylation) creates a hydrophilic sphere around the nanoparticles that sterically prevents the interaction of GNPs with each other, leading to increased particle stability and reduced aggregation. Moreover, PEG mitigates the adsorption of opsonin proteins on particle surfaces and decreases the particles' susceptibility to be cleared by the immune system [121, 157-160]. PEGylation is considered the most common method that has been used to form what is called "stealth nanoparticles".



## Part 2. Focus of this dissertation

Here in this dissertation is presented a study of the impact of serum protein adsorption on the cellular uptake of cancer-targeted nanoparticle MRI contrast agents. 4 and 10 nm GNPs were conjugated with a Dotarem thiol derivative gadolinium chelate, Gd (III)-DO3A, and cancer-targeted AS1411 aptamer with and without PEG of different molecular weights ( $M_w$ : 1, 2, and 5 kDa).

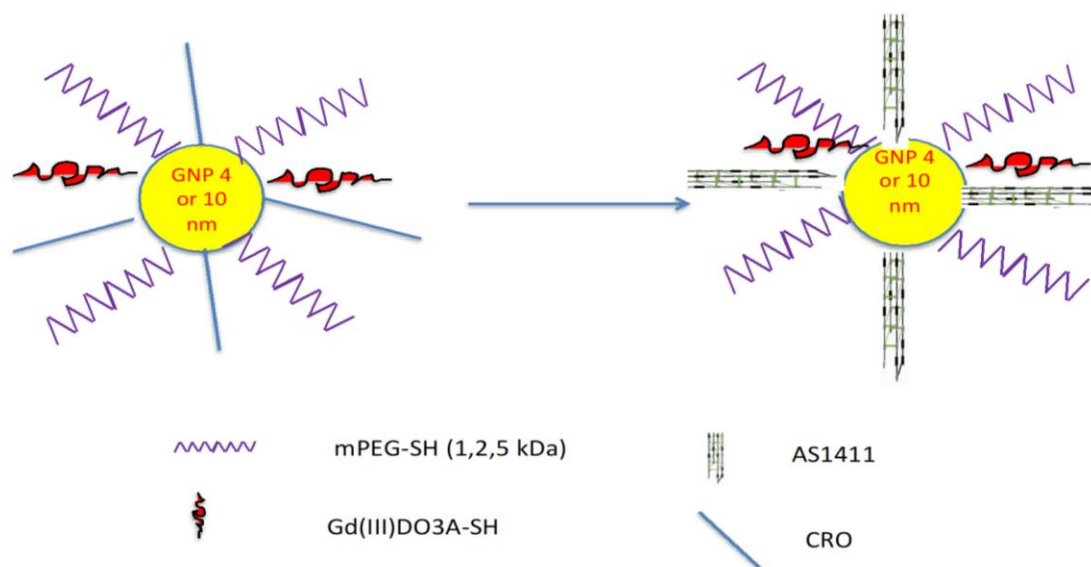


**Figure 1.4: Schematic illustration of the construction of the proposed MRI contrast agents**

- **AS1411** is a quartet G-rich, 26-mer, G-quadruplex-forming phosphodiester oligodeoxynucleotide. The 3D structure of AS1411 proves resistant against cellular and serum nucleases [161]. AS1411 specifically binds to a multifunctional phosphoprotein called nucleolin that presents in the nucleus of all cells but is overexpressed on the cell surface and in the cytoplasm of some cells including cancer cells and angiogenic endothelial cells. AS1411 has apoptotic induction activity through binding to nucleolin,

which inhibits nucleolin binding to BCL2 mRNA (BCL2 is a family of regulatory proteins that regulate cell apoptosis by either inducing or inhibiting apoptosis) [162-165]. AS1411 is taken up in cancer cells by macropinocytosis, and subsequently stimulates further macropinocytosis by nucleolin-dependant mechanism, which leads to specific accumulation in cancer cells [166].

The **Gadolinium:** most MRI contrast agents that used in clinic are gadolinium-based due to the highly paramagnetic nature of the trivalent metal. Gadolinium used to generate MRI contrast must be bound by a chelating agent because its ionic form is very toxic and interferes with calcium channel and protein binding sites [167]. In this study, we used DO3A (1,4,7,10-tetraazacyclododecane-N,N',N'',N'''-tetraacetic acid) as a chelating agent with a thiol group that allows conjugation of gadolinium to GNPs. As mentioned before, Conjugation of gadolinium chelate to GNPs avails improvement in Relaxivity without increasing the amount of gadolinium, as GNPs slow the rotational motion of gadolinium and thus boosts the relaxivity.

We have fulfilled our goal through the investigation of the following 3 specific aims:

**Specific aim 1:**

Develop and characterize 4 & 10 nm GNPs conjugates with AS1411/CRO, Gd (III)-DO3A, and PEGs (1, 2, and 5 kDa).

**Specific aim 2:**

- a) Determine the adsorption of serum proteins on the particles surfaces.
- b) Determine the uptake of the incubated particles with and without serum proteins

by macrophage and cancer cells.

### **Specific aim 3:**

Determine the uptake of the particles by tumor cells through *in vivo* biodistribution study.

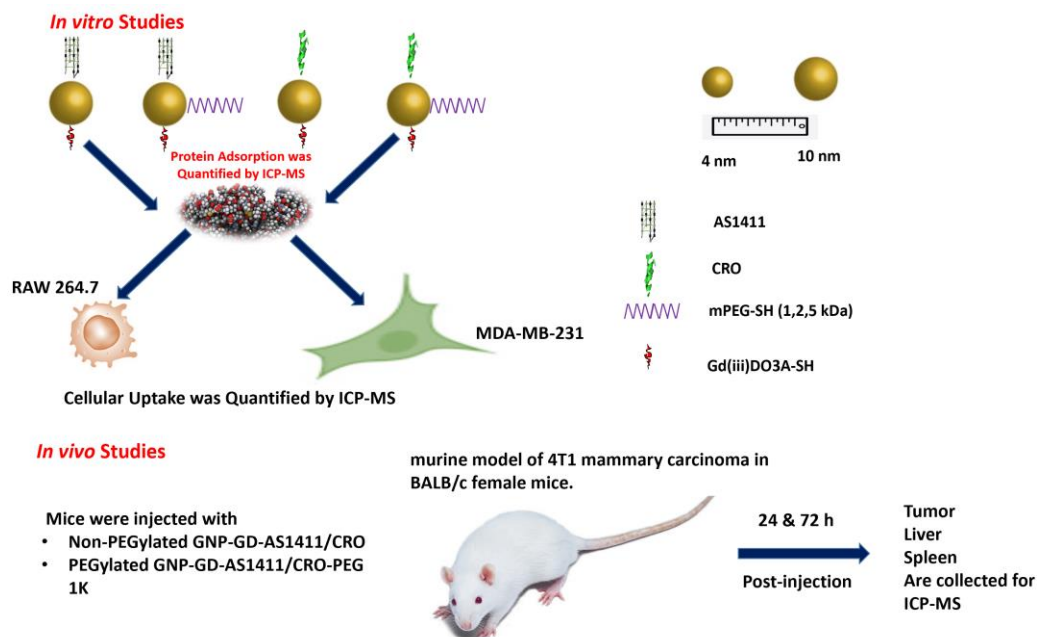


**Figure 1.5. Demonstration of the *in vitro* and the *in vivo* study**

We have synthesized and characterized 16 different formulations of MRI contrast agent GNPs candidates with 8 formulations for each GNP core size (4 and 10 nm). GNPs conjugated with Gd, either AS1411 or CRO (control), and with or without PEG (1, 2, and 5 kDa). Further, we have quantified the amount of adsorbed proteins after incubation of the PEGylated and non-PEGylated GNPs in human serum and quantified the uptake of the different nanoparticles with and without protein corona by the human breast cancer cell line MDA-MB-231 and the murine monocyte/macrophage cell line RAW 264.7.

In addition, we have looked into the *in vivo* biodistribution of GNPs using the

murine model of 4T1 mammary carcinoma in BALB/c female mice.

## CHAPTER 2

### MATERIALS AND METHODS

#### **2.1. Materials:**

Gold (III) Chloride Trihydrate ( $\text{HAuCl}_4 \cdot 3\text{H}_2\text{O}$ ) was purchased from Alfa Aesar (Tewksbury, MA). 10 nm GNPs were purchased from Nanopartz (Salt Lake, UT). Citric acid, trisodium salt ( $\text{Na}_3\text{C}_6\text{H}_5\text{O}_7$ ), Sodium Borohydride ( $\text{NaBH}_4$ ), Gadolinium trichloride hexahydrate ( $\text{GdCl}_3 \cdot 6\text{H}_2\text{O}$ ), dithiothreitol (DTT), Sodium dodecyl sulfate ( $\text{NaC}_{12}\text{H}_{25}\text{SO}_4$ ), anhydrous sodium bicarbonate ( $\text{NaHCO}_3$ ), sodium phosphate monobasic dihydrate ( $\text{NaH}_2\text{PO}_4 \cdot 2\text{H}_2\text{O}$ ), sodium phosphate dibasic ( $\text{Na}_2\text{HPO}_4$ ), 0.22  $\mu\text{m}$  syringe filter, and human serum (obtained from male AB plasma of multiple donors) were purchased from Sigma Aldrich (St.Louis, MO). 1,4,7,10-tetraazacyclododecane-1,4,7-tris (acetic acid)-10-(2-thioethyl) acetamide, DOTA, dodecane tetraacetic acid ( $\text{C}_{18}\text{H}_{33}\text{N}_5\text{O}_7\text{S} \cdot 2\text{CF}_3\text{CO}_2\text{H}$ , DO3ASH) was purchased from Macrocyclics, Inc. (Dallas, TX). 10.0X phosphate buffer saline (PBS, pH 7.4) and Pierce BCA protein assay kits (Bicinchoninic acid assay) were purchased from Thermo Fisher Scientific (Waltham, MA). Methoxy polyethylene glycol thiol (mPEG-SH),  $M_w$  1, 2, and 5 kDa were purchased from Creative PEGworks (Durham, NC). Nanopure ultrapure water (Sartorius Arium, resistivity of 18.2  $\text{M}\Omega\text{-cm}$ ) was used for preparing all aqueous solutions. Hydrochloric

acid (HCl) and Nitric Acid (HNO<sub>3</sub>) were analytical grades and purchased from VWR (Radnor, PA). Aqua regia solution (3 parts HCl and 1 part HNO<sub>3</sub>) was used to clean all glassware for GNP synthesis. Oligonucleotides (Oligo) having a regular DNA backbone (phosphodiester), a 5'-Thiol C6 S-S modification (Thio-MC6-D), 5'-6T spacer (for AS1411 and CRO), and high pressure-liquid chromatography (HPLC) purification were supplied by Integrated DNA Technologies (IDT) [Coralville, IA]. The oligonucleotide sequences used were 5'-/5ThioMC6-D/TTT TTT GGT GGT GGT GGT TGT GGT GGT GGT GGT TT-3' (AS1411), and 5'- /5ThioMC6-D/TTT TTT CCT CCT CCT CCT TCT CCT CCT CCT CCT TT-3 (CRO). 0.5 Trypsin- EDTA (10X) was purchased from Thermo Fisher Scientific (Waltham, MA). NuPAGE lithium dodecyl sulfate (LDS) sample buffer 4X, NuPAGE sample reducing agent 10X, NUPAGE compound 2-ethanesulfonic acid sodium dodecyl sulfate MES SDS running buffer 20X, NuPAGE 4 t0 12%, Bis-Tris, 1.0-1.5 mm, mini protein gels, and mini gel tank and blot module set were purchased from Thermo Fisher Scientific (Waltham, MA).

The MDA-MB-231 breast cancer cells, RAW 264.7 murine monocyte/macrophage cells, and 4T1 murine breast cancer cells were purchased from ATCC (Manassas, VA). Dulbecco's Modified Eagle Medium (DMEM) and Roswell Park Memorial Institute (RPMI) media were purchased from Corning (Manassas, VA). Fetal bovine serum (FBS) was purchased from Atlanta Biologicals (Flowery Branch, GA). Penicillin-Streptomycin was purchased from Hyclone/Cytiva (Marlborough, MA).

UV absorption spectra were measured with the UV Visible Spectrometer (Varian Cary 50 BIO UV, Agilent Technologies, Santa Clara, CA) using glass cuvette of 2 mL. Dynamic Light Scattering measurements (DLS) and the Zeta potential measurements

were acquired on samples using a NanoBrook Zeta PALS Zeta Potential Analyzer (Brookhaven Instruments, Holtsville, NY).

The concentrations of gold and gadolinium in cells and animal tissues were analyzed using an Agilent 7800 ICP-MS (Inductively Coupled Plasma Mass Spectrometry, Agilent Technologies Inc). Before the sample assay, ICP-MS machine performance was checked using a 1 ppb tuning solution and the assay program was auto-tuned using 10ppb tuning solution (Agilent Technologies, Cat# 5188-6564). Gd and Au standards were purchased from Agilent Technologies Inc (Cat# ICP-064-25 and Cat# ICP-079) and diluted in serial concentration as 0, 1, 2, 5, 10, and 50 ng/ml by 2% nitric acid/DI water solution as standards. A 500 ppb internal standard solution (Agilent Technologies, Cat# 5188-6525) containing Bi, Ge, Ln, Li, Lu, Rh, Sc, Tb was used to evaluate the recovery rate/machine operation condition. Samples were loaded with an Agilent SPS 4 Autosampler.

## **2.2. GNPs Synthesis:**

4nm GNPs were synthesized according to the procedure described by Murphy and coworkers [168]. All glassware were cleaned with aqua regia and rinsed with nanopure water before using. Briefly, 2.5 mL of 0.01 M trisodium citrate was added to 95.0 mL of nanopure water under intense stirring. Then, 2.5 mL of 0.01 M HAuCl<sub>4</sub> solution was added followed immediately by 3.0 mL of 0.1 M sodium borohydride at 4°C. The solution was stirred for 2 hours. GNP size was determined by UV/visible spectroscopy and dynamic light scattering [169]. 10 nm GNPs were purchased as mentioned before.

### **2.3. Chemical Synthesis of Gadolinium (III) DO3A-SH (Gd):**

1,4,7,10-tetraazacyclododecane-1,4,7-tris(acetic acid)-10-(2-thioethyl) acetamide,  $C_{18}H_{33}N_5O_7S \cdot 2CF_3CO_2H$  (DO3ASH) was chelated with  $GdCl_3$  by mixing an aqueous solution of DO3A-SH (17.1 mg in 200  $\mu$ L nanopure water) with an aqueous solution of  $GdCl_3$  (22.23 mg in 200  $\mu$ L nanopure water) at room temperature [170-172]. The reaction mixture pH was then adjusted to 6.0 by titrating 1.0 M sodium bicarbonate and the mixture was incubated overnight at 60°C. During the reaction, the pH was monitored three times and bicarbonate solution was added as necessary to keep the pH in the range of 6-7. Afterward, the reaction mixture pH was adjusted to 9-10 using sodium bicarbonate to precipitate the Gd-DO3A-SH complex which was isolated via centrifugation at 3000 g for 15 minutes.

### **2.4. Annealing and Preparing of AS1411 and CRO for Conjugation to GNPs:**

Oligonucleotide solutions were prepared as previously reported [173]. Briefly, 500.0  $\mu$ L of 500  $\mu$ M oligonucleotide solution was prepared by suspending AS1411 and CRO in nanopure water. Before use, the disulfide protecting group on the oligonucleotide was cleaved with dithiothreitol (DTT). A 250.0  $\mu$ L solution of 1M DTT was added to the oligonucleotide solution and heated to 90°C for 1 hour (0.1 M DTT, 0.18 M phosphate buffer (PB), pH 8.0). The cleaved oligonucleotides were purified using a NAP-25 column eluted with PB. Thereafter, the eluted solution of freshly cleaved oligonucleotides was added to gold nanoparticle dispersions.



## **2.5. Preparation of PEG solutions:**

Methoxy polyethylene glycol thiol (mPEG-SH), MW 1, 2, and 5 kDa were suspended in nanopure water and filtered using 0.22  $\mu$ m syringe filter before use.

## **2.6. Conjugation of Gd(III)-DO3A-SH (Gd), AS1411/ and or CRO, and mPEG to**

### **GNP:**

4 nm and 10 nm GNPs (~150 nM and ~10 nM for 4 and 10 nm, respectively) were functionalized with the MRI contrast agent Gd, either AS1411 or CRO, and with or without 1, 2, and 5 kDa mPEG chains [168]. The concentrations of the different agents were added X times the gold concentrations as shown in Table 1:

Table 2.1. Demonstration of the amount of functionalizing agents

<b>GNP</b>	<b>Gd</b>	<b>AS1411/CRO</b>	<b>PEG</b>
4 nm non-PEGylated	10X	15X	-
4 nm PEGylated	6X	10X	6X
10 nm non- PEGylated	120X	90X	-
10 nm PEGylated	72X	60X	36X

16 different formulations of GNPs were synthesized and incubated at room temperature for 20 minutes and then sonicated for 10 minutes. The solutions were incubated overnight

at 37°C, then 10X PBS solution was added gradually over 5 days until the concentration of the GNP solutions reached 137 mM NaCl (during each salting time, the GNP solutions were sonicated for 10 minutes and followed by incubation at 37°C). The excess oligonucleotide and Gd were removed via centrifugal filtration at 3000g for 30 min.

### **2.7. Quantification of AS1411 and CRO per nanoparticle:**

20.0 µl of each GNP sample was added to 200 µL of 1.0 M DTT and 2.28 mL of Phosphate Buffer (pH 8). The mixture was incubated for 24 h at 37°C to cleave the gold oligonucleotide-thiol bond. The mixture was purified using a NAP-25 column to separate the oligos from DTT, then the released oligonucleotides were quantified using UV absorption spectra. The concentrations of oligonucleotides were divided by the corresponding GNPs concentrations to determine how many aptamer/GNP.

### **2.8. Quantification of Gadolinium:**

20.0 µl of each GNPs sample was added to 800 µl of aqua regia and 600 µl of PBS solution and heated to 60°C for 2 hours. The sample then was diluted with nanopure water to 4% acid concentration and analyzed with ICP-MS. The concentrations of Gd were divided by the corresponding GNPs concentrations to determine how many Gd/GNP.

### **2.9. Protein Quantification by Bicinchoninic Acid (BCA) Assay:**

1 mL of 4 or 10 nm GNPs (100  $\mu$ L and 20  $\mu$ L, respectively) were mixed with 1 mL of 10% human serum (HS) and incubated for 24 h at 37°C under continuous shaking. GNPs and any protein corona were then separated from free HS by centrifugation 2 times at 20,000 g for 1 h to remove the unbound proteins. 5% of sodium dodecyl sulfate was added to GNPs-protein corona and samples were heated for 5 minutes at 60 °C to isolate the tightly bound proteins from GNPs. The samples were centrifuged and supernatants were analyzed using the BCA protein assay kit (Pierce) as directed by the manufacture. Bovine serum was used to generate a standard curve.

### **2.10. Gel Electrophoresis:**

The proteins isolated from GNPs were treated with LDS sample buffer and sample reducing agent, and loaded into 4 to 14% gel in a tank filled with MES SDS running buffer. Proteins samples were run at 200 V for 30 minutes. Gels were imaged on a ChemiDoc imaging system (Bio-Rad Laboratories, Hercules, CA, USA).

### **2.11. MDA-MB-231 and RAW 264.7 Cells Culture:**

MDA-MB-231 cells were cultured in DMEM media containing 10% FBS and 1% Penicillin-Streptomycin. RAW 264.7 cells were cultured in RPMI media containing

10% FBS and 1% Penicillin-Streptomycin. Both cell lines were subcultured using trypsin for passaging cells and incubated in a 5% CO<sub>2</sub> incubator.

### **2.12. Cellular Uptake Studies:**

100,000 MDA-MB-231 and RAW 264.6 cells per well were seeded in a 12-well plate and cultured in complete formulated media (DMEM and RPMI, respectively) for 24 h. Media were removed and cells, separated into separate sample wells, and each well treated with 4 or 10 nm GNPs (16 total samples of the contrast agents) in media (without FBS) in the presence or absence of 10% HS for 90 minutes or 4 h. Each treatment was performed in triplicate. At the designated endpoints cells were washed 3 times using 1X PBS, collected, and then counted using a hemocytometer. Cells were digested with aqua regia at 60°C for 2 h, then the samples were diluted with nanopure water to reach 4% acid concentration. Gold and gadolinium content in each sample was determined using ICP-MS.

### **2.13. In vivo biodistribution study:**

All animal experiments were performed under the approved protocol of The Institutional Animal Care and Use Committee (IACUC) of the University of Louisville, IACUC 22107. 4 week old female BALB/c mice were ordered from The Jackson Laboratory (Farmington, CT). Mice were quarantined for one week before starting the experiments. Mice were injected by 4T1 cells (500,000 cell count in 100 µL of PBS with MgCl<sub>2</sub>,

CaCl<sub>2</sub>, and glucose) via subcutaneous injection in the right flank. After 10 days, the tumors were developed (average volume ~ 300 mm<sup>3</sup>) and mice were divided randomly into 8 groups (n=6) and injected with 100 μL of either 4nm GNP-Gd-AS1411, GNP-Gd-AS1411-PEG 1K, GNP-Gd-CRO, GNP-Gd-CRO-PEG 1K or their 10 nm GNP analogs via intraperitoneal injection at a dose of 2 mg/kg of oligonucleotides. Mice were sacrificed at 24 and 72 h post injection. Following euthanasia, tumors, livers, and spleens were collected. Organs were dried in the oven at 60°C overnight (organs were weighed before and after drying). Dried organs were digested in aqua regia for 24 h then samples were centrifuged at 3000 g for 30 minutes, and diluted with nanopure water to be prepared for ICP-MS analysis.

#### **2.14. Statistical analysis:**

Unpaired t-test, one-way ANOVA and two-way ANOVA were performed for the obtained data using GraphPad Prism version 9.3.1 for Mac (Graphpad Software, San Diego CA USA, [www.graphpad.com](http://www.graphpad.com)). Differences were considered statistically significant with  $p < 0.05$ .

CHAPTER 3:  
RESULTS OF GNPs CHARACTERIZATION AND PROTEIN ADSORPTION  
STUDIES

**3.1. Development and characterization of 4 & 10 nm GNPs conjugates with AS1411/CRO, Gd (III)-DO3A, and PEGs (1, 2, and 5 kDa).**

***3.1.1. UV-vis spectra of GNPs***

16 different formulations of MRI contrast agent GNPs candidates were synthesized with 8 formulations for each GNP core size ( 4 and 10 nm). GNPs were conjugated with gadolinium (III) DO3A-SH (Gd), either AS1411 or CRO, and with or without PEG ( $M_w$ : 1, 2, and 5 kDa).

The UV-vis absorption spectra showed surface plasmon resonance (SPR) peaks at 504 and 515 nm for citrate capped 4 and 10 nm GNPs, respectively, while the conjugated 4 and 10 nm GNPs showed an average redshift in SPR to ~515 and ~520 nm, respectively, Figure 3.1. No significant broadening of UV/vis traces were noted, signifying successful conjugations with minimal aggregation of nanoparticles.

The molar concentration of each particle sample was calculated from the absorbance at the SPR peaks using the extinction coefficient of 4 and 10 nm GNPs ( $3.62 \times 10^6$  [169])

and  $1.21 \times 10^8$  [provided by 10 nm GNPs supplier], respectively). In addition, the ratio of the absorbance of GNPs (before coating) at the SPR peak ( $A_{spr}$ ) to the absorbance at 450 nm ( $A_{450}$ ) of 4 and 10 nm GNPs were 1.2 and 1.4, respectively, which confirm the correct diameters of both GNPs [169].

In all the graphs, GNPs formulations were denoted by the aptamer's name CRO or AS (for AS1411) and PEG of different  $M_w$  (denoted as 1K, 2K, and 5K in for 1, 2, and 5 kDa PEG, respectively).

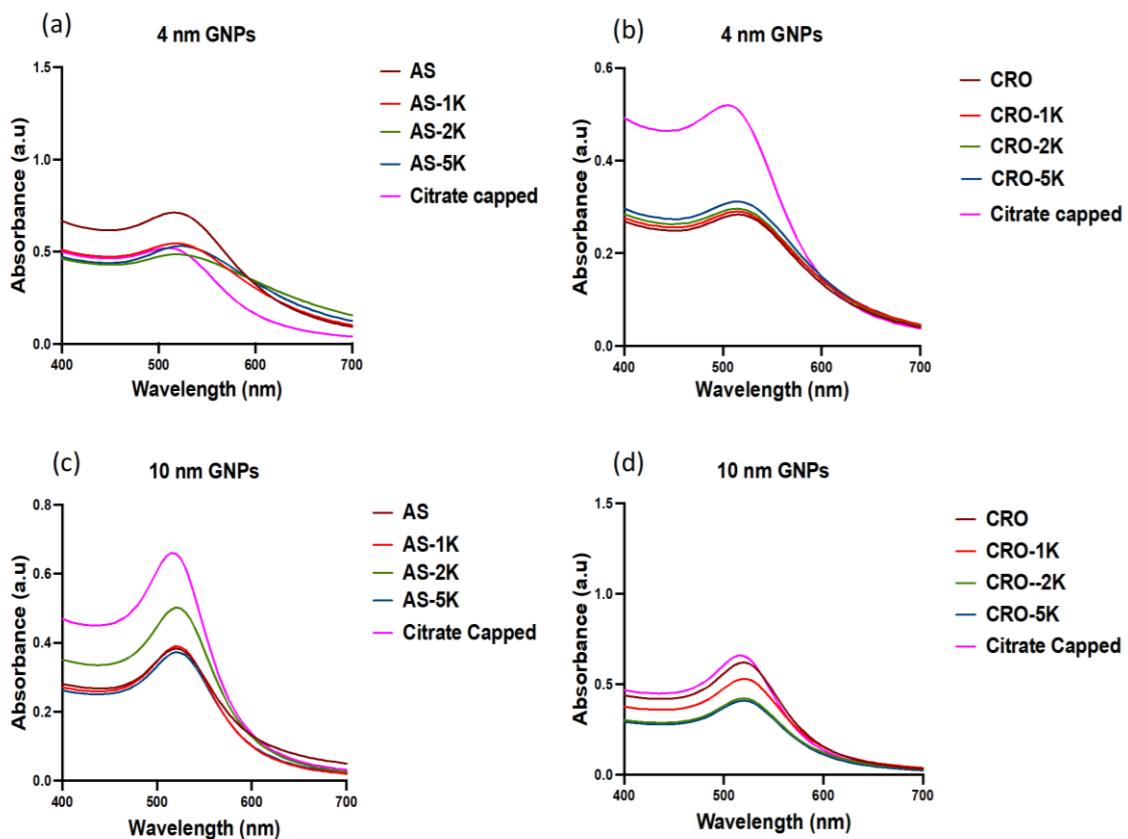


**Figure 3.1: UV-vis spectra of citrate capped, and conjugated GNPs.** All particles conjugated with Gd. GNPs formulations were denoted by the aptamer's name CRO or AS (for AS1411) and PEG of different  $M_w$  (denoted as 1K, 2K, and 5K in the graph for 1, 2, and 5 kDa PEG, respectively). (a) Citrate capped, Non-PEGylated, and PEGylated 4 nm GNPs conjugated with AS1411. (b) Citrate capped, Non-PEGylated and PEGylated 4 nm GNPs conjugated with AS1411. (c) Citrate capped, Non-PEGylated and PEGylated 10 nm GNPs conjugated with CRO. (d) Citrate capped, Non-PEGylated and PEGylated 10 nm GNPs conjugated with CRO.



### 1.2. Dynamic light scattering and zeta potential determination of GNPs

The average hydrodynamic diameters of 4 and 10 nm citrate-capped GNPs dispersed in nanopure water were  $4.8 \pm 0.5$  and  $13.4 \pm 1.2$  nm, respectively. While the average hydrodynamic diameters of the conjugated GNPs were measured in 1X PBS and ranged from 11.1 to 25.9 and from 18.2 to 32.2 for 4 and 10 nm, respectively, Figure 3.2. All GNPs were monodisperse with narrow size distribution and  $PDI < 0.4$ .

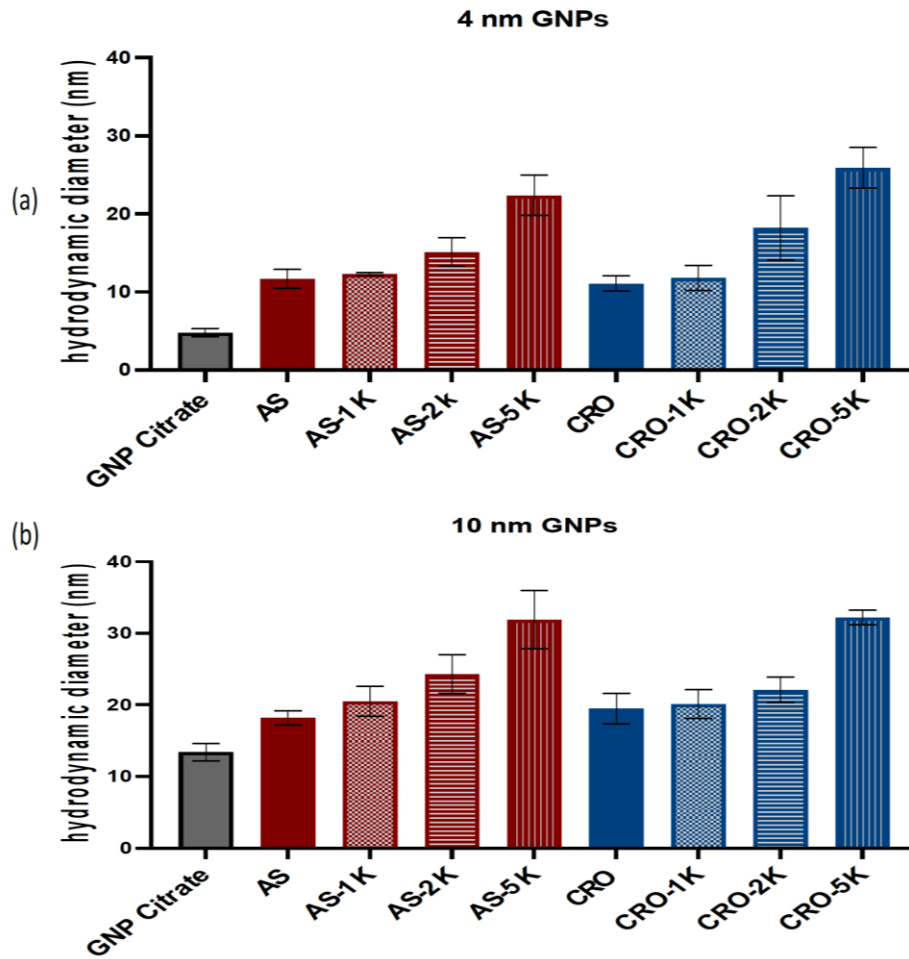
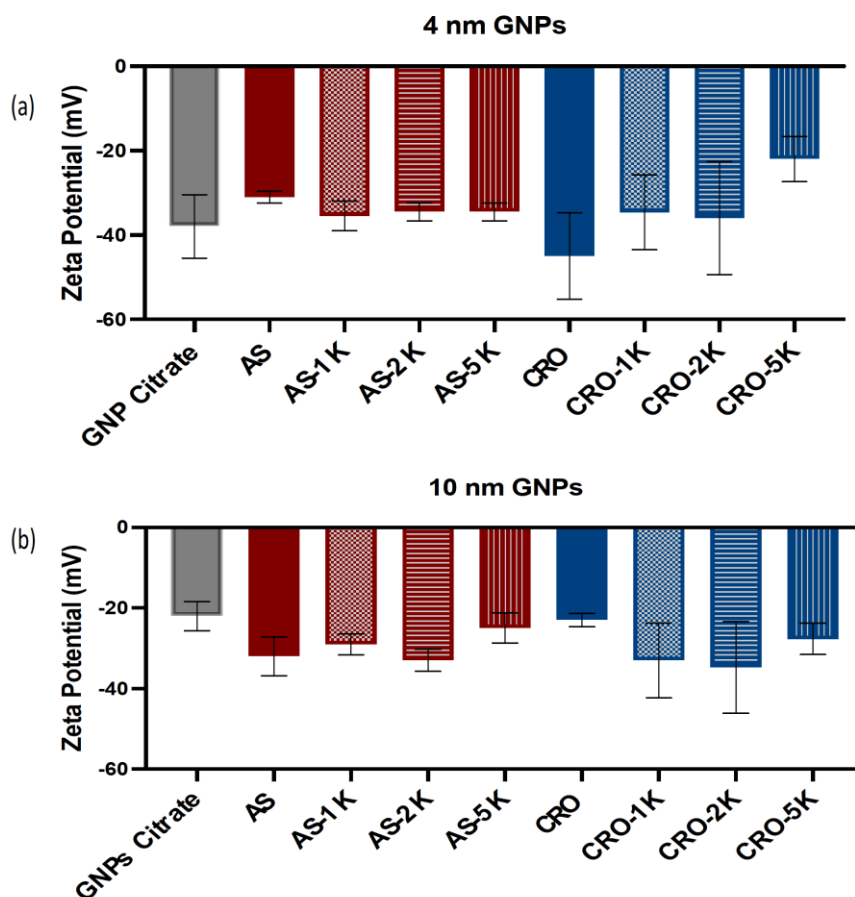


Figure 3.2: Characterization of GNPs: the average hydrodynamic diameter (a) This figure shows the average means of hydrodynamic diameters of 4 nm citrate capped and conjugated GNPs. (b) The average means of Hydrodynamic diameters of 10 nm citrate capped and conjugated GNPs.

The citrate capping and other functionalizing agents on GNPs conferred them a negative zeta ( $\zeta$ ) potential that ranged from -22 to -45 mV, implying that the applied coatings conferred stability in physiologically relevant levels of salt, Figure 3.3.

The citrate capped GNPs were dispersed in nanopure water during measuring and the functionalizing GNPs were dispersed in 1 X PBS.



**Figure 3.3: Characterization of GNPs:  $\zeta$  potential of citrate capped and conjugated GNPs** (a) This figure shows the average means of  $\zeta$  potential of 4 nm citrate capped and conjugated GNPs. (b) The average means of  $\zeta$  potential of 10 nm citrate capped and conjugated GNPs.

### 3.1.3. Quantification of oligonucleotides

The number of oligonucleotides (AS1411 and CRO) per GNP was quantified by UV-visible spectroscopy after cleaving the DNA from the particles using DTT solution and column purification, Table 3.1. The molar concentration of oligonucleotides were calculated using UV-vis spectra (the extinction coefficients provided by the supplier of AS1411 and CRO are 323500 and 268800, respectively), and divided by the corresponding concentration of GNPs prior to cleavage to get the number of DNA per GNP. Results showed that the numbers of oligonucleotides per 10 nm GNP was about 4 times of the number per 4 nm GNP, as 10 nm nanoparticle surface area is 6 times greater than that of 4 nm particles, while we didn't noticed a major difference between the numbers of oligonucleotides per GNP-AS1411 and GNP-CRO.

**Table 3.1: Quantification of the amount of oligonucleotides**

Sample	Oligonucleotides/4 nm GNPs	Oligonucleotides/10 nm GNPs
GNP-Gd-AS1411	10	43.2
GNP-Gd-AS1411-PEG 1K	7.4	43.7
GNP-Gd-AS1411-PEG 2K	7.6	46.8
GNP-Gd-AS1411-PEG 5K	7.0	31.5
GNP-Gd-CRO	12.3	44.9
GNP-Gd-CRO- PEG 1K	6.3	42.9
GNP-Gd-CRO- PEG 2K	8.3	38.9
GNP-Gd-CRO- PEG 5K	8.7	40.7

### 3.1.4. Quantification of gadolinium

The number of Gd ions per nanoparticle was quantified by ICP-MS after nanoparticle digestion in Aqua Regia, Table 3.2. The concentration of gadolinium in each sample was calculated and divided by the corresponding concentration of GNPs to determine the number of Gd per GNP.

**Table 3.2: Quantification of gadolinium**

Sample	Gd/4nm GNPs	Gd/10 nm GNPs
GNP-Gd-AS1411	6.5	77.2
GNP-Gd-AS1411-PEG 1K	5.7	64.7
GNP-Gd-AS1411-PEG 2K	5.9	55.1
GNP-Gd-AS1411-PEG 5K	6.5	72.6
GNP-Gd-CRO	9.0	150.0
GNP-Gd-CRO- PEG 1K	7.9	81.8
GNP-Gd-CRO- PEG 2K	6.4	115.2
GNP-Gd-CRO- PEG 5K	7.9	113.3

Results showed that nanoparticles coated with CRO (GNP-CRO) are loaded with higher amount of Gd than GNP coated with AS1411 (GNP-AS1411). This finding could be correlated with the configuration of the aptamer, as AS1411 forms quadruplex 3D structures on GNP, which may hinder the binding of Gd chelate with its larger footprint compared to CRO, which is linear and allows more room for Gd to bind to the particle

surface. Both oligonucleotide and Gd amount increase as GNP core size increases from 4 to 10 nm and decreases as larger molecular weight PEG is added to the coating. We couldn't quantify the amount of PEG per GNP, as the only method that we have seen to be effective and accurate is to set up a whole high performance liquid chromatography (HPLC), which was hard to perform at this time. The presence of DNA on GNP surface would interfere with the quantification using the common method of quantifying thiol-end of unbound PEG using Elman's reagent (5,5'-dithiobis (2-nitrobenzoic acid) or DTNB). The presence of PEG on GNP surface impacts the number of oligonucleotides as the longer chain of PEG the less the number of oligonucleotides, ex. GNP-Gd-AS1411-5K is coated only with 31.5 oligonucleotide.

### **3.2. Determination of the adsorption of serum proteins on the GNP surfaces.**

#### ***3.2.1. Quantification of the amount of bound proteins on the surface of GNPs by Bicinchoninic acid assay (BCA):***

To quantify the amount of adsorbed human serum proteins on PEGylated and non-PEGylated GNP surfaces, GNPs were incubated in 10% human serum for 24 h at 37°C with continuous shaking. Particles were then centrifuged 2 times to remove the unbound proteins and keep the solid protein coronae only. Then particles were treated with 5% SDS and heated to isolate the proteins followed by quantification of proteins ( $\mu\text{g}$  of protein/GNP) with a BCA assay using the standard curve of albumin protein. The results suggested that 4 and 10 nm PEGylated GNP MRI contrast agents conjugated with AS1411 adsorbed higher amounts of serum proteins than did the corresponding non-PEGylated versions, but the differences between the proteins amounts were non-significant. One-way ANOVA was used to compare among the means and unpaired t-test was used to compare between each two means. Moreover, we observed that the longer the chain of PEG, the higher the amount of proteins for 4 nm GNPs, Figure 3.4. (a). The same pattern was not consistent with 10 nm GNPs, but GNPs with PEG  $M_w$  5 kDa adsorbed the highest amount of proteins, Figure 3.4 (b).

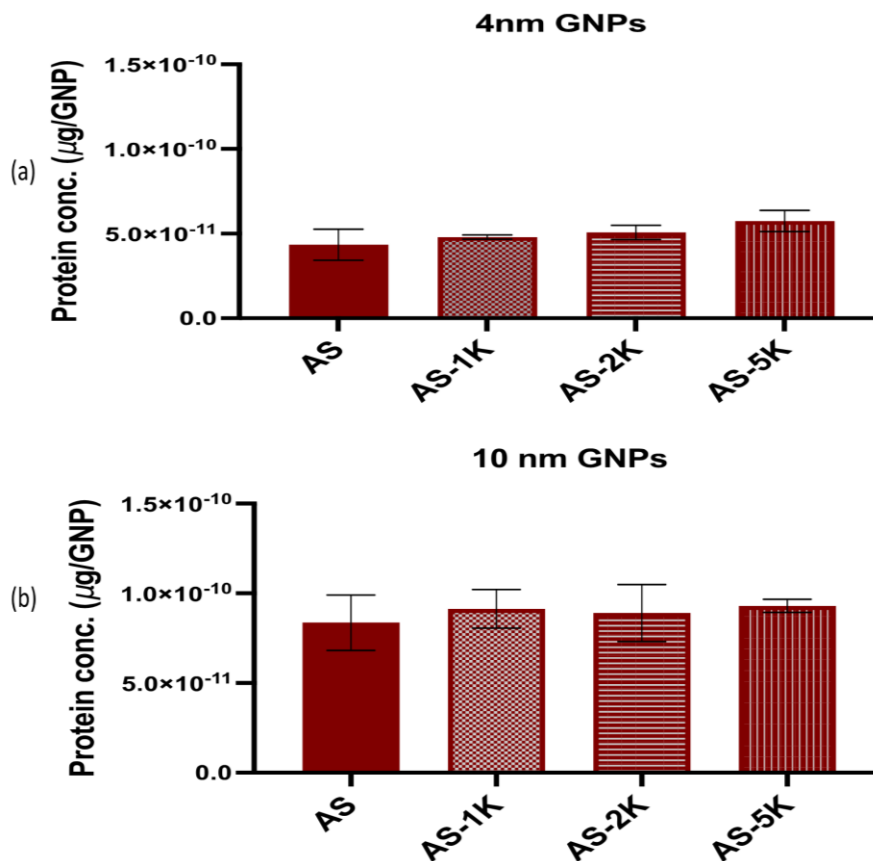


**Figure 3.4: Quantification of the amount of adsorbed proteins after incubation of 4 and 10 nm GNP-AS1411 with 10% human serum.** (a) Figure shows the average means of the amounts of proteins on the surface of 4 nm GNPs conjugated with AS1411. (b) The average means of the amounts of proteins on the surface of 10 nm GNPs conjugated with AS1411.

In contrast to the above, the 4 and 10 nm PEGylated MRI contrast GNPs conjugated with CRO mitigated the amount of adsorbed proteins with the highest reduction found with PEG  $M_w$  5 kDa, Figure 3.5 (a, b) (the reduction was significant among 10 nm GNPs). We suggest that these dissimilarities between the adsorbed

amounts of proteins on the PEGylated GNPs are attributable to the sequence and configuration of the aptamers. AS1411 is G-rich DNA, which forms a quadruplex 3D structure on the surface of GNPs, while CRO is T-rich linear DNA. The geometry of the DNA potentially affects the density and conformation of PEG chains on the GNPs surface, thereby impacting protein binding.

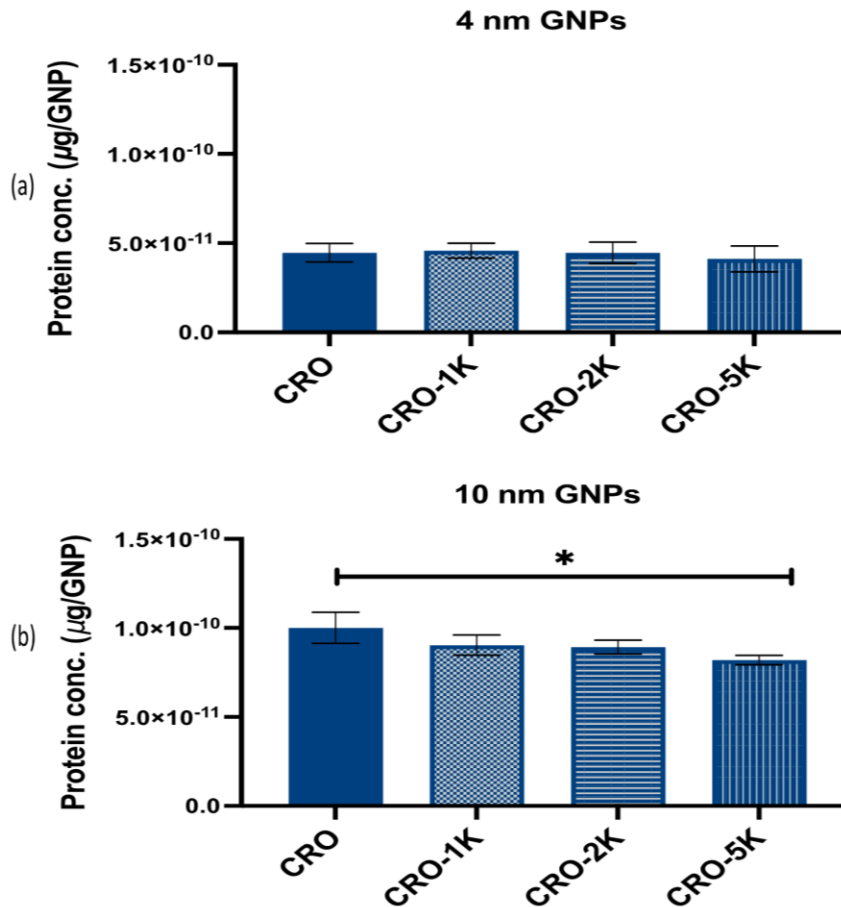


**Figure 3.5: Quantification of the amount of adsorbed proteins after incubation of 4 and 10 nm GNP-CRO with 10% human serum.** (a) Figure shows the average means of the amounts of proteins on the surface of 4 nm GNPs conjugated with CRO. (b) The average means of the amounts of proteins on the surface of 10 nm GNPs conjugated with CRO. \* denotes  $p < 0.05$ .



Additionally, we compared the amount of adsorbed proteins of all formulations of 4 nm GNP (conjugated with AS1411 and CRO) and found that the differences in protein binding were not significant. Comparatively the differences between all formulations of 10 nm was significant with PEG  $M_w$  5kDa with CRO showed a significant reduction of the amount of protein. Furthermore, we noticed that the amounts of adsorbed proteins on 10 nm GNPs are almost 2-fold the amounts found on 4 nm GNPs, Figure 3.6. Considering that the 10 nm nanoparticle surface area is 6 times greater than that of 4 nm particles, then smaller particles adsorbed a relatively higher amount of proteins per unit surface area.

### 4 & 10 GNPs

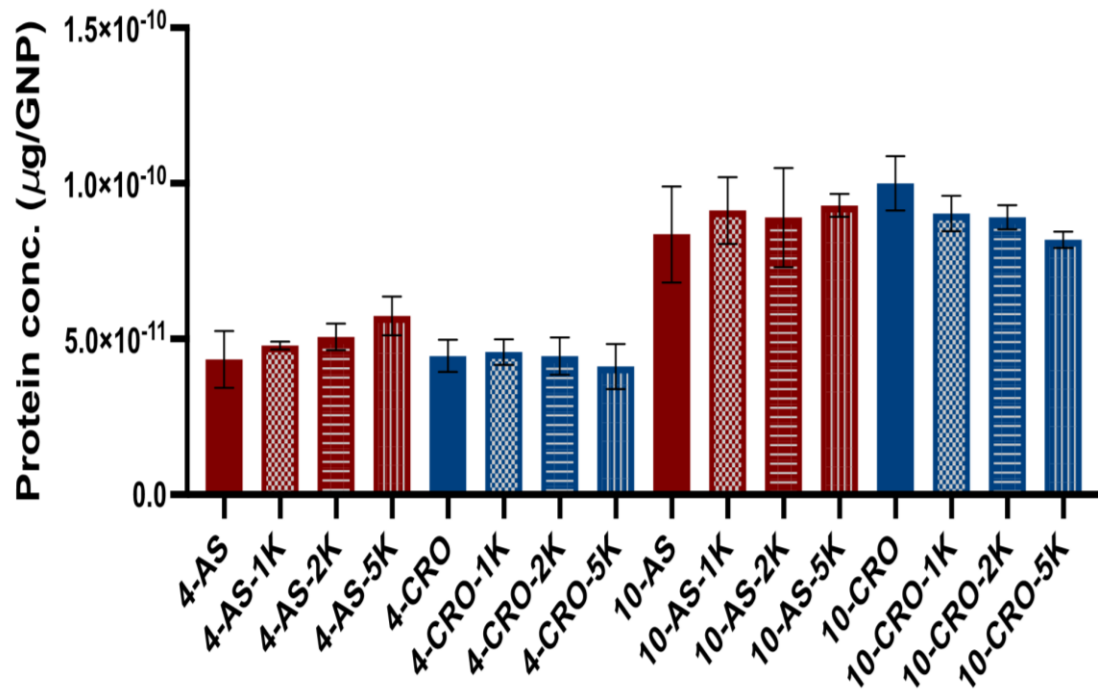
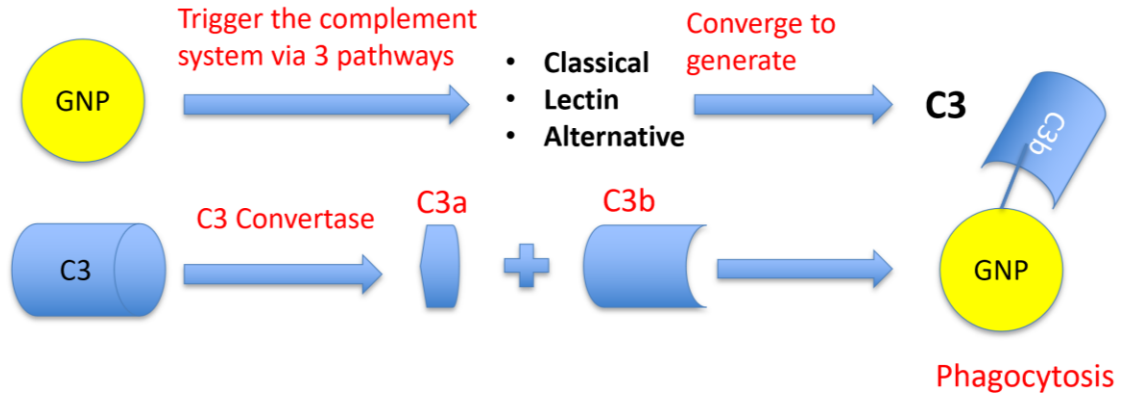


Figure 3.6: Comparison between 4 and 10 nm GNPs indicates that the amount of adsorbed proteins on 10 nm GNPs is almost 2-fold the amount found on 4 nm GNPs

**3.2.2 Quantification of the amount of bound proteins on the surface of GNPs by NuPAGE Bis-Tris gel electrophoresis:**

Once GNPs get in blood circulation, they activate the complement system, which is a critical component of the innate immune system. The complement system is a collection of over 40 soluble and membrane-bound proteins, which triggers via three distinct pathways: classical, lectin, and alternative. These pathways converge at the step where the central complement protein C3 is cleaved by C3 convertase to generate C3b and C3a. C3b (opsonin) is a major component of the complement system which prime the surface of GNPs for engulfment by macrophages and leukocytes through complement receptors [125], Figure 3.7. We used purified C3b protein in this experiment to investigate its presence in the isolated protein corona.



**Figure 3.7: Activation of the complement system by GNPs.**

Once the amounts of proteins adsorbed to GNPs were determined, we set out to identify which serum proteins adsorbed the most to the GNP surface. The proteins isolated from GNPs and purified C3b protein were treated with lithium dodecyl sulfate

(LDS) sample buffer, and sample reducing agent, and loaded into 4 to 14% gel in a tank filled with compound 2-ethanesulfonic acid sodium dodecyl sulfate (MES SDS) running buffer. C3b protein was run with the other isolated proteins samples to investigate which GNP type adsorbs more C3b protein on its surface. Protein samples were run and gels were imaged, Figures 3.8 and 3.9.

From the gels, a slight increase in the amount of proteins isolated from 4 nm GNP/AS1411 in comparison to 4 nm GNP-CRO was noticed. No difference between the thickness or the number of band of PEGylated and non-PEGylated GNPs was found, while we didn't find a difference between the amounts of isolated proteins from 10 nm GNP-AS1411 and GNP-CRO.

Purified separated into two bands representing the alpha and beta chains. Unfortunately, these bands were not clear enough for the isolated proteins of each GNPs sample to compare between them.

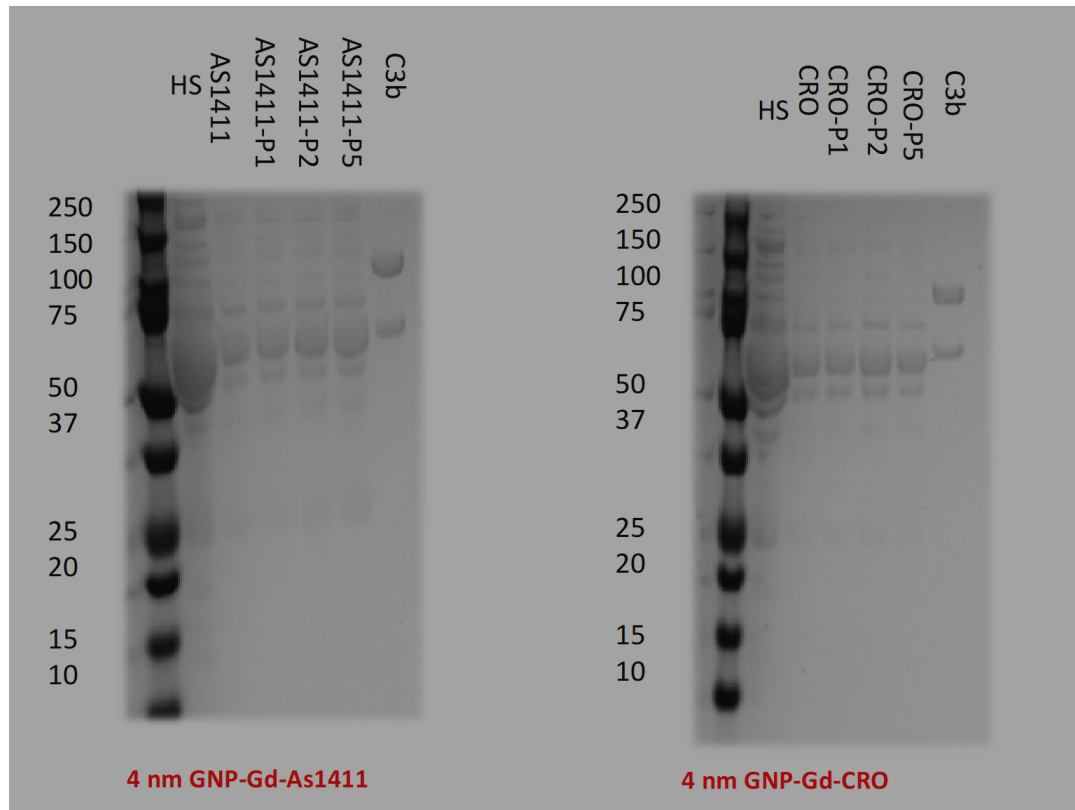


**Figure 3.8: Bis Tris gel electrophoresis of isolated protein from 4 nm GNP/AS1411 and GNP/CRO.**

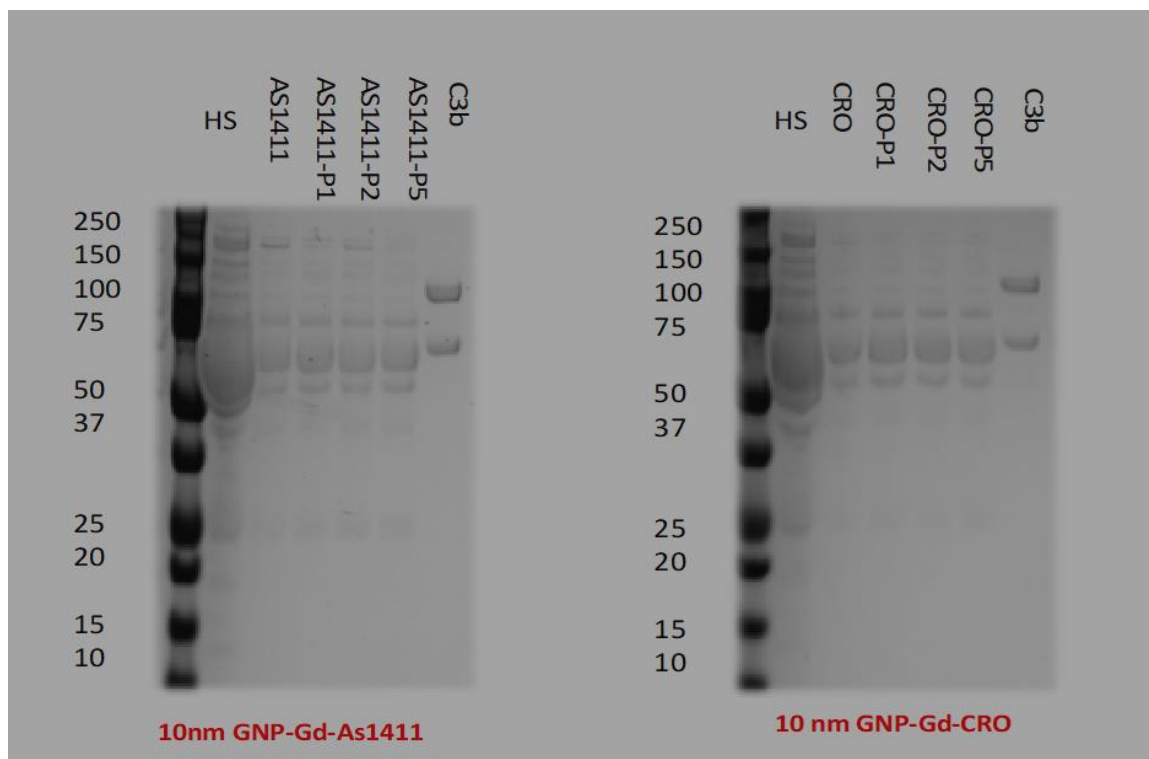


**Figure 3.9: Bis-Tris gel electrophoresis of isolated proteins from 10 nm GNP/AS1411 and GNP/CRO.**

## CHAPTER 4

### RESULTS OF *IN VITRO* AND *IN VIVO* STUDIES

#### **4.1.Determination of the uptake of the incubated particles with and without serum proteins by macrophage and cancer cells.**

##### ***4.1.1. Uptake by macrophage cells***

Uptake studies were performed using RAW 264.7 macrophage cells since the complement receptors for the corresponding proteins in human serum are expressed on their surface. Cells were treated with the 16 different GNP MRI contrast agents in both 10% human serum-containing and human serum-free culture media for either 90 minutes and 4 h. A 30 nM concentration was used for 4 nm GNPs (concentration was based on GNP) and normalized the concentrations of 10 nm GNPs to have the same content of aptamer as 4 nm GNPs. The cellular uptake of the particles was quantified by ICP-MS after cell digestion with aqua regia.

In general, we found that the uptake of all GNPs in RAW 264.7 in the human serum-containing media is significantly higher compared to the uptake in human serum-free media, which indicates that the serum proteins impact and increase the uptake of particles by the macrophage cells. These results reinforce the notion that complement proteins in the protein corona are getting recognized by macrophage complement receptors, thereby enhancing the uptake of particles by phagocytosis. Along with this, we observed that the uptake of GNPs is time-dependent, with higher amounts of gold internalized at 4 h in comparison to 90 minutes.

Additionally, all PEGylated 4 and 10 nm GNPs conjugated with AS1411 have a significantly higher uptake than the non-PEGylated ones (except the 4 nm PEGylated with PEG 5kDa, which has a lower uptake than non-PEGylated but the difference was not statistically significant), Figure 4.1, a and b. Furthermore, 4 nm GNPs showed higher uptake than 10 nm GNPs at the 4 h time point with serum-contained media, Figure 4.1. We used two-way ANOVA to compare between the means and unpaired t-test was used to compare between each two means.



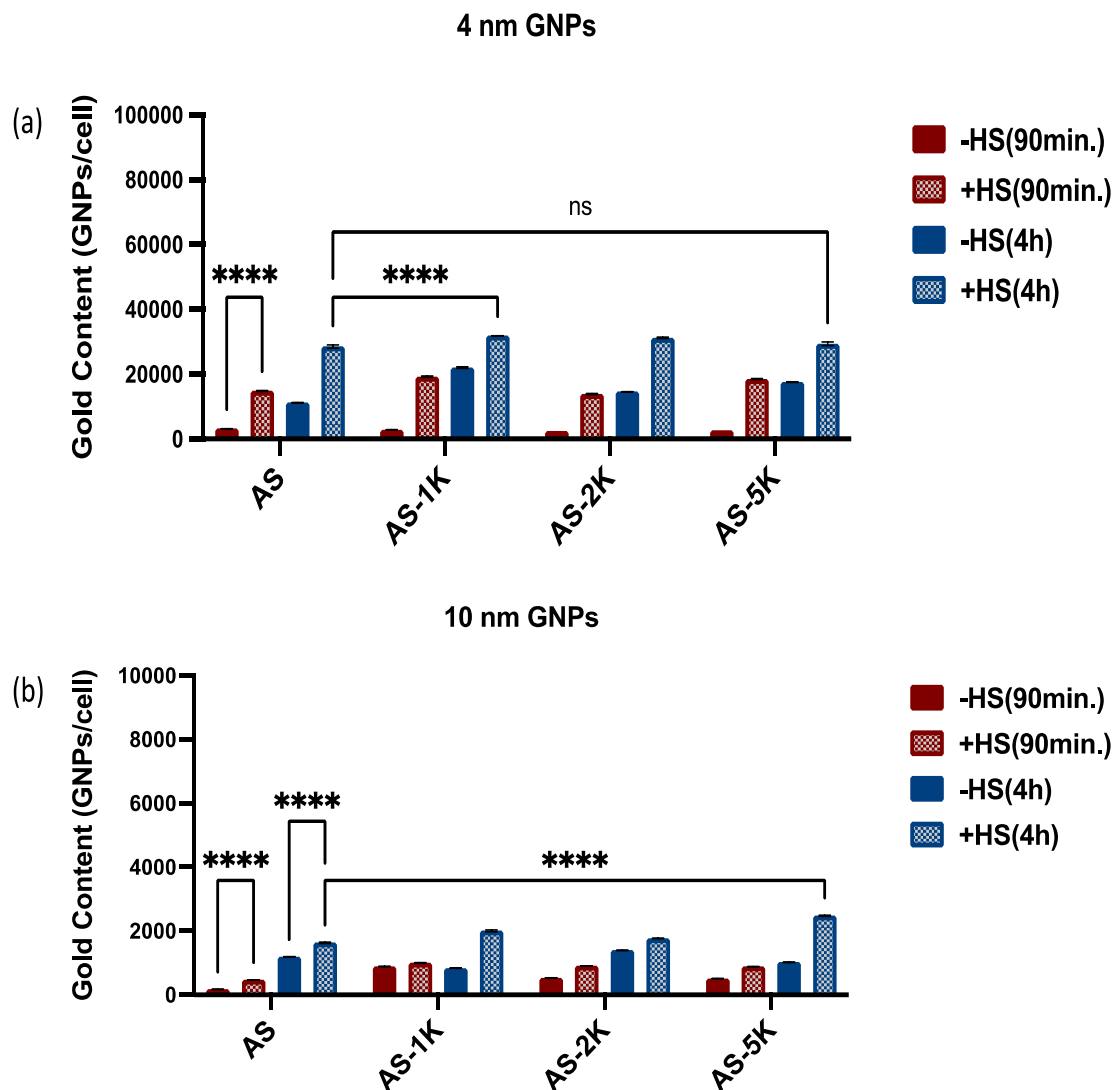


**Figure 4.1: Effect of 4 and 10 nm GNP-AS1411 human serum proteins corona on the uptake by macrophage RAW 264.7 cells.** (a) The figure shows the quantification of 4 nm GNP/AS1411 uptake. (b) Quantification of 10 nm GNP/AS1411 uptake.

\*\*\*\*denotes  $p < 0.0001$ , and ns denotes  $p$  non-significance.

In contrast to the above, we observed a significant reduction in the uptake of 4 nm PEGylated GNPs conjugated with CRO compared with non-PEGylated CRO particles. In these experiments, the longer the chain of PEG, the lower the uptake by the cells. While 10 nm PEGylated-1 and 2 kDa had higher uptake than non-PEGylated particles, GNPs-

CRO-PEG 5 kDa had the lowest uptake by macrophage cells, Figure 4.2, a and b. We found that these results are correlated to the results of the BCA assay, as the PEGylated GNPs with AS1411 did not mitigate the amount of adsorbed proteins while the PEGylated GNPs with CRO adsorbed less proteins than the non-PEGylated although the difference is only significant with 10 nm PEGylated-5kDa.

Furthermore, we found that the uptake of 4 and 10 nm GNPs conjugated with CRO is higher than 4 and 10 nm GNPs conjugated with AS1411 at 4 h with human serum. This result could be related to the aptamer sequence and configuration as AS1411 forms a quadruplex structure while CRO is linear, which seemingly affects the cellular internalization.

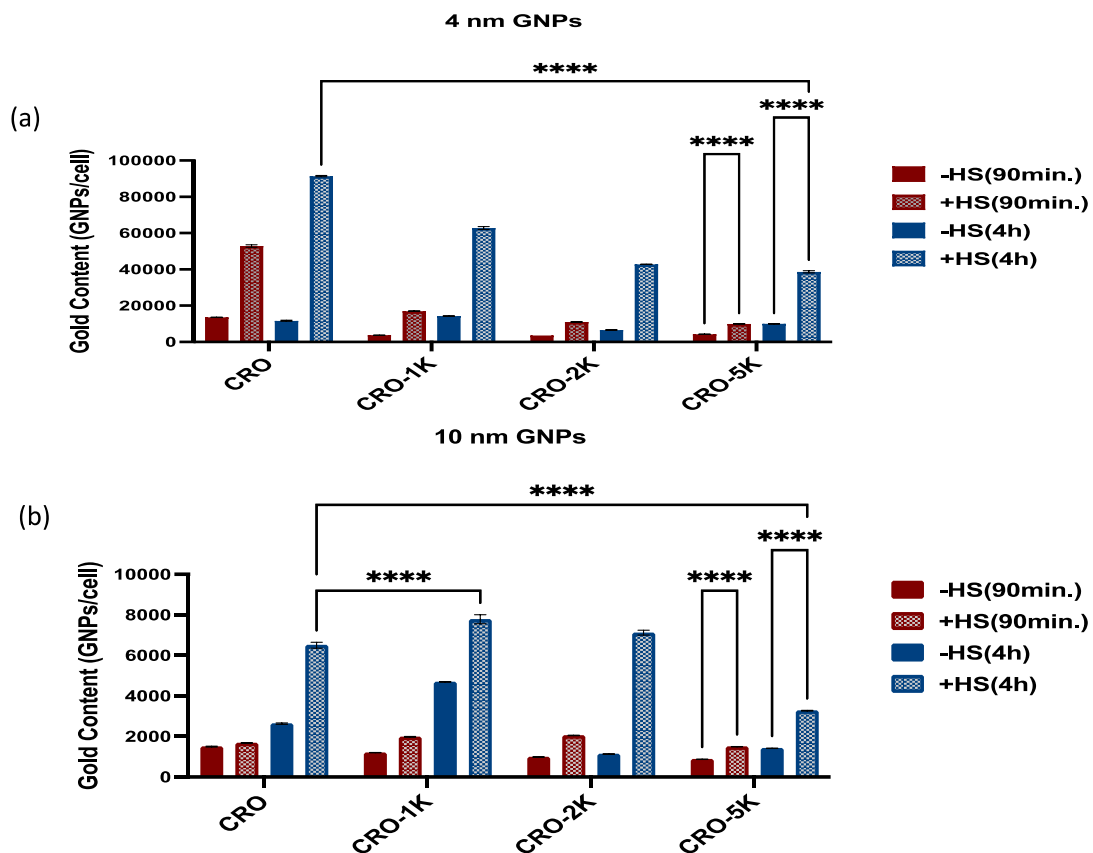


**Figure 4.2: Effect of 4 and 10 nm GNP-CRO human serum proteins corona on the uptake by macrophage RAW 264.7 cells.** (a) The figure shows the quantification of 4 nm GNP/CRO uptake. (b) Quantification of 10 nm GNP/CRO uptake. \*\*\*\*denotes  $p < 0.0001$ .

**Determination of the gadolinium uptake by macrophage cells:**

The amounts of gadolinium that have been taken by macrophage cells were quantified by ICP-MS. We have quantified the uptake after 90 minutes and 4 hours treatment with the particles with and without human serum, the same way as we quantified GNPs. We observed that the uptake of gadolinium does not correlate with the corresponding uptake of GNPs, Figure 4.3 and 4.4. While the uptake of all GNPs formulation in serum-containing media was significantly higher than the uptake of other particles in serum-free media, we did not observe the same trend with gadolinium. The highest uptake of 4 and 10 nm GNP-AS1411 was observed with PEGylated 5K and 2K without serum for 4 and 10 nm, respectively. For 4 and 10 nm GNP-CRO, we observed that non-PEGylated particles exhibited the highest uptake in serum-free media. Further, we noted that the uptake was not time dependent as some GNPs formulations showed higher uptake at 90 minutes than the uptake at 4 h.

We suggest the probability of releasing gadolinium from the particles during internalization by the cells or may be it may be loosely bound to the other functionalizing agents on the particle surface (oligonucleotides or PEG) and could be released upon uptake by cells.

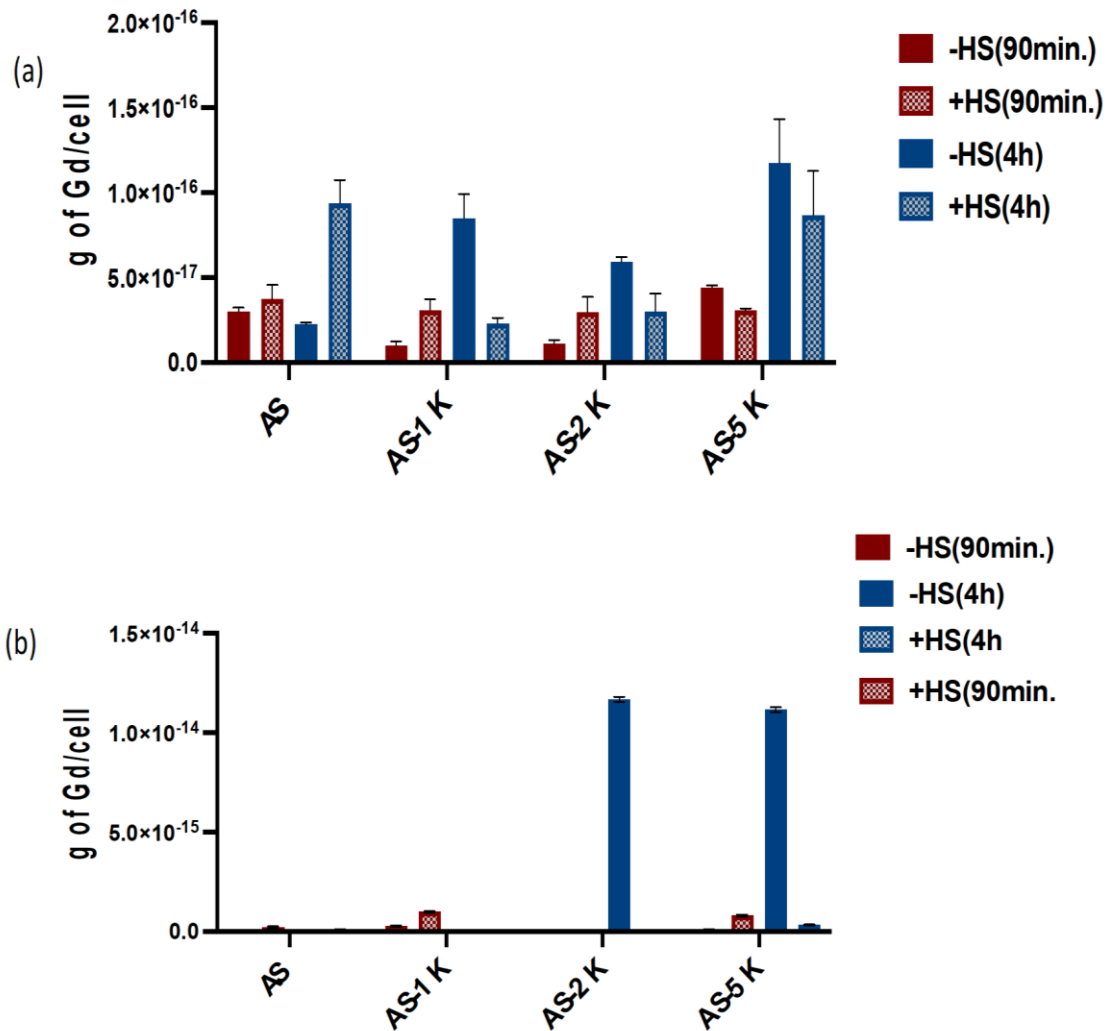


**Figure 4.3: Quantification of the amount of gadolinium in macrophage cells RAW 267.7 at 90 minutes and 4 h. after treatment with GNP-AS1411** (a) The figure shows the quantification of Gd after treating the cells with 4 nm GNP/AS1411. (b) The quantification of Gd after treating the cells with 10 nm GNP/AS1411.

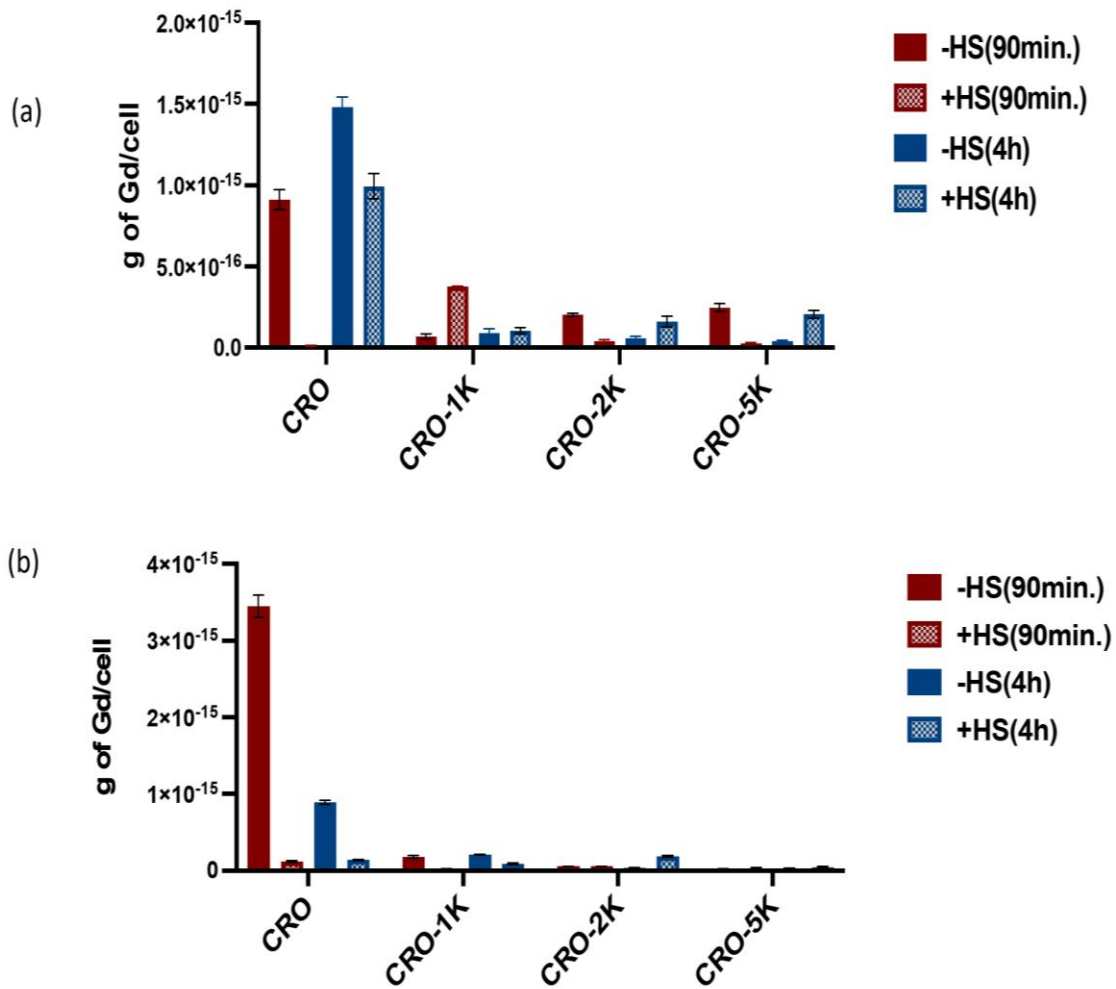


**Figure 4.4: Quantification of the amount of gadolinium in macrophage RAW 264.7 cells at 90 minutes and 4 h. after treatment with GNP-CRO** (a) The figure shows the quantification of Gd after treating the cells with 4 nm GNP-CRO. (b) The quantification of Gd after treating the cells with 10 nm GNP-CRO.

#### ***4.1.2. Uptake by cancer cells***

MDA-MB-231 cells were subjected to the same nanoparticle treatments as RAW246.7, and the up taken gold amounts were quantified by ICP-MS. Contrary to RAW 264.7 cells, MDA-MB-231 cells that were treated with the GNP contrast agents in serum-containing media, showed a significantly less gold amounts at the 2-time points compared to the samples in serum-free media, Figures 4.5 and 4.6, which suggests that serum proteins interfere with nanoparticle uptake in cancer cells. Further, all 4 and 10 nm PEGylated 5kDa GNPs exhibited the lowest uptake of gold regardless of the aptamer type, which differs from their uptake by macrophage cells. PEGylated (1 kDa) nanoparticles (AS1411 and CRO) showed the highest uptake among all GNP contrast agents, 4 and 10 GNPs conjugated with CRO and 4 GNPs conjugated with AS1411, figure 4.5, a, and Figure 4.6, a, and b. For 10 nm GNPs conjugated with AS1411, PEGylated 2 kDa was significantly higher than non-PEGylated and the PEGylated GNPs in the same group Figure 4.5, b. Furthermore, we noticed that the uptake of all 4 nm GNPs is much higher than the uptake of all 10 nm GNPs implying that the uptake by cancer cells relied more on the gold core size than the aptamer type or any other coating constituent. We used two-way ANOVA to compare between the means and unpaired t-test was used to compare between each two means.

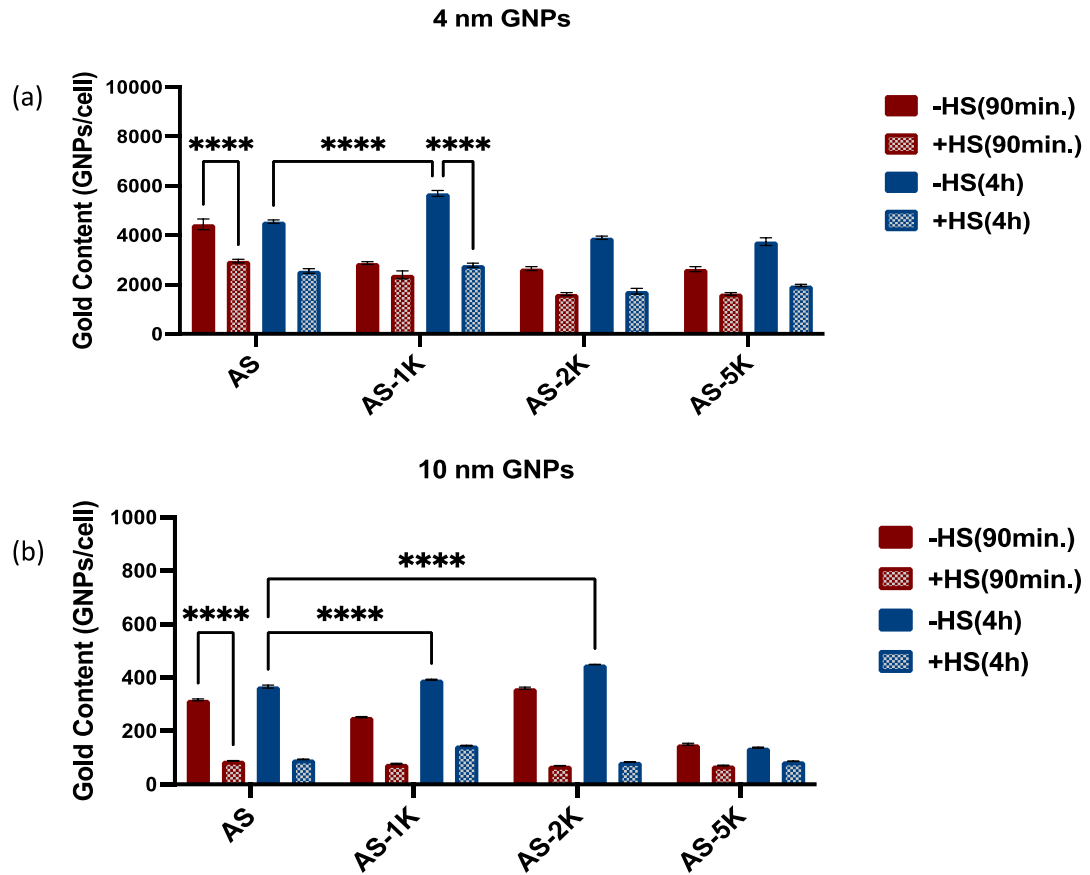


**Figure 4.5: Effect of 4 and 10 nm GNP-AS1411 human serum protein corona on the uptake by cancer MDA-MB231 cells.** (a) The graph shows the quantification of 4 nm GNP/AS1411 uptake. (b) Quantification of 10 nm GNP/AS1411 uptake. \*\*\*\*denotes  $p < 0.0001$ .



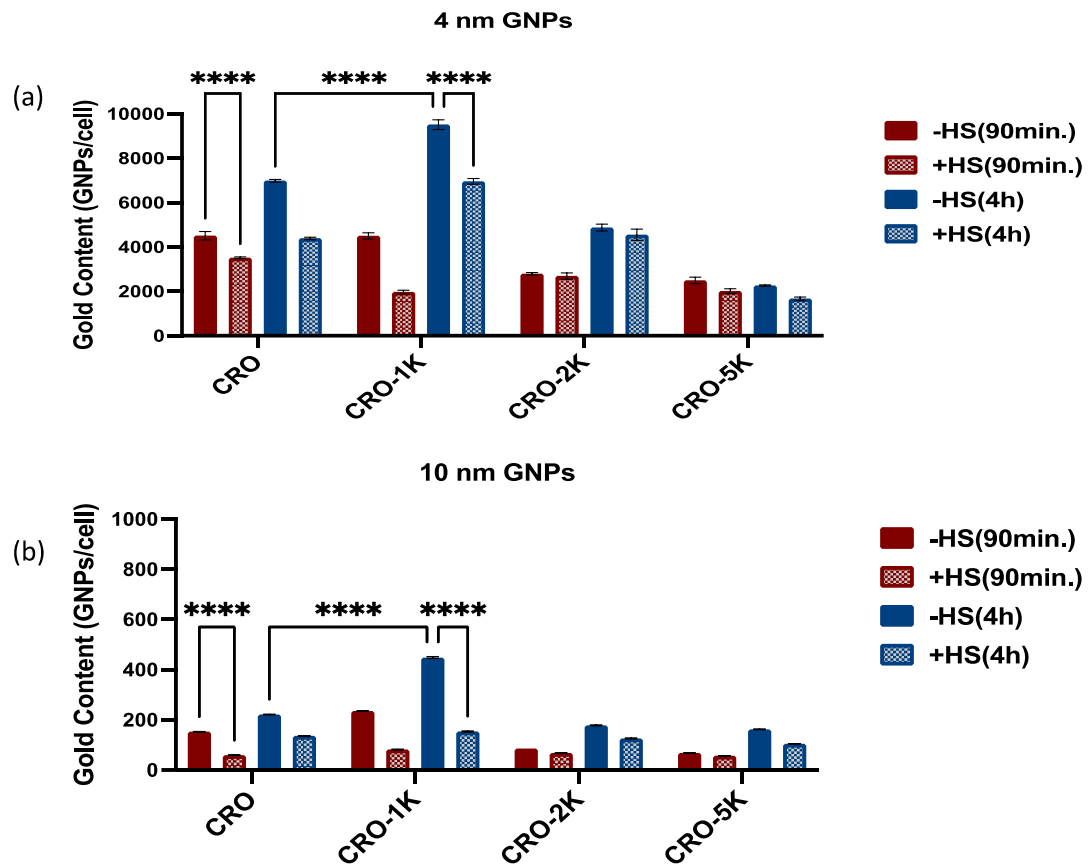


**Figure 4.6: Effect of 4 and 10 nm GNP-CRO human serum protein corona on the uptake by cancer MDA-MB231 cells. (a) The figure shows the quantification of 4 nm GNP/CRO uptake. (b) Quantification of 10 nm GNP/CRO uptake. \*\*\*\* denotes  $p < 0.0001$**

### Determination of the gadolinium uptake by cancer cells:

The amounts of gadolinium that were taken by cancer cells were quantified with ICP-MS. PEGylated 5K particles showed the highest uptake among 4 and 10 nm GNP-AS1411 at 90 minutes in serum-free media, Figure 4.7, while PEGylated 1K exhibited the highest uptake at 4 h in serum-containing media, Figure 4.8. We suggested the same thing that happened with macrophage cells that the gadolinium chelate released from GNPs during cellular uptake.

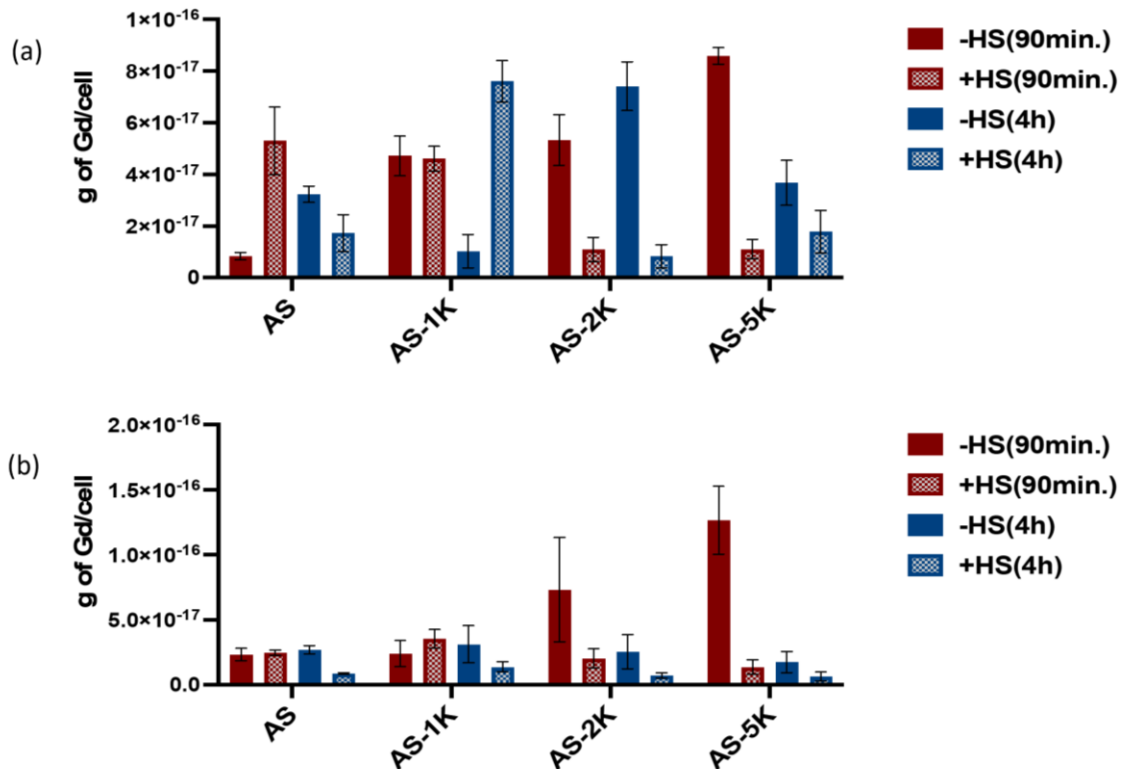


**Figure 4.7: Quantification of the amount of gadolinium in cancer cells MDA-MB-231 at 90 minutes and 4 h. after treatment with GNP-AS1411. (a) The figure shows the quantification of Gd after treating cancer cells with 4 nm GNP/AS1411. (b) The quantification of Gd after treating the cells with 10 nm GNP/AS1411.**

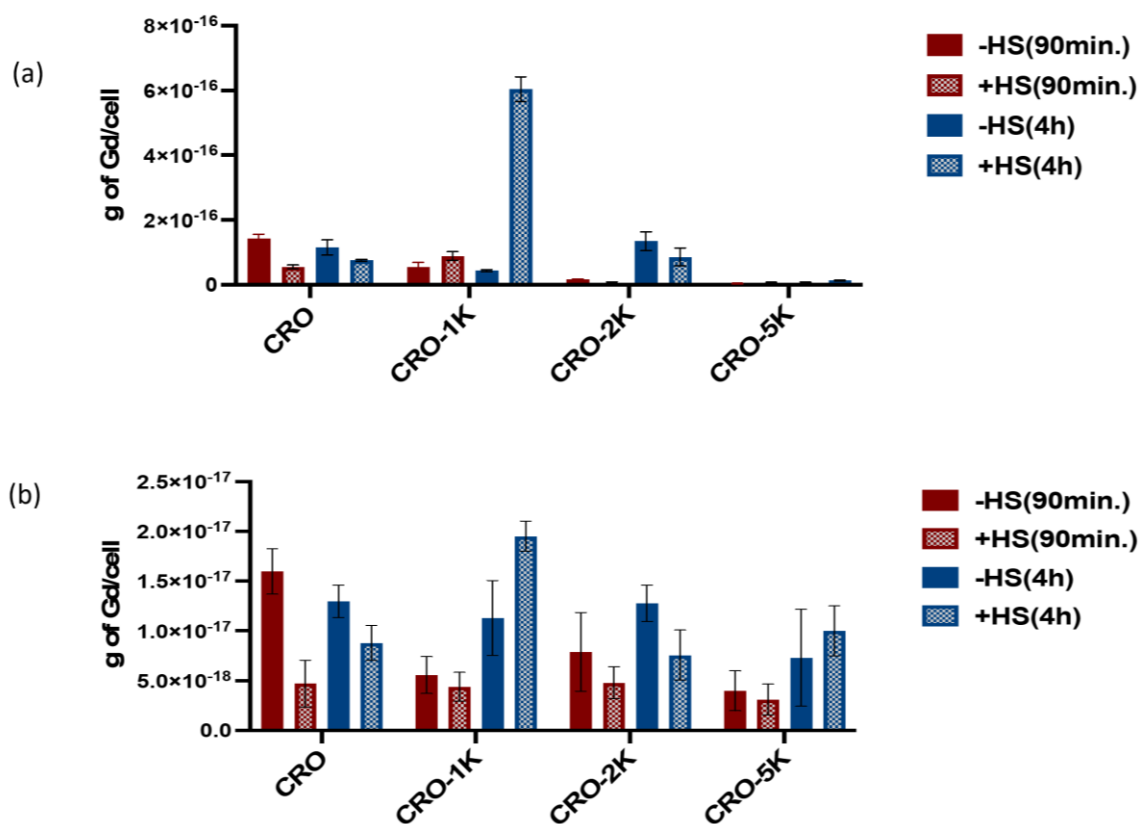


**Figure 4.8: Quantification of the amount of gadolinium in cancer cells MDA-MB-231 at 90 minutes and 4 h. after treatment with GNP-CRO** (a) The figure shows the quantification of Gd after treating the cells with 4 nm GNP-CRO. (b) The quantification of Gd after treating the cells with 10 nm GNP-CRO.

#### **4.2. Determination of the uptake of the particles by tumor cells through *in vivo* biodistribution study.**

An *in vivo* biodistribution study was conducted to better assess the differential uptake of the various GNP formulations by *in situ* tumor cells and macrophages functioning within an active immune system. A murine model of 4T1 mammary carcinoma in BALB/c female mice was used. While the *in vitro* uptake studies had been performed on human-derived MDA-MB-231 breast cancer cells, the use of those cells in an animal model would necessitate the use of animals with compromised immune systems. Thus, the 4T1 model was chosen to better assess the biodistribution of the GNPs with competition between tumor uptake and an intact reticuloendothelial system. Also, it is worth mentioning that 4T1 is a triple negative breast cancer cells and they very closely mimic human breast cancer cells MDA-MB-231. Additionally, the number of GNP variations used in the study were reduced from the initial set of GNPs used in the *in vitro* studies. For the *in vivo* studies, the  $M_w$  of PEG were restricted to only 1 kDa. PEG 1kDa was chosen because it had shown better uptake for 4 nm GNP in cancer cells, and protein adsorption assays for AS1411-GNP showed no significant difference among the 1, 2, and 5 kDa PEG-coated GNPs. We excluded the PEGylated particles with PEG 2 and 5 kDa since they showed the lowest uptake by cancer cells in *in vitro* studies. Since we were investigating the effects of PEGylation on biodistribution, the non-PEGylated GNPs served as a baseline group. When the subcutaneous allograft tumors reached  $\sim 300 \text{ mm}^3$ , mice were randomly divided into 8 groups and injected via intraperitoneal injection with GNPs. Mice were euthanized after either 24 and 72 h post-injection, and tumors, livers, and spleens were collected for ICP-MS analysis. Results showed that the uptake of most

PEGylated and non-PEGylated GNPs by liver and spleen is significantly higher than their uptake by tumor cells, Figure 4.9 and 4.10. The percentage of injected dose of the highest uptake by tumor cell was 0.22 % and 2.1% for 4 nm GNP-Gd-AS1411-1K (72 h) and 10 nm GNP-Gd-AS1411-1K (24 h) respectively, while the percentage of injected dose of the highest uptake by liver was 22 % and 35 % for 4 nm GNP-Gd-CRO-1k (24) and 10 nm GNP-Gd-CRO (72 h) respectively, and by spleen was 2.7 % and 6.6 % for 4 nm GNP-Gd-AS1411 (72 h) and 10 nm GNP-Gd-AS1411-1K (24 h) respectively.

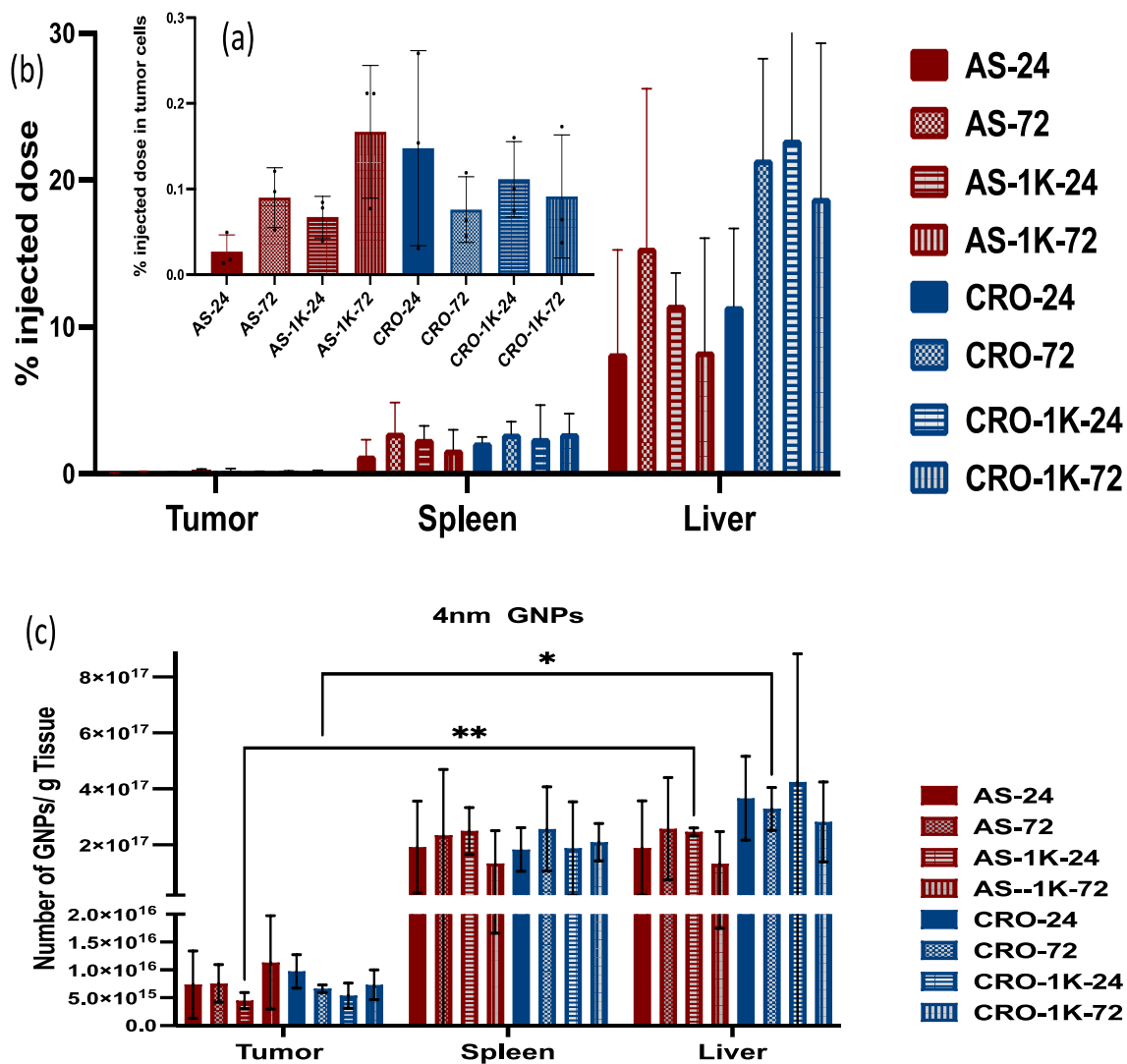


**Figure 4.9: Quantification of 4 nm GNPs accumulation in the tumor, liver, and spleen of mice that injected with non-PEGylated and PEGylated (PEG Mw: 1kDa) 24 and 72 h post injection.** (a) The percentage of the injected dose in tumor cells. (b) The percentage of the injected dose in liver and spleen. (c) The number of GNPs/g tissue. Each data point represents the mean  $\pm$  standard deviation (SD) of triplicate experiments. \*denotes  $P < 0.05$  and \*\*denotes  $P < 0.01$ .

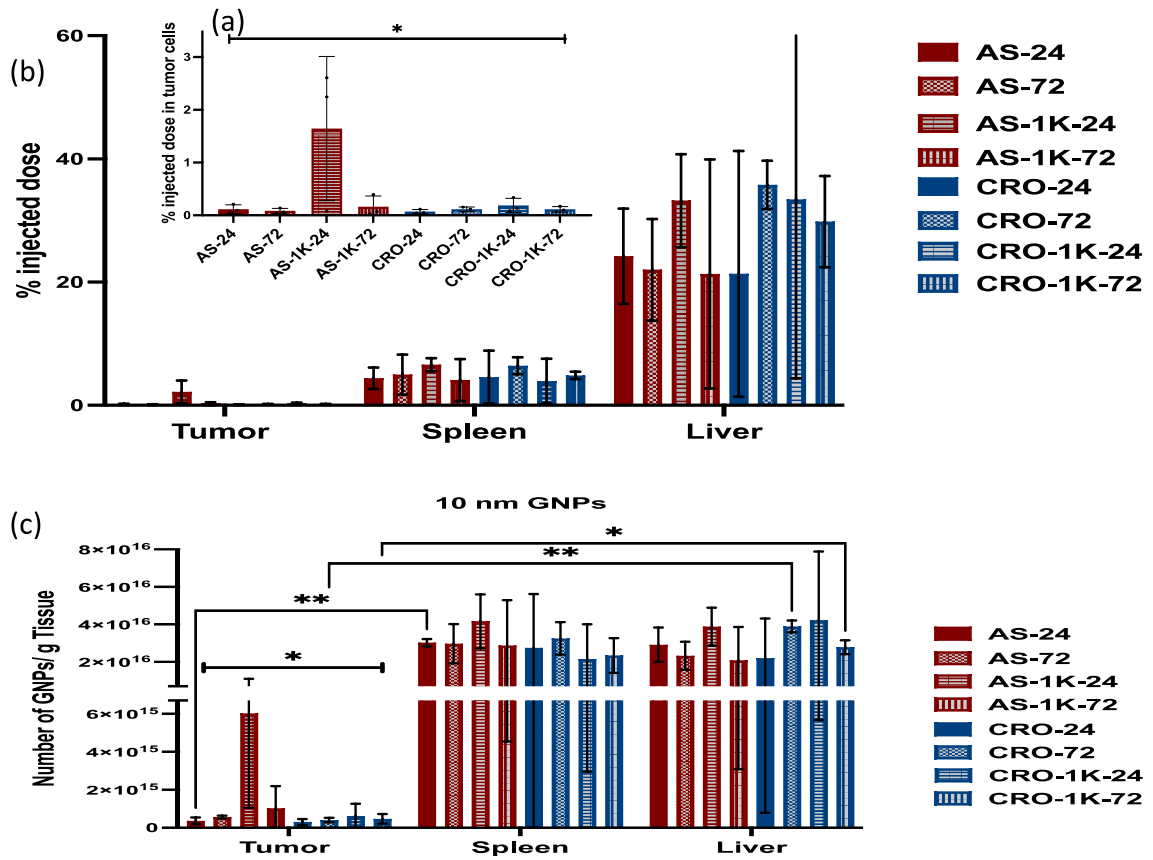


**Figure 4.10: Quantification of 10 nm GNPs accumulation in the tumor, liver, and spleen of mice that injected with non-PEGylated and PEGylated (PEG Mw: 1kDa) 24 and 72 h post injection.** (a) The percentage of the injected dose in tumor cells. (b) The percentage of the injected dose in liver and spleen. (c) The number of GNPs/g tissue. Each data point represents the mean  $\pm$  standard deviation (SD) of triplicate experiments.

\* denotes  $P < 0.05$  and \*\*denotes  $P < 0.01$ .

4 nm PEGylated GNPs/AS1411 exhibited the highest uptake by tumor cells at 72 h, but the difference is non-significant among the means, while the 4 nm non-PEGylated GNPs/CRO showed the highest uptake by tumor cells at 24 h and the difference is non-significant among the means as well, Figure 4.11.

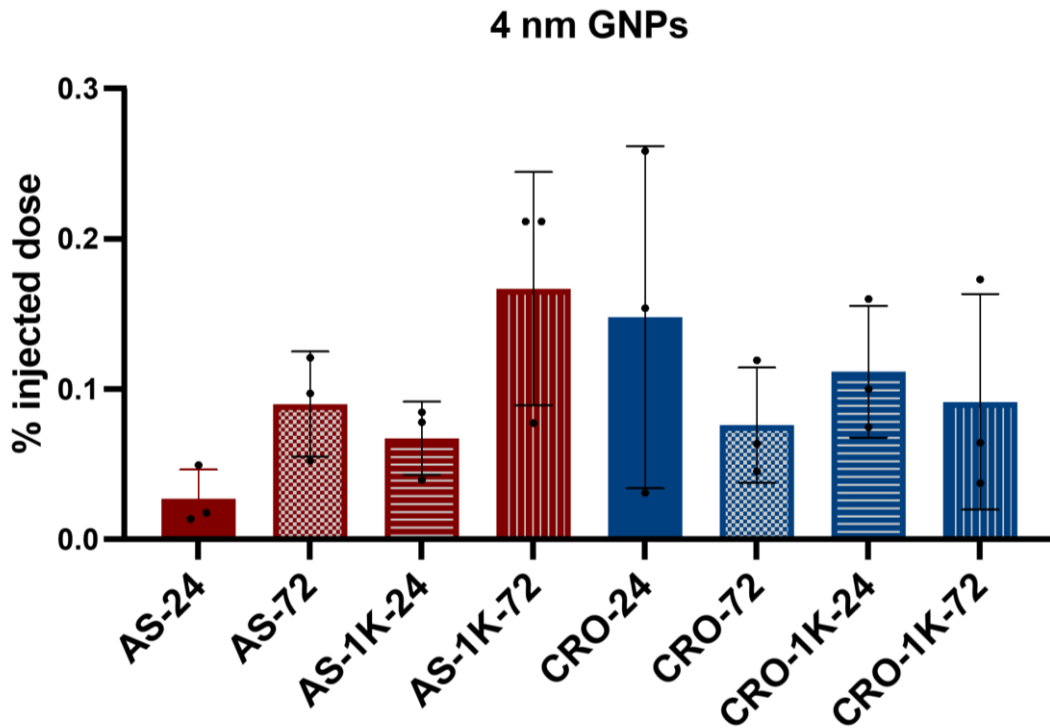


**Figure 4.11: Quantification of the uptake of 4 nm GNPs by tumor cells, the graph shows the percentage of the injected dose**

The uptake of 10 nm PEGylated GNPs-AS1411 by tumor cells was significantly higher than the other particles at 24 h ( $p = 0.0162$ ). 10 nm PEGylated GNP-CRO displayed a slight increase compare to non-PEGylated ones although the difference is non-significant, Figure 4.12. The results of the *in vivo* study revealed that PEGylation increases the uptake by tumor cells (especially 10 nm GNPs) for particles with AS1411, and in general we observed that the uptake of large particles (10 nm) by the liver and the spleen is



higher than the uptake of small ones. The results are consistent with previous findings that suggest that AS1411-GNP has a different uptake mechanism compared to other GNP (micropinocytosis vs general endocytosis) and are selectively retained in cancer cells.

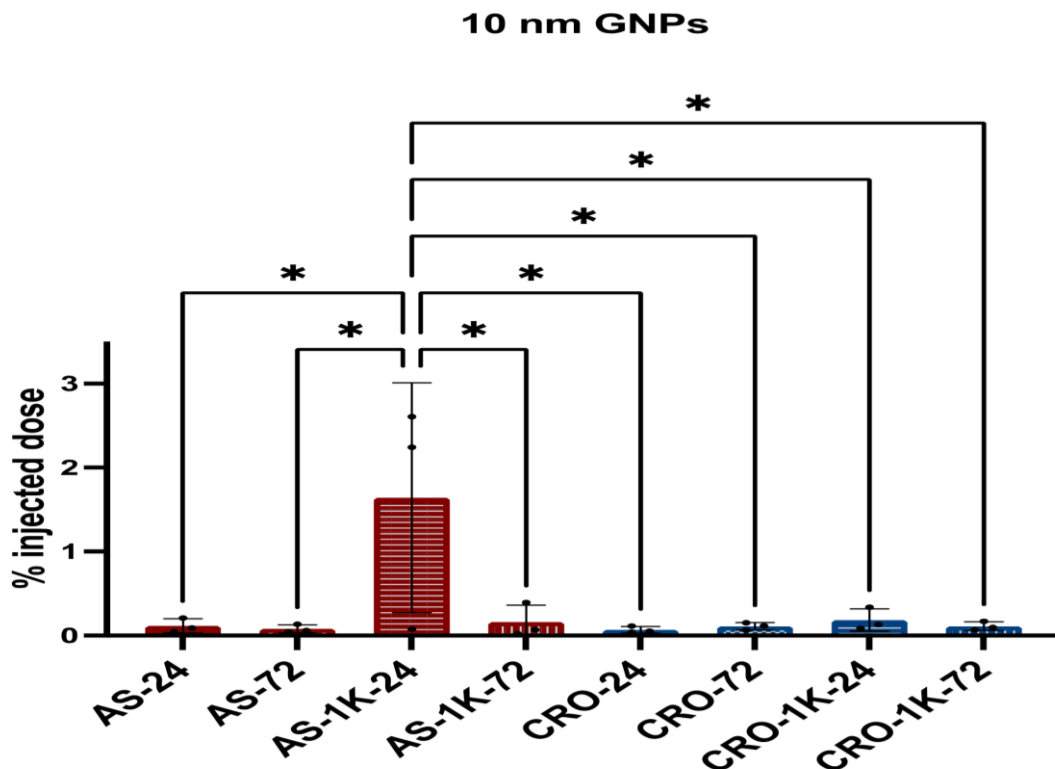


**Figure 4.12: Quantification of the uptake of 10 nm GNPs by tumor cells, the graph shows the percentage of the injected dose. \* denotes  $p < 0.05$ .**

The uptake of all types of 4 and 10 nm GNPs by the liver did not show any significance among the means of the PEGylated and non-PEGylated nanoparticle, and the same thing was observed in the spleen as well, which indicates that PEGylation did not decrease the uptake by macrophage-rich organs, nevertheless it increased the uptake by tumor cells for 10 nm GNP-Gd-AS1411-1k, Figures 4.13. and 4.14.

We used two-way ANOVA to compare between the means over the liver, spleen and tumor. Also, one-way ANOVA was used to compare between the means in each organ separately.

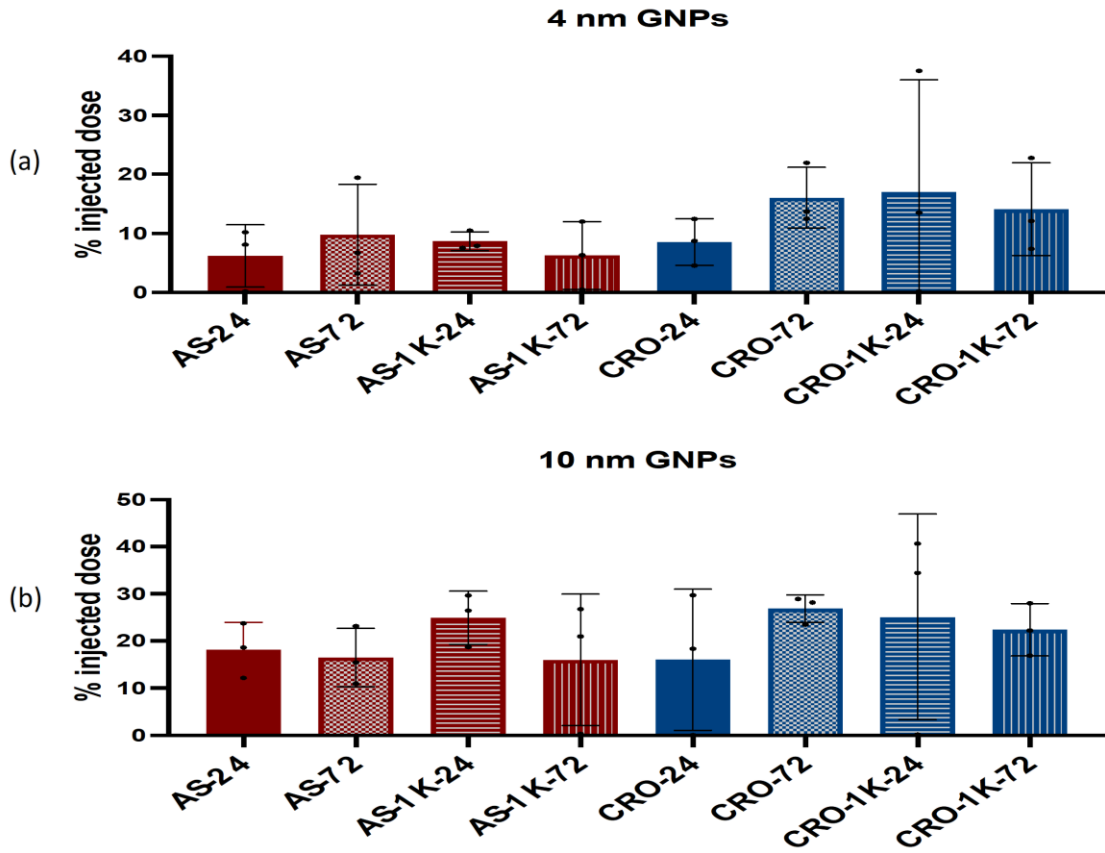


**Figure 4.13: Quantification of the uptake of GNPs by liver cells.** (a) The percentage of the injected dose of 4 nm GNPs. (b) The percentage of the injected dose of 10 nm GNPs

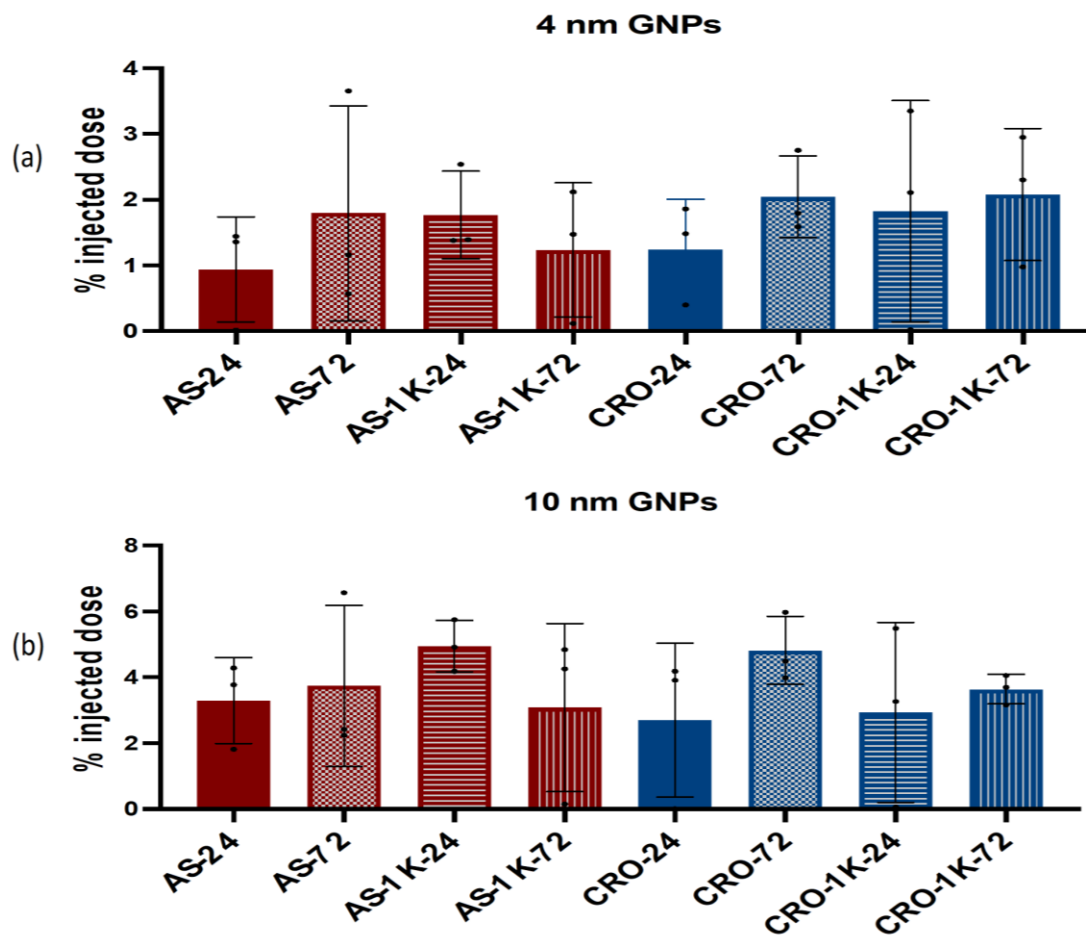


**Figure 4.14: Quantification of the uptake of GNPs by spleen cells.** (a) The percentage of the injected dose of 4 nm GNPs. (b) The percentage of the injected dose of 10 nm GNPs

**Quantification of gadolinium uptake in the tumors, liver and spleen:**

We have quantified the amount of gadolinium in the collected tumors, livers and spleen by ICP-MS after digesting them by aqua regia. The results showed that the amounts of gadolinium in liver and spleen tissues are significantly higher than the amount in tumor tissues even so they are not correlated to the corresponding amounts of GNPs, the same observation that we noted with the *in vitro* studies. Figures 4.15, 4.16, and 4.17 showed the amount of gadolinium in tumor, liver, spleen, respectively at 24 and 72 post-injection.

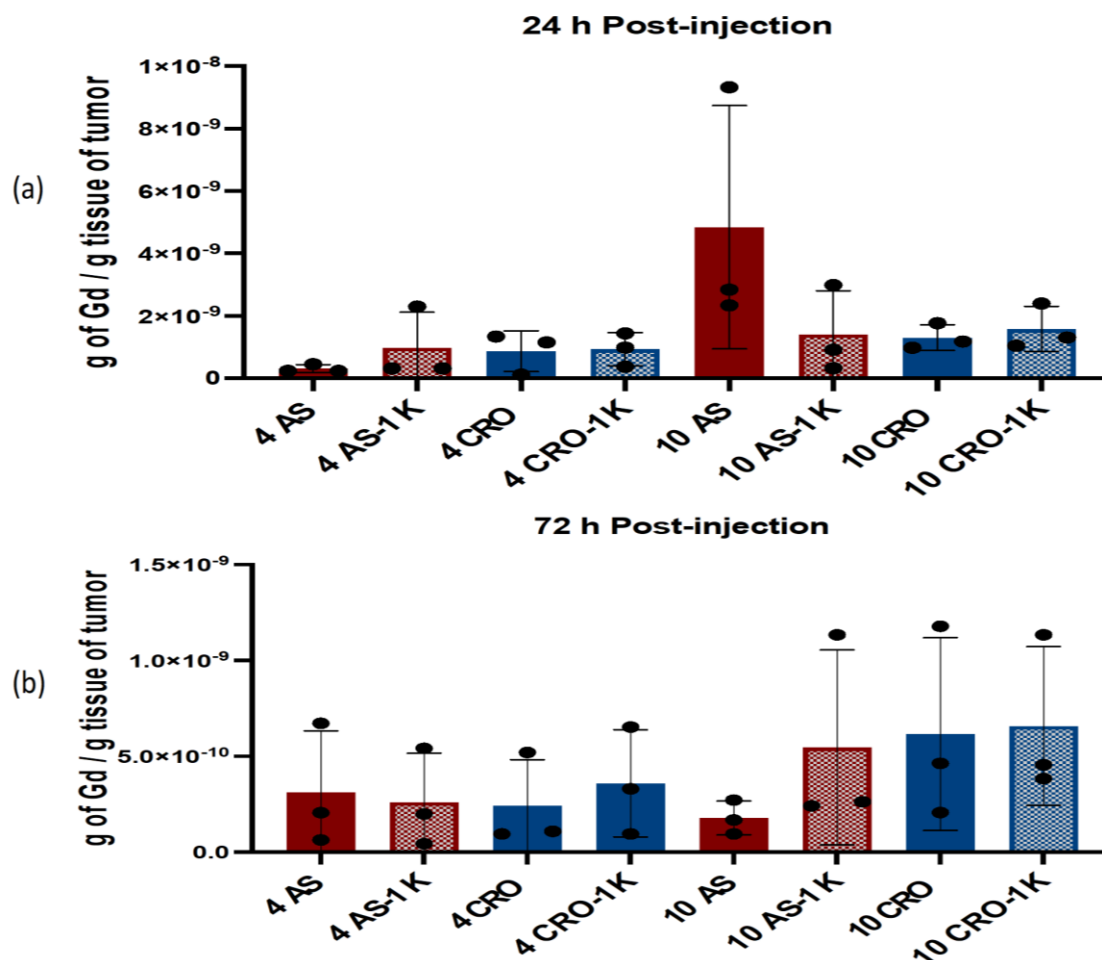


**Figure 4.15: Quantification of the amount of gadolinium in tumor tissues in g of Gd/g tissue at 24 post injection (a) and 72 post-injection (b).**

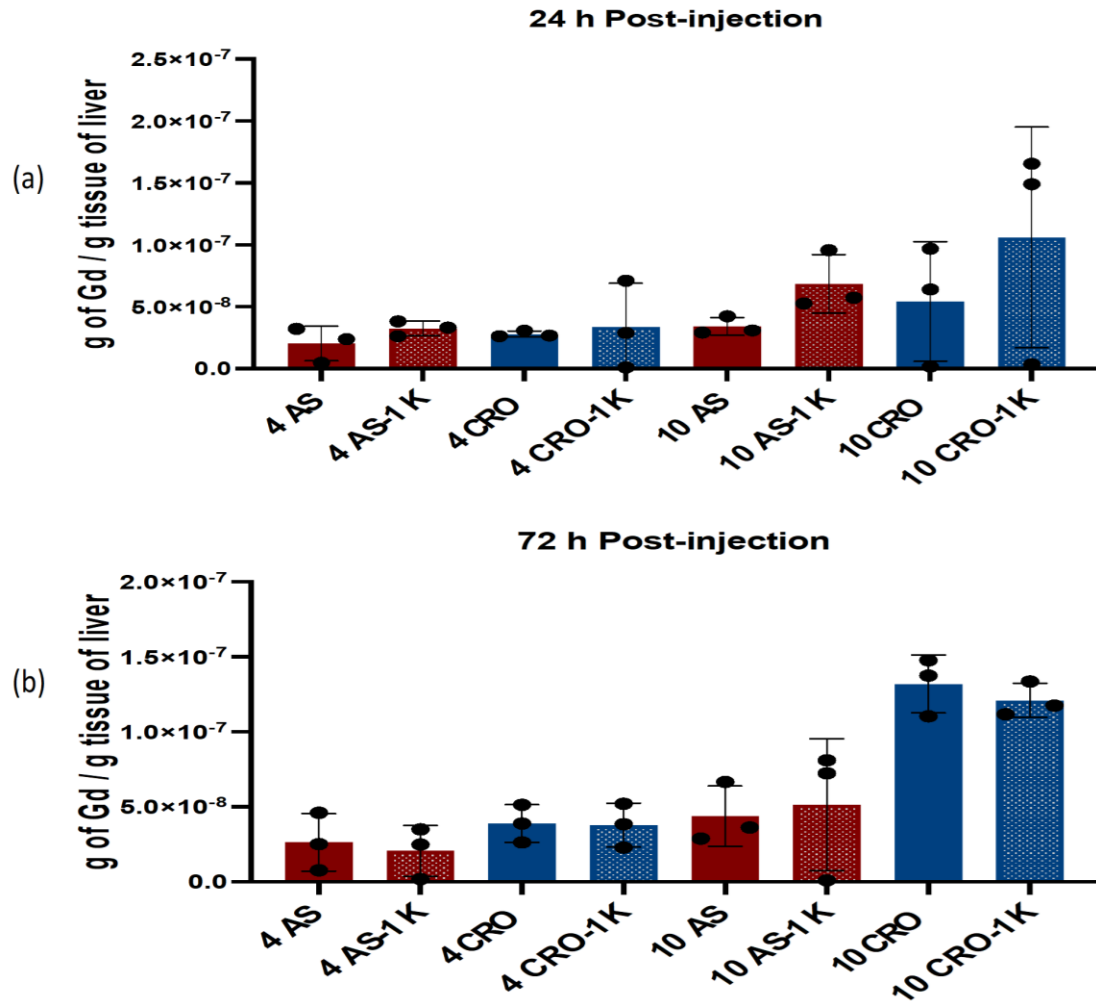


Figure 4.16: Quantification of the amount of gadolinium in liver tissues in g of Gd/g tissue at 24 post injection (a) and 72 post-injection (b).

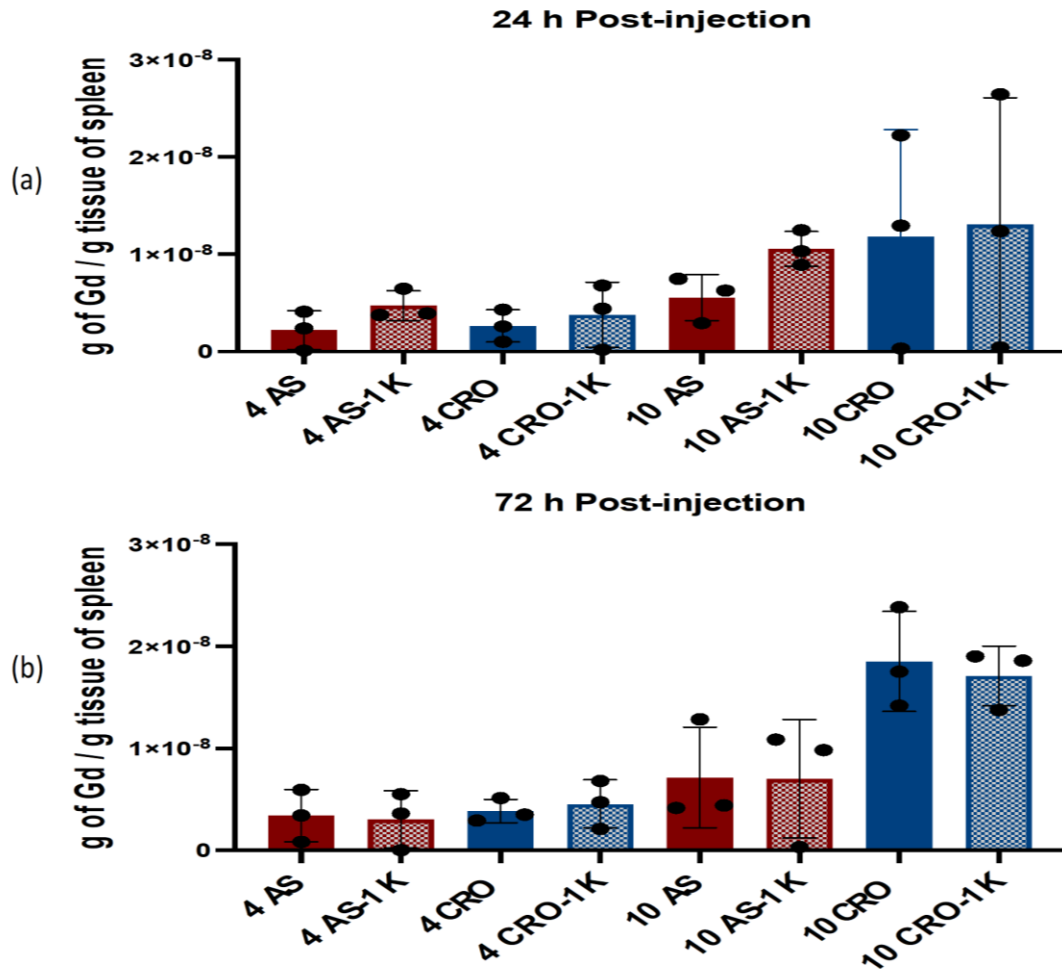


Figure 4.17: Quantification of the amount of gadolinium in spleen tissues in g of Gd/g tissue at 24 post injection (a) and 72 post-injection (b).

### 4.3. Magnetic resonance imaging (MRI) data analysis

To investigate if the amounts of gadolinium that have been delivered to the tumor cells are adequate to produce MRI contrast, we compared the amounts found in the tumors in the biodistribution study with previous data that we acquired and reported [194]. In the previous experiment, 4 nm GNPs functionalized with Gd (23 DO3A/GNP) and AS1411 (12 AS1411/GNP) at nanomolar concentrations 75, 300, and 1200 were mixed with agarose solution (7%) at a 1:1 ratio in 0.5 mL Eppendorf microcentrifuge tubes. The tubes were allowed to stand at room temperature for 30 min to solidify. Samples were mounted on a mesh grid and MRI images were acquired on a 9.4 T MRI instrument (Agilent, Santa Clara, CA, USA) for T1-W and T1 MRI measurements. All data from the 9.4T MRI system were converted to Digital Imaging and Communications in Medicine (DICOM) format using Varian NMR J (VNMRJ) 4.0 interface software (Palo Alto, CA, USA) before transferring to other software for further data processing. The contrast enhancement (relaxivity enhancement %) by 4 nm GNP-Gd-AS1411 was analyzed using a T1-weighted image analysis algorithm [194], Table 4.1, using the following equation:

$$\text{Relaxivity enhancement \%} = \frac{\sum_{i=1}^N (I_i)_{test} - (g_i)_{control}}{\sum_{i=1}^N (g_i)_{control}} \times 100$$

The control on this equation was for GNPs without gadolinium.

**Table 4.1: Relaxivity enhancement % by different concentrations of 4 nm GNP-Gd-AS1411:**

GNP concentration	Amount of Gadolinium (g)	Relaxivity enhancement %
75 nM	$3.39 \times 10^{-08}$	19
300 nM	$1.35 \times 10^{-07}$	44
1200 nM	$5.42 \times 10^{-07}$	64

In the recent *in vivo* study, the amounts of gadolinium in the digested tumor cells were quantified by ICP-MS after injecting the mice with the 8 MRI contrast agent candidates and mice were euthanized after 24 and 72 h post-injection.

Employing the data from Table 4.1, we used a 3<sup>rd</sup>-order polynomial to model the enhancement of MRI relaxivity and to estimate the enhancement of relaxivity on the test mice by applying an extrapolation technique on the estimated gadolinium quantity in each mouse that is implemented in Matlab 2021.

Tables 5 and 6 and Figures 4.18 show the estimated relaxivity enhancement % for each MRI contrast agent at 24 and 72 h post-injection respectively.

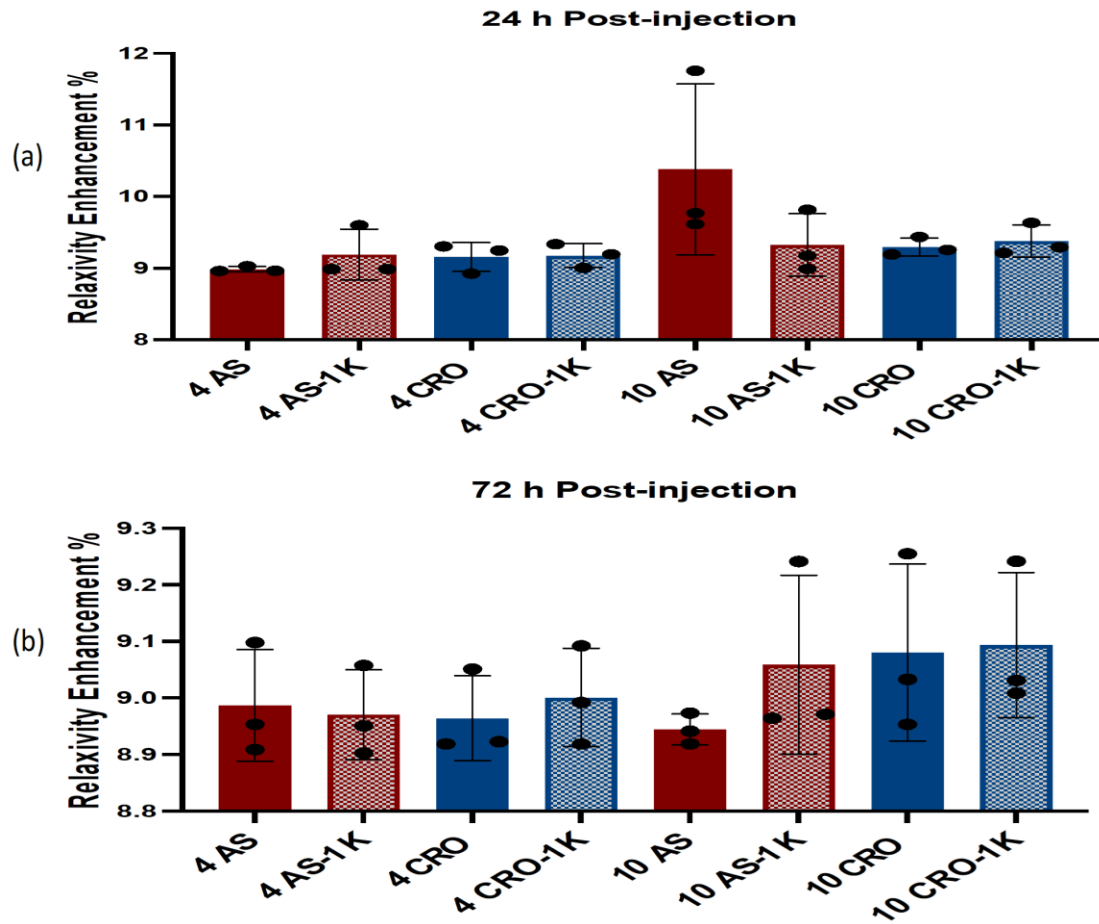


**Table 4.2: Relaxivity enhancement % of each MRI contrast agents at 24 h post-injection.**

MRI Contrast Agent	Amount of Gadolinium in g	Relaxivity enhancement %
4 nm GNP-Gd-AS1411	$3.10 \times 10^{-10}$	8.98
4 nm GNP-Gd-AS1411-1K	$9.76 \times 10^{-10}$	9.19
4 nm GNP-Gd-CRO	$7.33 \times 10^{-10}$	9.11
4 nm GNP-Gd-CRO-1k	$9.30 \times 10^{-10}$	9.17
10 nm GNP-Gd-AS1411	$4.83 \times 10^{-09}$	10.38
10 nm GNP-Gd-AS1411-1K	$1.41 \times 10^{-09}$	9.32
10 nm GNP-Gd-CRO	$1.30 \times 10^{-09}$	9.29
10 nm GNP-Gd-CRO-1K	$1.58 \times 10^{-09}$	9.38

**Table 4.3: Relaxivity enhancement % of each MRI contrast agents at 72 h post-injection.**

MRI Contrast Agent	Amount of Gadolinium in g	Relaxivity enhancement %
4 nm GNP-Gd-AS1411	$3.14 \times 10^{-10}$	8.98
4 nm GNP-Gd-AS1411-1K	$2.61 \times 10^{-10}$	8.97
4 nm GNP-Gd-CRO	$2.41 \times 10^{-10}$	8.96
4 nm GNP-Gd-CRO-1k	$3.60 \times 10^{-10}$	9.00
10 nm GNP-Gd-AS1411	$1.78 \times 10^{-10}$	8.94
10 nm GNP-Gd-AS1411-1K	$5.46 \times 10^{-10}$	9.05
10 nm GNP-Gd-CRO	$6.16 \times 10^{-10}$	9.08
10 nm GNP-Gd-CRO-1K	$6.57 \times 10^{-10}$	9.09



**Figures 4.18: Relaxivity enhancement % of each MRI contrast agents at 24 h post-injection (a) and 72 post-injection (b).**

The results showed that the estimated values of relaxivity enhancement % are not as high as the values of the previous experiment, but sufficient to enhance the MRI contrast. Along with this, we found that the higher the amount of gadolinium, the higher in the relaxivity enhancement %. In addition, we did not find a significant difference among the means of relaxivity enhancement % of PEGylated and non-PEGylated GNPs and among the means of the two-time points. Furthermore, the dissimilarity between the

aptamer did not affect the relaxivity enhancement and the differences were non-significant among the means of GNP-AS1411 and GNP-CRO.

Moreover, we observed that the highest amounts of Gd at 24 and 72 h inside the tumor cells were for 10 nm GNP-Gd-AS1411 and 10 nm GNP-Gd-CRO-1K, respectively, while the highest amounts of GNPs at 24 and 72 h were for 10 nm GNP-Gd-AS1411-1K and 4 nm GNP-Gd-AS1411-1K, respectively. This indicates that the amounts of Gd are not correlated with the corresponding amounts of GNPs. We suggest the possibility of releasing Gd from the nanoparticles during or after cellular internalization. The same phenomenon was observed in the *in vitro* studies as well, which requires more studies to investigate the stability of GNP-DO3A bond. It is also possible that some DO3A is only loosely bound to the particle through interactions with other members of the nanoparticle coating (PEG or oligonucleotide), and is released upon uptake into cells. It is worth noting that we quantified the Gd in the GNP samples before using them in our *in vitro* and *in vivo* studies and the values were correlated to the GNP and reflected the actual concentrations of Gd that we added to the nanoparticles during the synthesis.

## CHAPTER 5

### DISCUSSION And CONCLUSION

In this study, we have demonstrated the synthesis and characterization of series of GNP-based MRI contrast agents using 2 sizes of GNPs (4 and 10 nm) fabricated with a gadolinium chelate (Gd), either AS1411 or CRO oligonucleotides, and with or without PEG 1, 2, and 5 kDa.

UV-vis absorption spectrum, dynamic light scattering (DLS), and zeta potential ( $\zeta$ ) were acquired and reported to confirm particle size and the stability of the colloidal solutions.

Protein corona was purified from GNPs and quantified by BCA assay after incubation of the particles in 10% human serum for 24 h. PEGylation increased the amount of proteins binding with all GNPs containing AS1411, while it decreased protein binding to GNPs containing CRO oligonucleotide. Here, we suggest that the surface chemistry of GNPs plays a crucial role in the ability of PEG of impacting the protein corona, as the difference in the DNA sequence and the length of PEG together dictate the amount of adsorbed proteins [174, 175]. It has been reported that the density/confirmation of PEG is an important factor with the gold core size for determining the amount of proteins bound [176-179]. Additionally, we have shown that the size of particles affects the amount of bound proteins, as smaller GNPs adsorbed relatively more proteins/surface area in comparison with larger ones. This finding is supported by other reported studies [180].

The role of PEG in protein adsorption is controversial in the literature, some studies show that PEG provides a steric barrier that mitigates protein binding to nanoparticles [177,181], therefore decreasing opsonization, which is responsible for its stealth property. Adhere to this notion, studies correspond to the intensity of opsonization with the circulation half-life, as some serum proteins are recognized by the reticuloendothelial system (RES) and accelerate the blood clearance.

On the contrary, some researchers have demonstrated that PEGylation shortens the circulating time upon administration of the second dose in what is known as “accelerated blood clearance” (ABC) phenomenon due to the formation of anti-PEG IgM [182]. Albeit the effect of ABC seems temporary and scant in the third dose.

While others have reported that PEG increase the circulation time, but doesn't decrease the protein adsorption, suggesting that PEG may favorably binds to proteins that act as dysopsonin (mitigate the uptake by the RES). Furthermore, some studies have reported that some protein fragments adsorb on PEGylated particles that do not adsorb to non-PEGylated particles [183, 184].

The cellular uptake studies probed the impact of protein corona formation in the interaction of GNPs with macrophages and cancer cells. Serum proteins, including complement proteins, enhanced the uptake by macrophage cells due to recognition by complement receptors on the surface of macrophage cells. We demonstrated that the PEGylated GNPs/CRO reduced the uptake by macrophage cells with the highest reduction seen with PEG 5kDa, and the internalization of smaller-sized particles was slightly higher than the large ones [158,185]. While we noted that PEG did not mitigate the uptake of GNPs/AS1411 and indeed the highest uptake was with human serum-

contained media, such behavior is also seen in other studies, where it is reported that PEG activates the whole complement system, leading to the formation of sC5b-9 complex, also known as soluble membrane attack complex (sMAC) or terminal complement complex (TCC) (the endpoint of complement activation) [186, 187]. We suggest that the uptake by macrophage cells is related to the aptamer sequence and configuration (AS1411 forms a quadruplex structure while CRO is linear).

In contrast, serum proteins reduced the uptake of GNPs by cancer cells compared with the uptake of GNPs in serum-free media. More interestingly there was a reduction in the uptake of larger particles in comparison with the uptake of smaller ones by at least 15, and 20-fold for GNPs/AS1411 and GNPs/CRO respectively. These results are bolstered by many researchers [188-193], as it has been reported that protein corona strongly reduces the adhesion of GNPs to the cell surface and hence decreases GNPs uptake efficiency. Others also documented that the adsorbed proteins compete with the GNPs and prevent their interaction with cell surface. Further, some researchers have found that the cellular uptake of GNPs conjugated with oligonucleotides is negatively impacted by the protein corona and the intensity of internalization is dictated by density of oligonucleotides on particle surface.

The *in vivo* study investigated the uptake of our candidate contrast agents by the animal tumor model. We have excluded 2 and 5 kDa PEG as they showed a low cellular uptake by cancer cells. GNPs were injected via intraperitoneal injection. PEG significantly increased the uptake of 10 nm GNPs/AS1411 by tumor cells while the increase in uptake was non-significant for 4 nm. The uptake by macrophage-rich organs (liver and spleen) was significantly higher than the uptake by tumor cells, which seems to

be a fundamental challenge for using GNPs in biomedicine. It has been reported in the literature that the physicochemical properties of GNPs (e.g. shape, diameter, surface charge, surface loading, and hydrophobicity) dictate their interaction with the RES [127-130]. In addition, smaller particles, which have higher ratio of surface area to volume compared to larger particles, are more prone to aggregation and surface interaction with the biological components. Therefore, they distribute more in all body organs. Furthermore, the different routes of GNPs administration (e.g., intravenous, intradermal, nasal, subcutaneous, intraperitoneal, and inhalation) can evoke different immune responses. As it has been reported that the administration routes strongly affected both the magnitude and kinetics of the IgG2a response [131, 132].

In our study, we injected the mice via intraperitoneal injection (IP), which may affect the targeting and the efficacy of the particles. A group of researchers has reported that IP administration was significantly more effective in increasing the accumulation of the particles in tumor than intravenous injection (IV). Further, the area under the curve of tumors in the IP-injected group to those in the IV-injected group was 93 and 20, respectively. Also, the study showed that most of the particles accumulated in the RES after IV injection [195]. However another study has reported that injection of the particles through tail vein showed low toxic effect than the intraperitoneal administration [196].

We conclude that different route of administrations need to be investigated to determine which route is more effective and less toxic, in addition, the site of the tumor plays an important role as well.

Moreover, we assessed the ability of GNP-based MRI contrast agents to produce MRI contrast enhancement by comparing the amounts of gadolinium that have been

accumulated in tumor cells with previous data that we have acquired. The results showed that the contrast agents enhance the MRI contrast with non-significant difference between the contrast agents groups.

### **Strengths of this work**

In this dissertation, we have developed and characterized 16 different formulations of GNPs as MRI contrast agents that form stable colloidal solutions. We have quantified the protein corona upon the incubation of GNPs in 10% human serum. Also we have demonstrated the uptake of the 16 MRI contrast agents with and without protein corona by the human breast cancer cell line MDA-MB-231 and the murine monocyte/macrophage cell line RAW 264.7. The cellular uptake manifested the role of blood proteins on the cellular uptake of the two different cells.

We also have demonstrated the systemic delivery of GNPs to tumor cells through the *in vivo* study using the murine model of 4T1 mammary carcinoma in BALB/c female mice. We have used this model to evaluate the uptake of particles by tumor cell in the presence of active immune system. The proposed contrast agents showed a biological activity by enhancing the MRI contrast.

The conjugation of drugs and biomolecules with GNPs amplifies their efficacy, which leads to a decrease in the dose that is needed to achieve a desired outcome, therefore developing of GNP-based MRI contrast agent will decrease the amount of gadolinium that required to produce MRI signal, which could be beneficial to patients with compromised kidney function. In addition, conjugation of AS1411 with GNPs will help to selectively accumulation and target cancer cells.



## **Caveats and weaknesses**

We have hypothesized that PEG will mitigate the uptake by the RES and increase particles delivery to tumor cells. Results demonstrated that PEG increased the uptake by tumor cells for some contrast agents and failed to increase the delivery for others, while we could not see a significant effect on the uptake by the RES.

We have synthesized the PEGylated MRI contrast agents using one concentration of the coating agents for each particle size. The ratio of the concentrations of Gd, aptamer, and PEG to the gold concentrations was as follow: 6: 10: 6: 1 and 72: 60: 36: 1 for 4 and 10 nm, respectively. We suggest that using different concentrations of Gd, PEG and aptamer for each GNP core size could have a significant effect on the uptake by tumor and the RES, besides it will affect the enhancement of MRI contrast.

We have injected 4T1 cells in the right flank of the mice (air pouch heterotopic model), while we need to investigate the uptake of our proposed contrast agents in orthotopic murine model (injecting 4T1 in mammary fat pad) to investigate the impact of the tumor inoculation site in the tumor microenvironment and how this impact the particles delivery.

## **Future Directions:**

Using GNPs with different densities of coating agents could change the biological fate of the particles. The ratio of the concentration of PEG, Gd, and AS1411 will be modified to investigate which formula attains the highest uptake by tumor cells and which one achieves the lowest uptake by the reticuloendothelial cell cells, further,

scanning the live animal by MRI scanner after injection by the GNPs at different time points will be acquired. Addition to, different route of injection will be applied to.

In addition, the toxicity of the proposed contrast agents needs to be investigated. We have performed a general health profile chemistry analysis of 4 nm GNP conjugated gadolinium and either AS1411 or CRO in a previous study [197]. 50 Sprague Dawley (Crl: SD) rats were injected with the particles and phosphate buffer saline (PBS) as a control. Blood were collected from rats after 2 and 14 days post-injection. Five blood biomarker: alkaline phosphate (ALP), alanine transaminase (ALT), creatinine (CREA), total bilirubin (TBIL) and blood urea nitrogen (BUN) were obtained to evaluate liver and kidney functions. The blood biomarkers values of the test samples were compared to the biomarkers of the PBS and there were no significant difference among the means.

However more histopathological studies are required to determine any damage or abnormalities in the tissues of the organs, especially in liver and spleen.

## REFERENCES

- 1- Han G., Ghosh P., and Rotello V. "Multi-functional gold nanoparticles for drug delivery". Bio-applications of nanoparticles. 1st ed.; Warren C. W. Chan.; Springer. New York, NY, USA 2007; 620:48-56.
- 2- N. Khlebtsov and L. Dykman, "Biodistribution and toxicity of engineered gold nanoparticles: a review of *in vitro* and *in vivo* studies", *Chem Soc Rev.* 2011, 40(3), 1647-1671.
- 3- L. Dykman and N. Khlebtsov, "Gold nanoparticles in biomedical applications: recent advances and perspectives ", *Chem Soc Rev*, 2012.
- 4- The Keeley "Gold Cure" for Inebriety. *Br Med J.* 1892 Jul 9;2(1645):85-6
- 5- Ochsner E.H. "The use of colloidal gold in inoperable cancer", *Int. J. Med. Surg.* 1927.V.40.P.100-104.
- 6- Faulk, W. and Taylor, M., "An immunocolloid method for the electron microscope", *Immunochemistry*, 1971, 8, 1081–1083.
- 7- Freitas, L., Varca, G., Batista, J., and Lugao, A., "An Overview of the Synthesis of Gold Nanoparticles Using Radiation Technologies" *Nanomaterials*, 2018, 8(11): 939.
- 8- Buxton, G.V. "Radiation Chemistry: Principles and Applications". Verlag Chemie Publishers; Weinheim, Germany: 1987.
- 9- Soumya D. Critical Review of Water Radiolysis Processes, Dissociation Products, and Possible Impacts on the Local Environment: A Geochemist's Perspective. *Aust. J. Chem.* 2013;66:522–529.
- 10- S. Menon, Rajeshkumar S., V. Kumar S. "A review on biogenic synthesis of gold nanoparticles, characterization, and its applications", *Resource-Efficient Technologies*, 2017, Pages 516-527
- 11- Timoszyk A., "A review of the biological synthesis of gold nanoparticles using fruit extracts: scientific potential and application", *Bull. Mater Sci*, 2018, 41(6):154.
- 12- Mittal A K, Chisti Y and Banerjee U Ch, "Synthesis of metallic nanoparticles using plant extracts, *Biotechnol. Adv*, 2013, **31** 346.

- 13- Shankar S S, Ahmad A, Pasricha R and Sastr M, “Bioreduction of chloroaurate ions by geranium leaves and its endophytic fungus yields gold nanoparticles of different shapes”, *J. Mater Chem.*, 2003 13 1822.
- 14- Mittal J, Batra A, Singh A and Sharma M, “Phytofabrication of nanoparticles through plant as nanofactories”, *J. Nanosci Nanotechnol.*, 2014, 5 043002.
- 15- Santhoshkumar, Rajeshkumar S and Venkat Kumar S, “Phyto-assisted synthesis, characterization and applications of gold nanoparticles - A review”, *Biochem. Biophys. Rep.*, 2017, 21;11:46-57.
- 16- Makarov V V, Love A J, Sinitsyna O V, Makarova S S, Yamin- skyIV, “Green Nanotechnologies Synthesis of Metal Nanoparticles using Plant”, *ActaNat.*, 2013, 135.
- 17- Ahmad A, Mukherjee P, Senapati S, Mandal D, Khan MI, Kumar R, Sastry M, “Extracellular biosynthesis of silver nanoparticles using the fungus *Fusarium oxysporum*”, *Biointerfaces*, 2003, 28, 313–318.
- 18- Mandal D, Bolander ME, Mukhopadhyay D, Sarkar G, Mukherjee P, “The use of microorganisms for the formation of metal nanoparticles and their application” *Appl Microbiol Biotechnol*, 2006, 69, 485–492.
- 19- Patra CR, Bhattacharya R, Mukherjee P. “Fabrication and functional characterization of goldnanoconjugates for potential application in ovarian cancer”, *J. Mater. Chem.*, 2010;20:547–554.
- 20- Liu YL, Male KB, Bouvrette P, Luong JHT. “Control of the Size and Distribution of Gold Nanoparticles by Unmodified Cyclodextrins”, *Chem. Mater.* 2003;15:4172–4180.
- 21- Turkevich J, Stevenson PC, Hillier J. “A study of the nucleation and growth processes in the synthesis of colloidal gold”, *Discuss Faraday Soc.*, 1951;1 :55-75.
- 22- Chen DH., Chen CJ., “Formation and characterization of Au-Ag bimetallic nanoparticles in water-in-oil microemulsions”, *J. Mater. Chem.* 2002;12:1557–1562
- 23- Pastoriza-Santos I, Liz-Marzan LM. “Formation of PVP-Protected Metal Nanoparticles in DMF”, *Langmuir* 2002;18: 2888–2894.
- 24- Dong J, Carpinone P, Pyrgiotakis G, Demokritou Ph, and Moudgil B, “Synthesis of Precision Gold Nanoparticles Using Turkevich Method”, *Kona*, 2019, 10;37:224-232.
- 25- Frens G. *Kolloid-Zeitschrift and Zeitschrift Fur Polymere*, “Particle size and sol stability in metal colloids” *Originalarbeiten*, 1972;250:736–741.
- 26- Frens G. “Controlled Nucleation for the Regulation of the Particle Size in Monodisperse Gold Suspensions”, *Nat. Phys. Sci.*, 1973; 241:20–22.

- 27- Brust M, Walker M, Bethell D, Schiffrin DJ, Whyman R. "Synthesis of thiol-derivatised gold nanoparticles in a two-phase Liquid–Liquid system", *J. Chem. Soc, Chem. Comm.*,1994; 801–802.
- 28- Yi-Cheun Yeh, Brian Creran, and, Vincent Rotello," Gold Nanoparticles: Preparation, Properties, and Applications in Bionanotechnology" *Nanoscale*, 2012, 4,1871-1880.
- 29- Jain PK, Lee KS, El-Sayed IH, El-Sayed MA. "Calculated absorption and scattering properties of gold nanoparticles of different size, shape, and composition: applications in biological imaging and biomedicine", *J. Phys. Chem. B*. 2006; 110:7238–7248.
- 30- Eustis S, El-Sayed MA. "Why gold nanoparticles are more precious than pretty gold: Noble metal surface plasmon resonance and its enhancement of the radiative and nonradiative properties of nanocrystals of different shapes", *Chem. Soc. Rev.*, 2006;35:209–217.
- 31- Mie G. Ann, "Contributions to the optics of turbid media, particularly of colloidal metal solutions", *Phys.* 1908;25:377–445.
- 32- Templeton AC, Pietron JJ, Murray RW, Mulvaney P. "Solvent Refractive Index and Core Charge Influences on the Surface Plasmon Absorbance of Alkanethiolate Monolayer-Protected Gold Clusters" *J. Phys. Chem. B*. 2000;104:564–570.
- 33- Su KH, Wei QH, Zhang X, Mock JJ, Smith DR, Schultz S. "Interparticle Coupling Effects on Plasmon Resonances of Nanogold Particles", *Nano Lett.* 2003;3:1087–1090.
- 34- Elhai N, Kamali M, Baghersad H, " Recent biomedical applications of gold nanoparticles: A review", *Talanta*, 2018, vol. 184, Pages 537-556.
- 35- X. Ye, Y. Gao, J. Chen, D.C. Reifsnnyder, C.Zheng, C.B. Murray, "Seeded growth of monodisperse gold nanorods using bromide-free surfactant mixtures", *Nano Lett.*, 2013, 13, 5, 2163–2171.
- 36- Hill H, Mirkin Ch, "The bio-barcode assay for the detection of protein and nucleic acid targets using DTT-induced ligand exchange" *Nat. Protoc.*, 2006, 1, pages 324–336
- 37- Thaxton CS, Elghanian R, Thomas AD, Stoeva SI, Lee J-S, Smith ND, J.Schaeffer A, Klocker H, Horninger W, Bartsch G, Mirkin CA. "Nanoparticle-based bio-barcode assay redefines "undetectable" PSA and biochemical recurrence after radical prostatectomy", *Proc. Natl. Acad. Sci.* 2009;106:18437–18442.
- 38- Huang X, Kang B, Qian W, Mackey MA, Chen PC, Oyelere AK, El-Sayed IH, El-Sayed MA, "Comparative study of photothermolysis of cancer cells with nuclear-targeted or

- cytoplasm-targeted gold nanospheres: continuous wave or pulsed lasers”, *J Biomed Opt.* 2010; 15(5):058002.
- 39- Berciaud S, Cognet L, Blab GA, Lounis B. “Photothermal Heterodyne Imaging of Individual Nonfluorescent Nanoclusters and Nanocrystals”, *Phys. Rev. Lett.* 2004; 93:257402.
- 40- Kim CS, Wilder-Smith P, Ahn Y-C, Liaw L-HL, Chen Z, Kwon YJ. “Enhanced detection of early-stage oral cancer *in vivo* by optical coherence tomography using multimodal delivery of gold nanoparticles”, *J.Biomed. Opt.* 2009; 14:034008.
- 41- Zagaynova EV, Shirmanova MV, Kirillin MY, Khlebtsov BN, Orlova AG, Balalaeva IV, Sirotkina MA, Bugrova ML, Agrba PD, Kamensky VA. “Contrasting properties of gold nanoparticles for optical coherence tomography: phantom, *in vivo* studies and Monte Carlo simulation”, *Phys. Med. Biol.*, 2008; 53:4995–5009.
- 42- Zavaleta CL, Smith BR, Walton I, Doering W, Davis G, Shojaei B, J.Natan M, Gambhir SS. “Multiplexed imaging of surface enhanced Raman scattering nanotags in living mice using noninvasive Raman spectroscopy” *Proc. Natl. Acad. Sci.*, 2009, 106, 13511-13516.
- 43- Kattumuri, V., Katti, K., Bhaskaran, SH., Boote, E., Casteel, S., Fent, G., Robertson, D., Chandrasekhar, M., Kannan, R., Katti, K. “Gum arabic as a phytochemical construct for the stabilization of gold nanoparticles: *in vivo* pharmacokinetics and X-ray-contrast-imaging studies”, *Small*, 2007;3:333–341.
- 44- Hainfeld JF, Slatkin DN, Focella TM, Smilowitz HM. “Gold nanoparticles: a new X-ray contrast agent”, *Br J Radiol*, 2006;79:248–253.
- 45- Meir, R., Shamalov, K., Betzer, O., Motiei, M., Horovitz-Fried, M., Yehuda, R., Popovtzer, A., Popovtzer, R., and Cohen, “Nanomedicine for Cancer Immunotherapy: Tracking Cancer-Specific T-Cells *In Vivo* with Gold Nanoparticles and CT Imaging”, *ACS. Nano.* 2015; (9)6, 6363–6372.
- 46- Cao, Y., He, Y., Liu, H., Luo, Y., Shen, M., Xia, J., Shi, X. “Targeted CT imaging of human hepatocellular carcinoma using low-generation dendrimer entrapped gold nanoparticles modified with lactobionic acid”, *J Mater Chem B.*, 2015, 14;3(2):286-295.
- 47- Lux, J., and Sherry, A. “Advance in gadolinium-based MRI contrast agent designs for monitoring biological processes *in vivo*”, *Curr Opin Chem Biol*, 2018, 45:121-130.
- 48- Milne, M., Gobbo, P., McVicar, N., Bartha, R., Workentin, M., and Hudson, R. “water-soluble gold nanoparticles (AuNP) functionalized with a gadolinium (III) chelate via Michael addition for use as a MRI contrast agent”, *J. Mater. Chem. B.*, 2013, 1, 5628-5635.
- 49- Perry, H., Botnar, R., and Wilton-Ely, J., “Gold nanomaterials functionalized with gadolinium chelates and their application in multimodal imaging and therapy”, *Chem. Commun.*, 2020, 56, 4037-4046.

- 50- Conde, J., Tian, F., Baptista, P.V., de la Fuente, J.M. (2014). "Multifunctional Gold Nanocarriers for Cancer Theranostics: From Bench to Bedside and Back Again?". In: Alonso, M., Garcia-Fuentes, M. (eds) *Nano-Oncologicals. Advances in Delivery Science and Technology*. Springer, Cham.
- 51- Ma, J., Liu, Y., Gao, P. F., Zou, H. Y., & Huang, C. Z. "Precision improvement in dark-field microscopy imaging by using gold nanoparticles as an internal reference: a combined theoretical and experimental study", *Nanoscale*, 2016; 8(16), 8729–8736.
- 52- Patskovsky, S., Bergeron, E., Meunier, M. "Hyperpectral darkfield microscopy of PEGylated gold nanoparticle targeting CD44-expressing cancer cells", *J Biophotonics*, 2015, 8(1-2): 162-7.
- 53- Qian, W., Huang, X., Kang, B., & El-Sayed, M. A. "Dark- field light scattering imaging of living cancer cell component from birth through division using bioconjugated gold nanoprobes", *J. Biomed. Opt.*, 2010;15(4), 046025–046025-9.
- 54- Mieszawska, A. J., Mulder, W. J. M., Fayad, Z. A., & Cormode, D. P., "Multifunctional Gold Nanoparticles for Diagnosis and Therapy of Disease," *Mol. Pharm.*, 2013; vol. 10, no. 3, pp. 831-847.
- 55- Cordeiro, M., Ferreira Carlos, F., Pedrosa, P., Lopez, A., & Baptista, P. V. "Gold nanoparticles for diagnostics: advances towards points of care", *Diagnostics*, 2016; 6(4), 43.
- 56- Kang, J. W., So, P. T. C., Dasari, R. R., & Lim, D. K. "High resolution live cell Raman imaging using subcellular organelle-targeting SERS-sensitive gold nanoparticles with highly narrow intra-nanogap", *Nano Lett.* 2015; 15(3), 1766–1772.
- 57- Li, W., & Chen, X. "Gold nanoparticles for photoacoustic imaging". *Nanomedicine*. 2015; 10(2), 299–320.
- 58- Song, J., Kim J., Hwang, S., Jeon, M., Jeong, S., Kim, Ch., Kim, S. "Smart gold nanoparticles for photo- acoustic imaging: an imaging contrast agent responsive to the cancer microenvironment and signal amplification via pH-induced aggregation", *Chem. Comm.* 2016; 52(53), 8287–8290.
- 59- Huang, X., Jain, P. K., El-Sayed, I., and El-Sayed, M. "Plasmonic photothermal therapy (PPTT) using gold nanoparticles", *Lasers Med. Sci.* 2008; 23, 217–228.
- 60- Minton, J., Carlton, D., Dearman, J., McKnight, W., and Ketcham, A. "An evaluation of physical response of malignant tumor implants to pulsed laser radiation", *Surg. Gynaecol. Obstet.* 1965; 121, 538–544.
- 61- L. C. Kennedy, L. R. Bickford, N. A. Lewinski, A. J. Coughlin, Y. Hu, E. S. Day, J. L. West and R. A. "Drezek. A new era for cancer treatment: gold-nanoparticle-mediated thermal therapies", *Small*, 2011, 7, 169–183.
- 62- Pitsillides, C., Joe, E., Wei, X., Anderson R., and Lin, C. "Selective cell targeting with light-absorbing microparticles and nanoparticles", *Biophys. J.*, 2003, 84, 4023–4032.

- 63- Eun Ji Hong, Dae Gun Choi, Min Suk Shim. “Targeted and Effective Photodynamic Therapy For Cancer Using Functionalized Nanomaterials”. *Acta Pharmaceutica Sinica B*, 2016, volume 6, Pages 297-307.
- 64- B. C. Wilson, in *Handbook of Photonics for Biomedical Science*, ed. V. V. Tuchin, CRC Press, Boca Raton, 2010, pp. 649–686.
- 65- R. Wilson. “The use of gold nanoparticles in diagnostics and detection”, *Chem. Soc. Rev.*, 2008, 37, 2028–2045.
- 66- Bardhan, R., Grady, N., Cole, J., Joshi, A., and Halas, N. “Fluorescence enhancement by Au nanostructures: nanoshells and nanorods” *ACS Nano*, 2009, 3, 744–752.
- 67- Ming, T., Zhao, L., Chen, H., Woo, K., Wang, J., and Lin, H-Q, “Experimental evidence of plasmophores: plasmon-directed polarized emission from gold nanorod-fluorophore hybrid nanostructures”, *Nano Lett.* 2011; 11, 2296–2303.
- 68- Jing Lin, Shouju Wang, Peng Huang, Zhe Wang, Shouhui Chen, Gang Niu, Wanwan Li, Jie He, Daxiang Cui, Guangming Lu, Xiaoyuan Chen, and Zhihong Nile. “Photosensitizer-Loaded gold vesicles with strong plasmonic coupling effect for imaging-guided photothermal/photodynamic therapy”, *ACS Nano*. 2013; 7, 6, 5320–5329.
- 69- Farooq, M., Novosad, V., Rozhkova, E., Wali, H., Ali, A., Fateh, A., Neogi, P., Neogi, A., and Wang, Z. “Gold nanoparticles enabled efficient dual delivery of anticancer therapeutics to Hela cells”, *Nature Sci. Rep.* 2018, 8, 2907.
- 70- Han, G., Ghosh, P., and Rotello, V. “Functionalized gold nanoparticles for drug delivery”, *Nanomedicine*, 2007, 2,1.
- 71- Kim, CK., Ghosh, P., Pagliuca, C., Zhu, ZJ., Menichetti, S., Rotello, VM. “Entrapment of hydrophobic drugs in nanoparticle monolayers with efficient release into cancer cells”, *J Am Chem Soc.* 2009; Feb 4; 131(4):1360-1.
- 72- Zhang, XQ., Xu, X., Lam, R., Giljohann, D., Ho, D., Mirkin, CA. “Strategy for increasing drug solubility and efficacy through covalent attachment to polyvalent DNA-nanoparticle conjugates”, *ACS Nano*. 2011 Sep 27; 5(9):6962-70.
- 73- Giljohann, DA., Seferos, DS., Prigodich, AE., Patel, PC., Mirkin, CA. “Gene regulation with polyvalent siRNA-nanoparticle conjugates”, *J Am Chem Soc.* 2009 Feb 18; 131(6):2072-3.
- 74- Lee, SK., Han, MS., Asokan, S., Tung, CH. “Effective gene silencing by multilayered siRNA-coated gold nanoparticles”, *Small*. 2011; 7(3):364-70.
- 75- Yuan, F., Dellian, M., Fukumura, D., Leunig, M., Berk, DA., Torchilin, VP., Jain, RK. “Vascular permeability in a human tumor xenograft: molecular size dependence and cutoff size”, *Cancer Res.* 1995 Sep 1; 55(17):3752-6.
- 76- Yuan, F., Leunig, M., Huang, SK., Berk, DA., Papahadjopoulos, D., Jain, RK. “Microvascular permeability and interstitial penetration of sterically stabilized (stealth) liposomes in a human tumor xenograft”, *Cancer Res.* 1994; 54(13):3352-6.



- 77- Pluen, A., Boucher, Y., Ramanujan, S., McKee, TD., Gohongi, T., di Tomaso, E., Brown, E., Izumi, Y., Campbell, R., Berk, DA., Jain, R. "Role of tumor-host interactions in interstitial diffusion of macromolecules: cranial vs. subcutaneous tumors", *Proc Natl Acad Sci.*, 2001 Apr 10; 98(8):4628-33.
- 78- Maeda H. Review "Tumor-selective delivery of macromolecular drugs via the EPR effect: background and future prospects". *Bioconjug Chem.* 2010, 21(5):797-802.
- 79- Dreaden, E., Mwakwari, S., Sodji, Q., Oyelere, A., El-Sayed M. "Tamoxifen-poly(ethylene glycol)-thiol gold nanoparticle conjugates: enhanced potency and selective delivery for breast cancer treatment", *Bioconjug Chem.* 2009 Dec; 20(12):2247-53.
- 80- Dhar, S., Reddy, EM., Shiras, A., Pokharkar, V., Prasad, BL. "Natural gum reduced/stabilized gold nanoparticles for drug delivery formulations", *Chemistry*, 2008; 14(33):10244-50.
- 81- Brown, S., Nativo, P., Smith, J., Stirling, D., Edwards, PR., Venugopal, B., Flint, DJ., Plumb, JA., Graham, D., Wheate, NJ. "Gold nanoparticles for the improved anticancer drug delivery of the active component of oxaliplatin", *J Am Chem Soc.* 2010 Apr 7; 132(13):4678-84.
- 82- Paciotti, G., Zhao, J., Cao, Sh., Brodie, P., Tamarkin, L., Huhta, M., Myer, L., Friedman, J., and Knigston, D. "Synthesis and Evaluation of Paclitaxel-Loaded Gold Nanoparticles for Tumor-Targeted Drug Delivery". *Bioconjug Chem.* 2016, 27, 11, 2646–2657.
- 83- Chen, Y., Tsai, C., Huang, P., Chang, M., Cheng, P., Chou, C., Chen, D., Wang, C., Shiau, A., and Wu. C. "Methotrexate conjugated to gold nanoparticles inhibits tumor growth in a syngeneic lung tumor model", *Mol. Pharm.*, 2007, 4, 713–722.
- 84- Li, J., Wang, X., Wang, C., Chen, C., Dai, Y., Zhang, R., Song, M., Lv G., and Fu, D. "The Enhancement Effect of Gold Nanoparticles in Drug Delivery and as Biomarkers of Drug-Resistant Cancer Cells", *Chem. Med. Chem.*, 2007, 2, 374–378.
- 85- Huai, Y., Zhang, Y., Xiong, X., Das, SH., Bhattacharya, R., and Mukherjee, P. "Gold Nanoparticles sensitize pancreatic cancer cells to gemcitabine". *Cell Stress.* 2019 Aug; 3(8): 267–279.
- 86- Lundell, S., Brown A., Santora, A., Romanelli, S., Banerjee, I. "Development of Self-Assembled Gold Nanoparticle Bound Amino Hydroxy Mercaptopurine Hybrids as Sensors for DNA Binding", *Nano Hybrids and Composites*, 2018; Vol 18, 20-33.
- 87- Agasti, S., Chompoosor, A., You, C., Ghosh, P., Kim C., and Rotello. "Photoregulated Release of Caged Anticancer Drugs from Gold Nanoparticles", *V. J. Am. Chem. Soc.*, 2009, 131, 5728–5729.
- 88- Patra, C., Bhattacharya, R., and Mukherjee, P. "Fabrication and Functional Characterization of Goldnanoconjugates for Potential Application in Ovarian Cancer". *J. Mater. Chem.*, 2010; 20, 547–554.

- 89- Eghtedari, M., Liopo, A., Copland, J., Oraevsky, A., and Motamedi, M. “Engineering of Hetero-Functional Gold Nanorods for the in vivo Molecular Targeting of Breast Cancer Cells”, *Nano Lett.*, 2009, 9, 287–291. <sup>[1]</sup> <sub>[SEP]</sub>
- 90- Park, C., Youn, H., Kim, H., Noh, T., Kook, Y., Oh, E., Park, H., and Kim, C. J. “Cyclodextrin-covered gold nanoparticles for targeted delivery of an anti-cancer drug”, *Mater. Chem.*, 2009; 19, 2310–2315.
- 91- Rosi, N., Giljohann, D., Thaxton, C., Lytton-Jean, A., Han, M., Mirkin, Ch. “Oligonucleotide-modified gold nanoparticles for intracellular gene regulation”, *Science*, 312 (2006), pp. 1027-1030.
- 92- Giljohann, D., Seferos, D., Prigodich, A., Patel, P., Mirkin, Ch. “Gene regulation with polyvalent siRNA-nanoparticle conjugates”, *J Am Chem Soc*, 131 (2009), pp. 2072-2073.
- 93- Patel, P., Giljohann, D., Seferos, D., Mirkin, Ch. “Peptide antisense nanoparticles”, *Proc Natl Acad Sci*, 105 (2008), pp. 17222-17226.
- 94- Hao, L., Patel, P., Alhasan, A., Mirkin, D. “Nucleic acid-gold nanoparticle conjugates as mimics of microRNA”, *Small*, 2011, 18:7(22):3158-62.
- 95- Williams, D., Ehrman, S., Holoman, T. “Evaluation of the microbial growth response to inorganic nanoparticles”, *J. Nanobiotechnol*, 2006, 4, 38;4:3.
- 96- Rai, A., Prabhune, A., and Perry, C. “Antibiotics mediated synthesis of gold nanoparticles with potent antimicrobial activity and their application in antimicrobial coating”, *J. Mater. Chem.*, 2010.
- 97- Selvaraj, V., Alagar, M. “Analytical detection and biological assay of antileukemic drug 5-fluorouracil using gold nanoparticles as probe”, *Int J Pharm* 2007; 337:275–81.
- 98- Saha, B., Bhattacharya, J., Mukherjee, A., Ghosh, A., Santra, C., Dasgupta, A., and Karmakar, P. “In Vitro Structural and Functional Evaluation of Gold Nanoparticles Conjugated Antibiotics”, *Nanoscale Res. Lett.*, 2007, 2, 614–622.
- 99- Grace, A., and Pandian, K. “Antibacterial efficacy of aminoglycosidic antibiotics protected gold nanoparticles—A brief study”, *Colloids Surf.*, 2007, 297, 63–70.
- 100- Bowman, M., Ballard, T., Ackerson, C., Feldheim, D., Margolis, D., and Melander, C. “Inhibition of HIV Fusion with Multivalent Gold Nanoparticles”, *J. Am. Chem. Soc.*, 2008, 130, 6896–6897.
- 101- Joshi, H., Bhumkar, D., Joshi, K., Pokharkar, V., and Sastry, M. Chitosan “Reduced Gold Nanoparticles as Novel Carriers for Transmucosal Delivery of Insulin”, *Langmuir*, 2006, 22, 300–305.
- 102- Nie, Z., Liu, K., Zhong, C., Wang, L., Yang, Y., Tian, Q., and Liu, Y. “Enhanced radical scavenging activity by antioxidant-functionalized gold nanoparticles: a novel inspiration for development of new artificial antioxidants”, *Free Radical Biol. Med.*, 2007, 43, 1243–1254.

- 103- Pan, F., Yang, W., Li, W., Yang, X., Liu, Sh., Li, X., Zhao, X., Ding, H., Qin, L., and Pan, Y. "Conjugation of gold nanoparticles and recombinant human endostatin modulates vascular normalization via interruption of anterior gradient 2-mediated angiogenesis", *Tumour Bio*. 2017, Jul;39(7):1010428317708547.
- 104- Kemp, M., Kumar, A., Mousa, Sh., Dyskin, E., Yaicin M., Ajayan, P., Linhardt, R., and Mousa, Sh. "Gold and silver nanoparticles conjugated with heparin derivative possess anti-angiogenesis properties". *Nanotechnology*. 2009. 11;20(45):455104.
- 105- Song, H., Wi, J., Jo, D., Kim, Ji., Lee, S., Lee, T., Kim, Je. "Intraocular application of gold nanodisks optically tuned for optical coherence tomography: inhibitory effect on retinal neovascularization without unbearable toxicity", *Nanomedicine*. 2017. Aug;13(6):1901-1911.
- 106- Pan, F., Li, W., Yang, W., Yang, X., Liu, Sh., Li, X., Zaho, X., Ding, H., Qin, L., and Pan, Y. "Anterior gradient 2 as a supervisory marker for tumor vessel normalization induced by anti-angiogenic treatment", *Oncol Let*. 2018. Sep;16(3):3083-3091.
- 107- Jo, D., Hong, J., Kim, Ji., Han, S., and Kim Je. "Gold Nanocrystals with Well-Defined Crystallographic {111} Facets Suppress Pathological Neovascularization", *J Biomed Nanotechnol*. 2016. PMID: 29337491.
- 108- Satapathy SR, Nayak A, Siddharth S, Das S, Nayak D, Kundu CN. "Metallic gold and bioactive quinacrine hybrid nanoparticles inhibit oral cancer stem cell and angiogenesis by deregulating inflammatory cytokines in p53 dependent manner". *Nanomedicine*. 2018;14(3):883–896.
- 109- Arvizo RR, Rana S, Miranda OR, Bhattacharya R, Rotello VM, Mukherjee P. Mechanism of anti-angiogenic property of gold nanoparticles: role of nanoparticle size and surface charge. *Nanomedicine*. 2011;7(5):580–587. doi: 10.1016/j.nano.2011.01.011
- 110- Zhang, G., Yang, Z., Lu, W., Zhang, R., Huang, Q., Tian, M., Li, L., Liang, D., and Li, Ch. "Influence of anchoring ligands and particle size on the colloidal stability and in vivo biodistribution of polyethylene glycol-coated gold nanoparticles in tumor-xenografted mice", *Biomater*. 2009;30(10):1928–1936.
- 111- Douglas SJ, Davis SS, and Illum L. "Nanoparticles in drug delivery", *Crit Rev Ther Drug Carrier Syst*. 1987;3(3):233–261.
- 112- Hillyer J, Albrecht R. "Gastrointestinal persorption and tissue distribution of differently sized colloidal gold nanoparticles", *J Pharm Sci*. 2001;90:1927–1936
- 113- Semmler-Behnke M, Kreyling WG, Lipka J, Fertsch S, Wenk A, Takenaka S, Schmid, G., and Brandau, W. "Biodistribution of 1.4- and 18-nm Gold Particles in Rats", *Small*. 2008;4(12):2108–2111
- 114- Sonavane, G., Tomoda, K., Sano, A., Ohshima, H., Terada, H., and Makino, K., "In vitro permeation of gold nanoparticles through rat skin and rat intestine: Effect of particle size" *Coll. and Surf B: Biointerfaces*. 2008;65(1):1–10

- 115- Sonavane, G., Tomoda, K., and Makino, K. “Biodistribution of colloidal gold nanoparticles after intravenous administration: Effect of particle size” *Coll. and Surf B: Biointerfaces*. 2008;66(2):274–280.
- 116- De Jong, WH., Hagens, WI., Krystek, P., Burger, MC., Sips, AJAM., and Geertsma, RE. “Particle size-dependent organ distribution of gold nanoparticles after intravenous administration”, *Biomater*. 2008;29(12):1912–9.
- 117- Balogh L, Nigavekar SS, Nair BM, Lesniak W, Zhang C, Sung LY, Kariapper, M., El-Jawahri, A., Llanes, M., Bolton, B., Mamou, F., Tan, W., Huston, A., Minc, L., and Khan, K. M. “Significant effect of size on the in vivo biodistribution of gold composite nanodevices in mouse tumor models”, *Nanomedicine*. 2007;3(4):281–296.
- 118- Albanese, A., Walkey, C., Olsen, J., Guo, H., Emili, A., and Chan, W. “Secreted Biomolecules Alter the Biological Identity and Cellular Interactions of Nanoparticles”, *ACS Nano*. 2014, 8, 6, 5515–5526.
- 119- Fadeel, B., Feliu, N., Vogt, C., Abdelmonem, A., and Parak, W. “Bridge over troubled waters: understanding the synthetic and biological identities of engineered nanomaterials”, *WIREs Nanomedicine and Nanobiotechnology*. 2013.
- 120- Liu, Y., Hardie, J., Zhang, X., and Rotello, V. “Effects of engineered nanoparticles on innate immune system”, *Semin Immunol*. 2017, 34: 25, 32.
- 121- J., Xu Q., Kim N., Hanes J., and Ensign L. “PEGylation as a strategy for improving nanoparticle-based drug and gene delivery”, *Adv Drug Deliv Rev*. 2015. 1;99(Pt A):28-51.
- 122- Chinen A., Guan Ch., Ko C., and Mirkin Ch. “The impact of protein formation on the macrophage cellular uptake and biodistribution of spherical nucleic acids”. *Small*. 2017; 13(16).
- 123- Zhang W., Meckes B., Mirkin Ch. “Spherical nucleic acids with tailored and active protein coronae”, *ACS cent. Sci*. 2019; 1983-1990.
- 124- Akhter M., Khalilullah H., Gupta M., Alflaleh., Alhakamy N., Riadi Y., Md Sh. “Impact of protein corona on the biological identity of nanomedicine; understanding the fate of nanomaterials in the biological milieu”, *Biomedicines*. 2021; 9(10): 1496.
- 125- Chen F., Wang G., Griffin J., Brenneman B., Banda N., Holers V., Backos D., Wu L., Moghimi S., and Simberg D. “Complement proteins bind to nanoparticles protein corona and undergo dynamic exchange in vivo”, *Nature Nanotechnol*. 2017; 12(4): 387–393.
- 126- Tekie F., Hajiramezanali M., Geramifar P., Raoufi M., Dinarvand R., Soleimani M., and Atyabi F. “Controlling evolution of protein corona: a prosperous approach to improve chitosan-based nanoparticles biodistribution and half-life”, *Nature Scientific Reports*. 2020; 10(1): 9664.

- 127- Petrarca C, Clemente E, Amato V, Pedata P, Sabbioni E, Bernardini G, Iavicoli I, Cortese S, Niu Q, Otsuki T, Paganelli R, Di Gioacchino M. “Engineered metal based nanoparticles and innate immunity”, *Clin Mol Allergy*. 2015;13:13
- 128- Luo YH, Chang LW, Lin P. “Metal-Based Nanoparticles and the Immune System: Activation, Inflammation and Potential Applications” *Biomed Res Int*. 2015;2015.
- 129- Moyano DF, Liu Y, Peer D, Rotello VM. Modulation of Immune Response Using Engineered Nanoparticle Surfaces. *Small*. 2016;12:76–82.
- 130- Getts DR, Shea LD, Miller SD, King NJC. “Harnessing nanoparticles for immune modulation”, *Trends Immunol*. 2015;36:419–427.
- 131- Cheng CJ, Tietjen GT, Saucier-sawyer JK, Saltzman WM. “A holistic approach to targeting disease with polymeric nanoparticles”, *Nat Rev Drug disc*, 2015;14:239–247.
- 132- Mohanan D, Slütter B, Henriksen-lacey M, Jiskoot W, Bouwstra JA, Perrie Y, Kündig TM, Gander B, Johansen P. “Administration routes affect the quality of immune responses: A cross-sectional evaluation of particulate antigen-delivery systems”, *J Control Release*. 2010;147:342–349.
- 133- Pricop D, Andrieş M. “Endocytosis and Exocytosis of Gold Nanoparticles”, *Int J Nano*. 2014;25:1–9.
- 134- Fievez V, Garinot M, Schneider Y, Pr at V. “Nanoparticles as potential oral delivery systems of proteins and vaccines: A mechanistic approach”, *J Control Release*. 2006;116:1–27.
- 135- Fang RH, Kroll AV, Zhang L. “Nanoparticle-Based Manipulation of Antigen-Presenting Cells for Cancer Immunotherapy”, *Small*. 2015;11:5483–5496.
- 136- Ilinskaya AN, Dobrovolskaia MA. “Immunosuppressive and anti-inflammatory properties of engineered nanomaterials”. *Br J Pharmacol*. 2014;171:3988–4000.
- 137- Sani, A., Cao, C., and Cui, D. “Toxicity of gold nanoparticles (AuNPs): A review”, *Biochem Biophys Rep*. 2021 26: 100991.
- 138- Chithrani B.D., Ghazani A.A., Chan W.C.W. “Determining the size and shape dependence of gold nanoparticle uptake into mammalian cells”, *Nano Lett*. 2006;6:662.
- 139- Jennings T., Strouse G. “Past, present, and future of gold nanoparticles”. *Adv. Exp. Med. Biol*. 2007;620:34.
- 140- Van Doren E.A.F., Temmerman P.R.H.D., Francisco A.D., Mast J. “Determination of the volume specific surface area by using transmission electron tomography for characterization and definition of nanomaterials”, *Journal of Nanobiotechnology*. 2011;9:17

- 141- Donaldson K., Borm P.J.A., Castranova V., Gulumian M. “The limits of testing particle-mediated oxidative stress in vitro in predicting diverse pathologies; relevance for testing of nanoparticles”, *Part. Fibre Toxicol.* 2009;6:13.
- 142- Cho, W., Cho, M., Jeong, J. Choi, M., Cho, H., Han, B., Kim, Sh., Kim, H., Lim, Y., Chung, B., Jeong, J. “Acute toxicity and pharmacokinetics of 13 nm-sized PEG-coated gold nanoparticles”, *Toxicol. Appl. Pharmacol.* 2009. 1;236(1):16-24.
- 143- Chen Y.S., Hung Y.C., Liao I., Huang G.S. “Assessment of the in vivo toxicity of gold nanoparticles”. *Nanoscale Res Lett.* 2009;4:858–864. doi: 10.1007/s11671-009-9334-6.
- 144- Pedata P, Petrarca C, Garzillo EM, Di Gioacchino M. “Immunotoxicological impact of occupational and environmental nanoparticles exposure: The influence of physical, chemical and combined characteristics of the particles” *Int J Immunopathol Pharmacol.* 2016;29:343–353.
- 145- Bolanos K., Kogan M., and Araya E. “Cappin gold nanoparticles with albumin to improve their biomedical properties”, *Int J Nanomedicine.* 2019; 9;14:6387-6406.
- 146- Swiercz, R., Mo, M., Khare, P., Schneider, Z., Ober, R., and Ward, E. “Loss of expression of the recycling receptor, FcRn, promotes tumor cell growth by increasing albumin consumption”, *Oncotarget.* 2017. 10;8(2):3528-3541.
- 147- Larsen, M., Kuhlmann, M., Hvam, M., Howard, K. “Albumin-based drug delivery: harnessing nature to cure disease”, *Mol Cell Ther.* 2016. 27;4:3.
- 148- XIA, Q., Zhang, Y., Li, Z., Hou, X., and Feng, N. “Red blood cell membrane-camouflaged nanoparticles: a novel drug delivery system for antitumor application”, *Acta Pharm Sin B.* 2019. 9(4): 675–689.
- 149- Dehaini, D., Wei, X., Fang, R., Masson, S., Angsantikul, P., Luk, B., Zhang, Y., Ying, M., Jiang, Y., Kroll, A., Gao, W., and Zhang, L. “Erythrocyte-Platelet Hybrid Membrane Coating for Enhanced Nanoparticle Functionalization”, *Adv Mater.* 2017. 29(16):10.
- 150- Patel, P., Dand, N., Hirlekar, R., and Kadam, V. “Drug loaded erythrocytes: as novel drug delivery system”, *Curr Pharm Des.* 2008.14(1):63-70.
- 151- Hamidi, M., and Tajerzadeh. “Carrier erythrocytes: an overview”, *Drug Deliv.* 2003. 10(1):9-20.
- 152- Laradji, A., Karakocak, B., Kolesnikov, A., Kefalov, V., and Ravi, N. “Hyaluronic Acid-Based Gold Nanoparticles for the Topical Delivery of Therapeutics to the Retina and the Retinal Pigment Epithelium”, *Communication.* 2021,13,3324.
- 153- Sanfilippo, V., Caruso, V., Cucci, L., Inturri, R., Vaccaro, s., and Satriano, C. “Hyaluronan-Metal Gold Nanoparticle Hybrids for Targeted Tumor Cell Therapy”. *Int J Mol Sci.* 2020; 21(9): 3085.

- 154- Karakocak, B., Liang, J., Biswas, P., and Ravi, N. "Hyaluronate Coating Enhances the Delivery and Biocompatibility of Gold Nanoparticles", *Carbohydro Polym.* 2018. 186: 243-251.
- 155- Hans ML, Lowman AM. "Biodegradable nanoparticles for drug delivery and targeting. Current Opinion in Solid State", *J. Mater Sci.* 2002;6:319–327.
- 156- Jaggupilli A, Elkord E. "Significance of CD44 and CD24 as Cancer stem cell markers: an enduring ambiguity", *Clinical & Developmental Immunology.* 2012:11.
- 157- Li D., Wang F., Di H., Liu X., Zhang P., Zhou W., and Liu D. "Cross-Linked poly (ethylene glycol) shells for nanoparticles: enhanced stealth effect and colloidal stability", *Langmuir.* 2019; 2:35(26):8799-8805.
- 158- Quach Q., Kong R., and Kah J. "Complement activation by PEGylated gold nanoparticles", *Bioconjugate Chem.* 2018; 29, 4, 976–981.
- 159- Pelaz B., Pino P., Maffre P., Hartmann R., Gallego M., Rivera-Fernandez S., de la Fuente J., Nienhaus G., and Parak W. "Surface functionalization of nanoparticles with polyethylene glycol: effects on protein adsorption and cellular uptake". *ACS Nano.* 2015; 9, 7, 6996–7008.
- 160- Otsuka H., Nagasaki Y., Kataoka K. "PEGylated nanoparticles for biological and pharmaceutical applications", *Adv Drug Deliv Rev.* 2003; 24;55(3):403-19.
- 161- Reyes-Reyes, E., Teng, Y., and Bates, P. "A new paradigm for aptamer therapeutic AS1411 action: Uptake by macropinocytosis and its stimulation by a nucleolin-dependent mechanism" *Cancer Res.* 2010. 1; 70(21): 8617-8629.
- 162- Bates PJ, Kahlon JB, Thomas SD, Trent JO, Miller DM. "Antiproliferative activity of G-rich oligonucleotides correlates with protein binding", *J Biol Chem.* 1999;274:26369–26377.
- 163- Dapić V, Abdomerović V, Marrington R, et al. Biophysical and biological properties of quadruplex oligodeoxyribonucleotides. *Nucleic Acids Res.* 2003;31:2097–2107.
- 164- Dapić V, Bates PJ, Trent JO, Rodger A, Thomas SD, Miller DM. "Antiproliferative activity of G-quartet-forming oligonucleotides with backbone and sugar modifications", *Biochemistry.* 2002;41:3676–3685.
- 165- Soundararajan, S., Chen, W., Spicer, E., Courtenay-Luck, N., and Fernandes D. "The Nucleolin Targeting Aptamer AS1411 Destabilizes *Bcl-2* Messenger RNA in Human Breast Cancer Cells", *Cancer Res.* 2008. 68(7): 2358-2365.
- 166- Bates, P., Reyes-Reyes, E., Malik, M., Murphy, E., O’Toole, M., and Trent, J. "G-quadruplex oligonucleotide AS1411 as a cancer-targeting agent: Uses and mechanisms" *Biochem Biophys Acta Gen Subj,* 2016,1861(5Pt):1414-1428.

- 167- Zhou, Z., and Lu, Z. “Gadolinium-based contrast agents for MR cancer imaging”, *Wiley Interdiscip Rev Nanomed Nanobiotechnol.* 2013; 5(1): 1-18.
- 168- Masitas, R. A.; Zamborini, F. P., “Oxidation of highly unstable <4 nm diameter gold nanoparticles 850 mV negative of the bulk oxidation potential”, *J. Am. Chem. Soc.* 2012; 134 (11), 5014-5017.
- 169- Haiss, W.; Thanh, N. T. K.; Aveyard, J.; Fernig, D. G., Determination of size and concentration of gold nanoparticles from UV–Vis spectra. *Analytical Chemistry.* 2007; 79 (11), 4215-4221.
- 170- Lebduskova, P.; Hermann, P.; Helm, L.; Toth, E.; Kotek, J.; Binnemans, K.; Rudovsky, J.; Lukes, I.; Merbach, A. E., “Gadolinium(iii) complexes of mono- and diethyl esters of monophosphonic acid analogue of DOTA as potential MRI contrast agents: solution structures and relaxometric studies”, *Dalton Transactions.* 2007; (4), 493-501.
- 171- Lacerda, S.; Campello, M. P.; Marques, F.; Gano, L.; Kubicek, V.; Fouskova, P.; Toth, E.; Santos, I., “A novel tetraazamacrocyclic bearing a thiol pendant arm for labeling biomolecules with radiolanthanides”. *Dalton Transactions.* 2009; (23), 4509-4518.
- 172- Chang, T.-C.; Yu, S. J., “Microwave-assisted catalytic acetylation of alcohols by gold-nanoparticle-supported gadolinium complex”, *Synthetic Communications.* 2015; 45 (5), 651-662.
- 173- Hurst, S. J.; Lytton-Jean, A. K. R.; Mirkin, C. A., “Maximizing DNA loading on a range of gold nanoparticle sizes”, *Analytical Chemistry.* 2006; 78 (24), 8313-8318.
- 174- Perera, Y., Xu, J., Amarasekara, D., Hughes, A., Abbood, I., and Fitzkee, N. “Understanding the adsorption of peptides and proteins onto PEGylated gold nanoparticles”, *Molecules.* 2021, 26(19): 5788.
- 175- Li, M., Jiang, Sh., Simon, J., Pablick, D., Frey, M., Wanger, M., Mailander, V., Crespy, D., and Landfester, K. “Brush conformation of polyethylene glycol determine the stealth effect of nanocarriers in the low protein adsorption regime”, *Nano lett.* 2021, 21, 4, 1591-1598.
- 176- Verhoef J., and Anchordoquy Th. “Questioning the use of PEGylation for drug delivery”. *Drug Deliv Transl Res.* 2013, 3(6): 499-503.
- 177- Walkey, C., Olsen, J., Guo, H., Emili, A., and Chan, W. “Nanoparticle size and surface chemistry determine serum protein adsorption and macrophage uptake”, *J. Am. Chem. Soc.* 2011, 134, 4, 2139–2147.
- 178- Gref, R., Luck, M., Quellec, P., Marchand, M., Dellacherie, E., Harnisch, S., Blunk, T., and Muller, R.H. “Stealth’ corona-core nanoparticles surface modified by polyethylene glycol (PEG): influences of the corona (PEG chain length and surface density) and of the core composition on phagocytic uptake and plasma protein adsorption”, *Colloids Surf. B. Biointerfaces.* 2000, 18, 3-4, 301-313.



- 179- Hamad I, Al-Hanbali O, Hunter AC, Rutt KJ, Andresen TL, Moghimi SM. “Distinct polymer architecture mediates switching of complement-activation pathways at the nanosphere-serum interface: implications for stealth nanoparticle engineering”, *ACS Nano*. 2010, 4(11):6629–6638.
- 180- Schaffler, M., Semmler-Behnke, M., Sarioglu H., Takenaka, Sh., Wenk, A., Schleh, C., Hauck, S., Johnston B., and Kreyling W. “Serum protein identification and quantification of the corona of 5,15 and 80 nm gold nanoparticles”, *Nanotechnology*. 2013, 265103 (9pp).
- 181- Dos Santos N., Allen C., Doppen AM., Anantha M., Cox KA., Gallagher RC., Karlsson G., Edwards K., Kenner G., Samuels L., Webb MS., and Bally MB. “Influence of poly(ethylene glycol) grafting density and polymer length on liposomes: relating plasma circulation lifetimes to protein binding” *Biochim Biophys Acta*. 2007,1367–1377.
- 182- Abu Lila A., Kiwada H., and Ishida T. The accelerated blood clearance (ABC) phenomenon: clinical challenge and approaches to manage. *J Control Release*. 2013, 127, 38-47.
- 183- Betker, J., Gomez, J. and Anchordoquy Th. “The effects of lipoplex formulation variables on the protein corona and comparisons with in vitro transfection efficiency”, *J Control Release*. 2013, 171(3): 261-268.
- 184- Xu, L., and Anchordoquy Th. “Drug delivery trends in clinical trials and translational medicine: challenges and opportunities in the delivery of nucleic acid-based therapeutics” *J Pharm Sci*. 2012, 100 (1): 38-52.
- 185- Oh, N., and Park, Ji. “Surface chemistry of gold nanoparticles mediates their exocytosis in macrophages”, *ACS Nano*. 2014, 8, 6, 6232–6241.
- 186- Quach, Q., and Kah, J. “Non-specific adsorption of complement proteins affects complement activation pathways of gold nanomaterials”, *Nanotoxicology*. 2017, 11, NO.3, 382-394.
- 187- Dezsi, L., Fulop, T., Meszaros, T., Szenasi, G., Urbanics, R., Vazsonyi, C., Orfi, E., Rosivall, Laszlo, L., Nemes, R., Kok, R., Metselaar, C., Storm, G., Szebni, J. “Features of complement activation-related pseudoallergy to liposomes with different surface charge and PEGylation: comparison of the porcine and rat responses”, *J Control Release*. 2014, 10: 195:2-10.
- 188- Patel, P., Giljohann, D., Daniel, W., Zheng, D., Prigodich, and A., Mirkin, Ch. “Scavenger receptors mediate cellular uptake of polyvalent oligonucleotide-functionalized gold nanoparticles”, *Bioconjug Chem*. 2010, 21(12): 2250-2256.

- 189- Brun, E., and Sicard-Roselli, C. “Could nanoparticle corona characterization help for biological consequence prediction?”, *Cancer Nanotechnol.* 2014, 5(1): 7.
- 190- Cheng, X., Tian, X., Wu, A., Li, J., Tian, J., Chong, Y., Chai, Z., Zhao, Y., Chen, Ch., and Ge C. “Protein corona influences cellular uptake of gold nanoparticles by phagocytic and nonphagocytic cells in a size-dependent manner”, *ACS Appl. Mater. Interfaces.* 2015, 7, 37, 20568-20575.
- 191- Mosquera, J., Gracia, I., Henriksen-Lacey, M., Martinez-Calvo, M., Dhanjani, M., Mascarenas, J., and Liz-Marzan, L. “Reversible control of protein corona formation on gold nanoparticles using host–guest interactions”, *ACS Nano.* 2020, 14(5), 5382-5391.
- 192- Lesniak, A., Salvati, A., Santos-Martinez, M., Radomski, M., Dawson, K., and Aberg, Ch. “Nanoparticle adhesion to the cell Membrane and Its effect on nanoparticle uptake efficiency”. *J.Am. Chem. Soc.* 2013, 135, 4, 1438-1444.
- 193- Mosquera, J., Gracia, I., and Liz-Marzan, L. “Cellular uptake of nanoparticles versus small molecules: a matter of size”, *Acc. Chem. Res.* 2018, 51,9, 2305-2313.
- 194- Chauhan R., **El-Baz N.**, Keynton R., James K., Malik D., Zhu M. El-Baz A., Ng Ch., Bates P., Malik M., O’Toole M. Targeted gold nanoparticle–oligonucleotide contrast agents in combination with a new local voxel-wise MRI analysis algorithm for in vitro imaging of triple-negative breast cancer. *J. Nanomater.* 2019, 9(5): 709.
- 195- Chen, Ch., Li, J., Guo, N., Chang, D., Wang, Ch., Chen, J., Lin, W., Chi, K., Lee, Y., Liu, R., Chen, Ch., and Wang, H. “Evaluation of the Biological Behavior of a Gold Nanocore-Encapsulated Human Serum Albumin Nanoparticle (Au@HSANP) in a CT-26 Tumor/Ascites Mouse Model after Intravenous/Intraperitoneal Administration” *Int J MolSci.* 2019 Jan 8;20(1):217.
- 196- Yahyaei, B., Nouri, M., Bakherad, S., Hassani, M., and Poralı, P. “Effects of biologically produced gold nanoparticles: toxicity assessment in different rat organs after intraperitoneal injection” *AMB Expr.* 2019, 9, 38.
- 197- Nagwa El-Baz,” A Cancer-Targeted Gold Nanoparticle-Based MRI contrast Agent”, M.S. Thesis, University of Louisville, 2018.

## LIST OF ABBREVIATION

GNPs	Gold Nanoparticles
EPR	The Enhanced Permeability and Retention Effect
MW	Microwave Irradiation
UV	Ultraviolet
SPR	Surface Plasmon resonance
NIR	Near-infrared
MMP	Magnetic Microparticle
CT	Computed Tomography
PAT	Photoacoustic Tomography
OCT	Coherence Tomography
LA	Lactobionic Acid
HCC	Hepatocellular Carcinoma
MRI	Magnetic Resonance Imaging
DFM	Darkfield Microscopy
SERS	Surface-Enhanced Raman Scattering (SERS)

PAI	Photoacoustic imaging
PTT	Photothermal therapy
PDT	Photodynamic therapy
PBS	Phosphate Buffer saline
PB	Phosphate Buffer
Gd	Gadolinium
DO3A-SH or DOTA	Dodecane Tetraacetic Acid
Ce6	Chlorin e6
PEG	Polyethylene glycol
DOX	Doxorubicin
PRKC $\epsilon$	Protein kinase C epsilon
5FU	5-Fluorouracil
DPPH	2,2-Diphenyl-1-Picrylhydrazyl
VEGF-A	Vascular Endothelial Growth Factor-A
RhoA	Ras Homolog Family Member A
ROS	Reactive Oxygen Species
RBCs	Red blood cell
HS	Human Serum

DTT	Dithiothreitol
mPEG-SH	Methoxy polyethylene glycol thiol
HPLC	High Performance Liquid Chromatography
LDS	Lithium dodecyl sulfate
MES SDS	Compound 2-ethanesulfonic acid sodium dodecyl sulfate
DMEM	Dulbecco's Modified Eagle Medium
RPMI	Roswell Park Memorial Institute
DLS	Dynamic Light Scattering measurements
ICP-MS	Inductively Coupled Plasma Mass Spectrometry
BCA	Bicinchoninic acid assay
FBS	Fetal bovine serum
IACUC	The Institutional Animal Care and Use Committee
$A_{450}$	Absorbance at 450 nm
$A_{spr}$	SPR peak
DTNB	5,5'-dithiobis (2-nitrobenzoic acid)
DICOM	Digital Imaging and Communications in Medicine
S MAC	Soluble Membrane Attack Complex
TCC	Terminal Complement Complex

RES

Reticuloendothelial system

## CURRCULUM VITAE

Nagwa El-Baz

Ph.D. Candidate, Department of Pharmacology and Toxicology

Mailing Address: Nanotherapeutics Laboratory

Department of Bioengineering, University of Louisville

200 E Shipp Ave

Louisville, KY 40208 USA

University of Louisville

n0elba01@louisville.edu

---

### **Education**

2022-Present      Ph.D. candidate in Pharmacology and Toxicology, University of Louisville, USA.

Mentor: Dr. Martin O'Toole, Department of Bioengineering.

Dissertation Title: The Impact of PEGylation on Cellular Uptake and *In Vivo* Biodistribution of Gold Nanoparticle MRI Contrast Agents.

Anticipated graduation date: December 2022.

- 2015-2018 M.S. Pharmacology and Toxicology, University of Louisville, USA.  
Thesis Title: A Cancer-Targeted Gold Nanoparticle-Based MRI Contrast Agent.
- 1996-2001 B.S. School of Pharmacy, Mansoura University, Egypt.

### **Professional Experience**

- 2015-Present Research Assistant, Nanotherapeutic Laboratory, Bioengineering Department, University of Louisville, USA.
- 2001-2002 Pharmacist, Elsinblaween Hospital, Egypt.
- 1996-2001 Summer Internship, at Elsinblaween Hospital, Egypt.

### **Fellowships and Awards**

- Graduate Dean's Citation Award, 2022
- Graduate Student Council Travel Award, 2022.
- Graduate Student Council Research Grant, 2021.
- Graduate Student Council Research Grant, 2020.
- Integrated Programs in Biomedical Science, Fellowship 2018-2020.

### **Publications**

#### **Peer-Reviewed Journal Manuscript**

- 1- Rajat Chauhan+, Nagwa El-Baz+, Robert Keynton, Kurtis James, Danial Malik, Mingming Zhu, Ayman El-Baz, Chin Ng, Paula Bates, Mohammad Tariq Malik, and Martin O'Toole, "Targeted Gold Nanoparticle-Oligonucleotide Contrast Agents in Combination with a New Local Voxel-Wise MRI Analysis Algorithm for In Vitro Imaging of Triple-Negative Breast Cancer", *Nanomaterials*, 2019, 7;9(5):709. + means



co-first author.

- 2- **Nagwa El-Baz**, Paula Bates, Martin O'Toole, "The Impact of PEGylation on Cellular Uptake and *In Vivo* Biodistribution of Gold Nanoparticle MRI Contrast Agents", *Bioengineering*.

### **Peer-Reviewed Conference Proceeding Manuscript**

- **Nagwa El-Baz**, Rajat Chauhan, Kurtis T. James, Danial A. Malik, Mingming Zhu, Ayman ElBaz, Robert S. Keynton<sup>1</sup>, Chin K. Ng, Paula J. Bates<sup>2</sup>, Tariq Malik, Martin G. O' Toole, "Gold Nanoparticles Conjugate Cancer-Targeting Aptamer and Gadolinium Chelate for MR Cancer Imaging", *IEEE International Symposium on Signal Processing and Information Technology*, 12/6/2018.

### **Abstracts Published in Proceedings and Invited Presentations**

- 1- **Nagwa El-Baz**, Paula Bates, Martin O'Toole, "Complement Proteins Adsorption by PEGylated and Non-PEGylated Cancer-Targeted Gold Nanoparticle MRI Contrast agents", *Society for Biomaterials*, April 2022 in Baltimore, USA.
- 2- **Nagwa El-Baz**, Paula Bates, Martin O'Toole, "Assessment Of The amount Of Serum Proteins On The surface Of Cancer- Targeted Gold Nanoparticles" October 2021 in Orlando, USA.
- 3- **Nagwa El-Baz**, Paula Bates, Martin O'Toole," Non- Specific Adsorption of Serum Proteins on the Surface of Cancer-Targeted Gold Nanoparticle MRI Contrast Agents", *UofL graduate school conference*, March 2021 in Louisville, USA.
- 4- **Nagwa El-Baz**, Rajat Chauhan, Betty Nunn, Paula Bates, Martin O'Toole," Characterization of Serum Protein Adsorption on Cancer-Targeted Gold Nanoparticles MRI Contrast Agents", *Research!Louisville*, September 2019 in Louisville, USA.
- 5- **N. El-Baz**, K. James, R. Chauhan, D. Malik, B. Nunn, A. Switala, A. El-Baz, R. Keynton, P. Bates, T. Malik, M. O'Toole, "In Vivo Assessment of Toxicity of Gold Nanotheranostic Agent", *Society for Biomaterials*, April 2018 in Atlanta, USA.

- 6- **N.El-Baz**, R. Chauhan, K. T. James, D. A. Malik, M. Zhu, Junling Li, A. El-Baz, D. M. Miller, R. S. Keynton, C. K. Ng, P. J. Bates, T. Malik, M. G. O' Toole, "A Novel Image Monitoring Algorithm For Triple Negative Breast Cancer," *Biomedical Engineering Society (BMES)*, October 2017 in Phoenix, USA.
- 7- M. Malik, M. O'Toole, D. Malik, R. Chauhan, M. Zhu, C. Ng, J. Li, H. Zheng, K. James, **N. El-Baz**, N. Bilcuhuk, A. El-Baz, R. Keynton, A. Dragun, B. Wang, N. Dunlap, D. Miller and P. Bates, "AS1411-GNS: A Platform Technology for Cancer-targeted Therapy and Imaging," *Imaging 2020: The Future of Precision Medicine Molecular Imaging for Diagnosis and Surgery/Therapy*, Wyoming, September, 2016.
- 8- D. Malik\*, **N. ElBaz\***, R. Chauhan\*, K. James, M. Zhu, J. Li, A. ElBaz, D. Miller, R. Keynton, C. Ng, P. Bates, , M. O' Toole, M. Malik, "Nanotheranostic: Targeted Aptamer Nanoparticles for Breast Cancer Therapy and Imaging," *Nanotheranostic*, Boston, USA, June 2016. Note that '\*' means co-first author.
- 9- **N. El-Baz**, D. Malik<sup>1</sup>, R. Chauhan, K. James, M. Zhu, J. Li, A. El-Baz, D. Miller, R. Keynton, C. Ng, P. Bates, M. Tariq Malik, M. O' Toole, "Targeted Theranostic Gold Nanoparticles for Imaging and Therapy of Triple Negative Breast Cancer," *Biomedical Engineering Society (BMES)*, October 5-8, 2016 in Minneapolis.

### **Talk and Oral Presentations**

1. **N. El-Baz**, "The Impact of PEGylation on Protein Adsorption and Cellular Uptake of Gold Nanoparticle MRI Contrast Agents," Pharmacology and Toxicology Department Research Seminar, May 2022.
2. **N. El-Baz**, "Gold Nanoparticles as promising agents in Biomedicine: Applications and Challenges," Pharmacology and Toxicology Department Research Seminar, September 2019.
3. **N. El\_Baz**, "Gold Nanoparticles Conjugate Cancer-Targeting Aptamer and Gadolinium Chelate for MR Cancer Imaging" Oral presentation at IEEE International Symposium on Signal Processing and Information Technology, 12/6/2018.
4. **N. El-Baz**, "A Cancer-Targeted Gold Nanoparticle-based MRI Contrast Agent," Pharmacology and Toxicology Department Research Seminar, M.S Thesis/Ph.D. Proposal, July 2018.
5. **N. El-Baz**, "Cancer Targeting MRI Contrast Agent," JGBCC Seminar Series, May 2016.

6. **N. El-Baz**, “Cancer Targeting MRI Contrast Agent,” Pharmacology and Toxicology Department Research Seminar, March 2016.

### **Memberships in Professional Societies**

- Biomedical Engineering Society (BMES)

### **Volunteer and Community Work**

- Poster Judge, Nur Islamic School Science Fair, 2020.
- Poster Judge, Meyzeek and Manual Regional Science Fair, 2018.